Microwave measurement techniques for wearable antennas

Microwave Measurement Techniques for Wearable Antennas

by

Muhammad Irfan Khattak

Doctoral Thesis

Submitted in partial fulfillment of the requirements for the award of

Doctor of Philosophy of Loughborough University

2010

Certificate of Originality

This is to certify that I am responsible for the work submitted in this thesis, that the original work is my own except as specified in acknowledgments or in footnotes, and that neither the thesis nor the original work contained therein has been submitted to this or any other institution for a higher degree.

Author's signature   ……………………………………………………

Date   …………………………………………

Abstract

This research is germane to the area of on-body antennas and the characterisation of antennas in close proximity to biological matter. The ranges of frequencies discussed are currently popular for mobile communications, namely 0.9GHz to 6GHz with spot frequencies of GSM900, GSM1800 and WiFi2.5GHz. Particular attention is given to the elimination of errors in measurement. This is achieved by the characterisation of an anechoic chamber; a study of the effects of cables; a study of the interaction of surface currents and the human body; a study of tissue simulating liquid; the design of a simple body phantom; the characterisation of the on-body channel for human males in wet and dry clothing and a comparison of perturbation on antennas close to humans and a phantom.

To my dearest (Late) father, mother, my sisters and my loving brother

Muhammad Arif Ullah

Acknowledgements

Publications

- Ma, L., Edwards, R. M., Bashir, S., **Khattak, M. I**., *'A wearable flexible multi-band antenna based on a square slotted printed monopole',* Antennas and Propagation Conference, 2008. LAPC 2008. Loughborough, 17-18 March 2008 Page(s):345 – 348.

- Bashir, S., Hosseini, M., Edwards, R. M., **Khattak, M. I**., Ma, L.,' *Bicep mounted low profile wearable antenna based on a non-uniform EBG ground plane – Flexible EBG Inverted-L (FEBGIL) Antenna',* Antennas and Propagation Conference, 2008. LAPC 2008. Loughborough, 17-18 March 2008 Page(s):333 - 336

- **M. I. Khattak**, R. M. Edwards, S. Bashir, L. Ma, "*A study of the on-body channel for a human male with wet and dry clothing*", in WWRF 21ST Meeting, 13th – 15th October 2008, Stockholm, Sweden.

- **M. I. Khattak,** R. M. Edwards, J. Ma, "*A Study of Perturbations due to Antennas in close proximity with the Human Body and Body Simulating Liquid Filled Phantoms at 1.8GHz*", Loughborough Antennas & Propagation Conference, 16th and 17th November, 2009.

- **M. I. Khattak**, R. M. Edwards, J. Ma and C. J. Panagamuwa, "*A Study of Perturbations in Linear and Circular Polarised Antenna in close proximity of Human Body and Dielectric Liquid Filled Phantom at 1.8 GHz*", 4th European Conference on Antennas and Propagation, EuCAP 2010, Barcelona, Spain, on 12-16 April 2010.

- R. M. Edwards, J. A. Brister and **M. I. Khattak**, "*Application of Pareto Ranked Genetic Algorithm to a Wearable Ball Spiral Antenna*", IEEE International Conference on Wireless Information Technology and Systems, Honolulu, Hawai'i, USA, August 28th - September 3rd, 2010.

Table of Contents

List of Figures

List of Tables

Chapter 1:
Introduction

This research is concerned with techniques for microwave measurement of antennas that are worn by humans. There is a great deal of information available about how to measure the characteristics of antennas in isolation. Two books on this subject are [1, 2] both of these books consider antennas and their measurements in free space, and both can be considered to be landmark publications. However, with the advent of personal communication systems there has been a trend for antennas to move even closer to humans. Unlike antennas in free space that can be characterised using commonly available analysis [1, 2], information about antennas on the body is far more incomplete. In many papers the effects of the body on antennas parameters are investigated but left unexplained. For example Zhi Ning Chen [3] presents a paper on Human Head effects on Planar Antennas, but results for on body are simply stated without explanation.

Many papers for example [3-10] give scant consideration to the perturbing effects of the body. Perhaps one explanation for lack of information about the influence of humans on measurements is that bodies come in many shapes and sizes and that an antenna designer may not be able to predict who might use an antenna. However my hypothesis is that there will be general laws that might be used to predict the range of perturbing effects on antenna parameters due to the body that is the effects of humans on antenna characteristics can be reliably predicted in a more exacting way than is currently the case. It is upon this premise that this PhD is based.

1.1 Thesis Outline

This thesis presents results and discussion relevant to on-body channel characterisation at microwave frequencies including cabling errors associated with on-body measurements, on-body channel characterisation procedures and on-body propagation models. A particularly novel section of this thesis will be concerned with on-body channel characterisation for dry and wet clothing on a human body inside and outside of an anechoic chamber. Perturbation of patch antennas near a human body and dielectric filled human body simulating phantoms and the effects of antenna polarisation on these perturbations at mobile communication frequencies is also researched. In this chapter a literature review of wearable antenna is given along with comments on design and applications.

Due to the flexible nature of coaxial cables that tend to have to move with the body, wearable antenna measurements are always vulnerable to cabling errors. Therefore Chapter 2 is used to introduce types of cabling errors associated with on-body measurements. Chapter 2 includes an introduction to the cabling errors that are germane to on-body measurements for wearable antennas. Phase and amplitude errors linked with the surface currents on the coaxial cable, bending of the cables, mismatch losses and systematic errors are explained. Possible solutions to avoid these errors are also proposed. Later in this chapter the permittivity and conductivity of biological matter is also discussed. Knowledge of these properties is necessary in order to find the energy losses in the body.

In Chapter 3 some electrical properties of human body are further discussed. These include dielectric constant and conductivity; the wave speed in human tissue; propagation of power through human tissues and propagation properties of waves around the human body are highlighted. On-body propagation of electromagnetic waves around the human body is illustrated using a lossy cylinder near an antenna. At the end of the chapter further interaction of the human body with electromagnetic

waves is explained and a review of human body effects on wearable antenna parameters are summarised.

The purpose of Chapter 4 has been to review the work of several leading authors who made significant contributions to the area of on body antenna measurements. In particular techniques used to propose propagation models for the on-body surface wave will be discussed. Three points would seem to be common. Firstly on body channels are highly dynamic. Secondly, ground planes and insulation layers between antennas and supporting tissue are particularly important. Lastly, many on body measurements can be done in quiet areas outside of an anechoic chamber.

In Chapter 5 the application of techniques used in the measurement of wearable antennas is presented. Normalised Site Attenuation (NSA) measurements in anechoic chamber used to check performance will be discussed. It was found that the available chamber performed within recommended limits across the range of frequencies that was used in this work. Complimentary research is also undertaken to access the impact of absorber orientation and the addition of a polystyrene walkway. A novel phone mount and tissue simulating liquid phantom, over the air (OTA) measurement to check the sensitivity of mobile phone, is also presented in the chapter.

Chapter 6 give an insight into on-body channels and the effects of wet clothing are investigated. This research which essentially measures on-body propagation channels, using a quarter wave monopole and square loop antennas. A later section explains how a Specific Anthropomorphic Mannequin (SAM) commonly used to measure on-body antenna properties may produce different results from actual. Results presented will be useful in assessing optimal antenna/body separation for wearable antennas in Body Area Networks using both intra and inter wireless connectivity. At the end the effects of antenna polarisation will also be checked.

1.2 Wearable Antennas

Wearable antennas have received interest due to the introduction of personal communications technology which provides momentum to make mobile phones smaller and simpler to carry and use. Clothing may now have a variety of consumer electronics integrated into it. In personal electronics antennas play a paramount role in the optimal design of the wearable or hand-held units used in communications. Such antennas can increase range, reduce infrastructure, increase battery life and improve diversity. The antenna requirements are given by the particular specification, but common to many applications of wearables are the requirements to be light weight, inexpensive, low maintenance and robust. They should also be comfortable to wear and this has resulted in demand for flexible antennas, which can be easily attached to clothing.

The earliest wearable antenna discovered in this review was made for a military application where the authors of [11] designed a wearable whip antenna. The rationale for this was that soldiers who showed a typical whip antenna were popular targets where a wearable antenna would be less obvious. Also in an early paper (2003) an RF helmet antenna and RF vest antenna were put forward by the authors of [12] and [13] respectively, which could be operated over the frequency range of 500-2000MHz. A conductive cloth and polyester interwoven with nickel and copper were used to construct the helmet antenna whilst the vest antenna was made of canvas and flectron. The main advantages of these antennas were light weight, inexpensive manufacture and low maintenance.

Medical imaging is another application of wearable antennas. Detection of cancer cells as early as possible is an area of concern and very promising results were put forward by the authors of [14, 15] for the early detection of breast cancer. The idea behind this research was that the breast tumours have different electrical properties than healthy breast tissues at certain frequencies. The breast was illuminated with electromagnetic

waves and the transmitted or reflected waves were then measured and compared with known results. Monopole antennas were used by the authors of [14], but research is also being done to develop textile antennas for the medical imaging as these antennas are comfortable against the skin.

The concept of "Smart Clothing" may date back to as early as 1993 [16, 17]. Smart clothes are augmented clothes improved by intelligent wearable systems. In these systems new textiles, now known as technical textiles, are beginning to appear. Technical textiles may be conductive but also flexible. A term associated with technical textiles used in wearable antennas is dupability.   In other words the usual purpose of clothing can be extended to new tasks such as calling emergency assistance and continuous health checkups and etc. Smart clothes were recently introduced by the authors of [17, 18] for arctic environment.

1.3 Wearable Antenna Design:

Since wearable antennas can be incorporated with clothes, so the textile material can used as a substrate for these type of antennas. One of the main advantages of this type of substrate is that clothing tends to have low permittivity and having low dielectric constants means that surface wave losses are decreased and impedance bandwidth is increased. On the other hand fabric stretch and compression changes the dimensions of the antenna influences the antennas characteristics. Typical changes are as detuning in the frequency band and loss of Q.

1.4 Wearable Technology and its Applications:

The definition of wearable technology describes wearables as any kind of electronic device, material and/or components that maybe considered a part of ordinary clothing. Wearables tend to facilitate technological additions to clothing. Current advancements in the field of wearable antennas have made them more useful for wearable technology.

1.4.1 Space and Military Applications:

Previously body sensors have divided into two groups, sensors that can be implanted inside the body and sensors that are worn on or as a part of clothing. These types of sensors have already been used widely in space, military and medical applications. An interesting example was written up by the authors of [19] who have developed a biotelemeter. This device, which was implantable, was used to find out the impacts of spaceflight on the living systems. Similarly the Smart Shirt discussed in [20] uses a special type of sensor made up of optical fibres. This sensor can be used for the detection of bullet entry and exit points, wounds, heartbeat, respiration rate, electrocardiogram (EKG), temperature and pulse oximetry, all during combat conditions.

1.4.2 Telemedicine:

By definition telemedicine means Medicine at a distance, a service to improve the quality of medical treatment. The authors of [21] have given an overview of the completed, ongoing, and emerging applications of wireless information-technology applications in health systems. Emergency telemedicine, the diagnostic accuracy of an ECG telecardiology service, a teleradiology system using a mobile CT van and High-speed Satellite Communication, Mobile Medical Data (MOMEDA) and a collaborative virtual medical team for home healthcare of cancer patients, were the main projects they have discussed.

1.4.3 Medical Implants:

Medical implant communication systems are a growing application of body-centric communication systems. The main challenge in these system is that the antenna is placed inside the human body (a lossy object), which considerably changes the antenna characteristics along with the requirements of non-hazardous nature of these implants.

Many projects have been deployed or under development stages, which includes implantable drug pumps [22], vagus nerve simulator for epilepsy treatment [23] and muscle actuators for paraplegic patients [24] and many more.

1.5 Hypothesis

Although the subject of on-body antennas has become highly topical it is apparent from an extensive literature review that that researchers often pay little or no attention to the types of error that are likely to occur in measurements of antennas close the body. This leads to experiments that are often unrepeatable with the available information; pin head solutions and a general lack of precision for antennas close to the body. The hypothesis supported by the research of this thesis is that the measurement of the properties of on-body antennas can be done reliably and accurately.

Chapter 2:
Supporting Theory for Cabling Errors and Losses in the Human Body in Wearable Antenna Measurements

2.1 Introduction:

The purpose of this chapter is to introduce techniques germane to the accurate measurement and simulation of on-body wearable antennas designed to be used at mobile communications frequencies. It turns out that an antenna on the body should treat that body as an integral part of a system in which in terms of volume it is only a minor component. In general therefore the measurement of an antenna close to any amount of biological tissue has to be done using special techniques that are not usually required when looking at antennas in free space. The electrical properties of matter are therefore very important and as such are also discussed here.

This chapter is therefore structured as follows: section 2.2 contains errors associated with on-body antenna measurements due to the use of Vector Network Analyzers (VNAs). Section 2.3 contains discussion of errors in antenna measurements due to bending of flexible coaxial cables. Section 2.4 contains errors in wearable antenna measurements due to impedance mismatch. Later in this chapter is included a description of conductivity, permittivity and energy losses in biological matter.

2.2   Uncertainties in On-Body Measurements due to the Use of Vector Network Analyser (VNA)

As of 2010 the measurement instrument of choice for most antenna experiments is the vector network analyser (VNA). This device can be used to analyse electrical

networks and can reliably be used for the assessment of antenna parameters. In this thesis it is assumed that the properties of reflection and transmission related to S-parameters are already understood. In the work described in this thesis an analyser with a frequency range of 0.3 to 6GHz was used.

VNAs are designed to measure low and high frequency (microwave) devices, but the measurements of high frequency devices pose great level of difficulties in calibrating the instrumentations because these devices cannot be easily connected directly to VNA which supports coaxial or waveguide media. Device under test (DUT), in our case it is antenna under test (AUT), are manufactured in non-coaxial or wave guide media, so some sort of fixtures are required to connect them to the ports of VNA. A block diagram representing this idea is given below in figure 2.1.
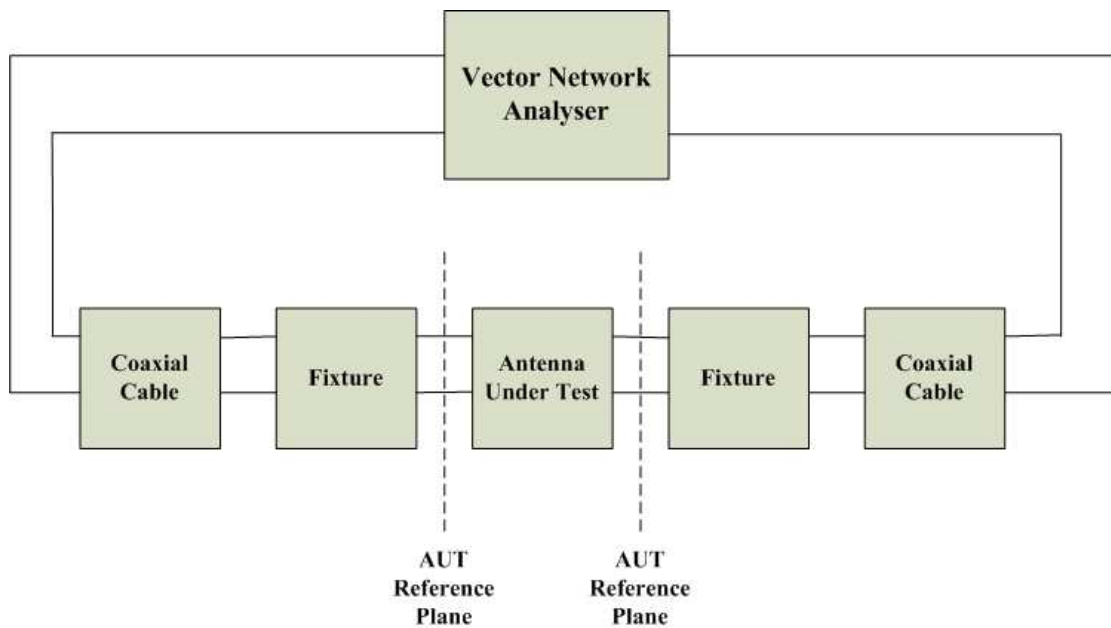
Figure 2-1: A typical antenna measurement setup.

There are three general types of errors associated with measurements performed using VNAs, which are systematic errors (repeatable errors due to imperfection in components, connectors and fixtures), drift errors and random errors. The latter two are connected to noise, connector repeatability, temperature variations and physical

changes within the VNA. *Random errors* vary randomly as a function of time. Since they are not predictable, they cannot be removed by calibration. The main reason for random errors in VNA is instrument noise (e.g., sampler noise, and the IF noise floor), switch repeatability, and connector repeatability. These noise errors associated with VNAs can be reduced by increasing source power and narrowing the IF bandwidth. *Drift errors* occur when a test system's performance changes after a calibration has been performed. They are primarily caused by temperature variation and can be removed by additional calibration. The rate of drift determines how frequently additional calibrations are needed and by making a test environment with stable ambient temperature, drift errors can usually be minimized.

These are typically too costly to be removed and therefore constitute the so called noise floor of the VNA.

2.2.1 Quantification of Systematic Errors through Process of Calibration

The point where AUT is connected to the measurement system figure 2.1 is known as AUT reference point and it is this point where all measurements are desired to be referenced. It turns out that wherever there are used fixtures and cables along with the AUT contribute errors to the measurement. These effects increase with increase in frequency but can be calibrated out up to the reference plane [25-27].

Basic measurements of calibration consist of the calculation of incident, reflected and transmitted wave by applying a stimulus. The network scattering parameters are determined by taking the ratio of these vector quantities. This concept is shown in figure 2.2 given below.
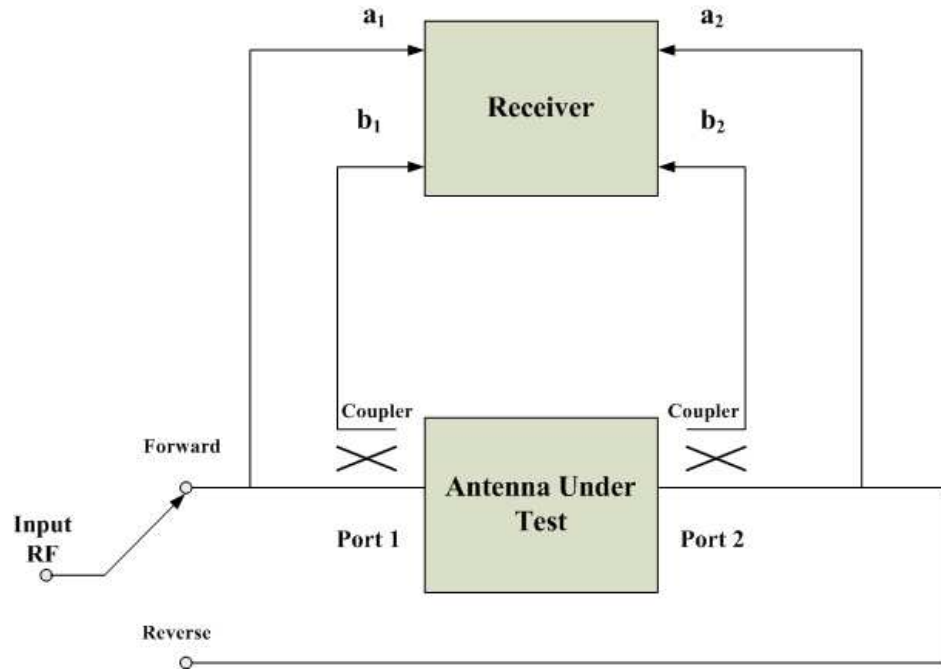
Figure 2-2: A simplified block diagram of vector network analyser.

The RF switch provides stimulus at either of the two ports of VNA and RF couplers connected to both ports are there to measure the reflected voltages. The letter "a" represents the incident signal and "b" represents reflected signal.

With stimulus at port 1 and assuming ideal source to load termination that is $a_2 = 0$:

$$S_{11} = \frac{b_1}{a_1} \quad \text{and} \quad S_{21} = \frac{b_2}{a_1}$$

And stimulus at port 2 and assuming ideal source to load termination that is $a_1 = 0$:

$$S_{22} = \frac{b_2}{a_2} \quad \text{and} \quad S_{12} = \frac{b_1}{a_2}$$

A form of calibration that is performed locally given in Appendix A, usually each time the instrument is set up and configured for a given series of measurements. This type of calibration is intended to remove systematic errors from the instrument hardware (and to take into account the presence of any accessories that may have been added to enable specific measurements to be performed) at the required frequencies for the

measurements. For example in an antenna reflection measurement where a coaxial cable is connected to the front panel connector of VNA followed by coaxial adaptor and finally to antenna prob. Calibration will correct for the effects of these added components as well as correct the systematic errors in the VNA. This is why this type of calibration is often referred to as *error correction.*

The details of the calibration procedures used in our research work are given in Appendix A and the supporting analysis can be found in [28-30].

With regard to wearable antennas in which the likely-hood of impedance mismatch is high an understanding of the way choke baluns work is essential. These should be used on the VNA side of the calibration plane. Both power splitters and active devices present problem worthy of further study with regard to calibration.

2.3 Uncertainty in On-Body Measurements due to Bending of the Coaxial Cables.

We assume here that the cable when in use has not been subjected to bending (flexure) beyond its design limit. In an anechoic chamber the antenna under test is normally the only source of primary radiation. By primary we mean that the source is on the conductor (antenna), rather than off the conductor as in a reflector. In this research we have seen two types of re-radiation problem associated with the measurement of small antennas. Often as an antenna is brought close to the body a severe mismatch can occur. This leads to unwanted current on the outside of the outer conductor which may re-radiate. Section 2.4 below deals with this type of problem. More rarely a leak in a cable due to age or over-flexure may allow a leak in the cable sheath which will cause a secondary source in the chamber. Variations in antenna measurements due to cable movements are situation dependent, they maybe as high as 10dB in case of [31] due to large movements of the antenna cable, on the other hand in some case these

uncertainties are only up to $\pm$0.5dB when the movements are small like in the cases of [32]. Such perturbation is the norm in realistic wearable antenna experiments where the coaxial cables are flexible in nature. Note that in general the less flexible a cable is designed to be the better its phase stability is likely to be. According to the authors of [33], among many of the factors which contribute to the changes in the electrical length of the coaxial cable is bending. When the electrical length of the cable is altered, it results in two types of effects, which are group delay and frequency offset. The voltage handling capacity of the coaxial cables is reduced due to the sharp bending producing weak points in the power handling ability. This allowable bend radius for most of the cables is approximately five-to-six times the cable's outer diameter.

2.4 Uncertainty in On-Body Measurements due to Mismatch Loss

The fields generated by the current on a typical wearable antenna will interact strongly with the body. This means that as either the antenna moves in relation to the body or the properties of the body change, for example gets wet or changes temperature; the antenna match will also change. Currently, it is not practical to match a wearable antenna to the range of impedances it is likely to see and therefore a best match for a relatively static position is normally designed for. A factor which contributes to the antenna measurement error is the impedance mismatch. Mismatch loss is the measure of how much power is lost when the signal faces an impedance mismatch. The mismatch loss, usually expressed in dB, describes how much power is not being absorbed by the terminating load which in this case is usually an antenna. Not all the power available at the interface between the transmission line and the load is delivered into the load; part of it is reflected. The general rule is that for maximum power transfer to the antenna the impedance of the generator must be equal to the impedance of the antenna. If the antenna impedance is very low then the power lost in the generator is maximal. An antenna with high input impedance is in most cases better than an antenna with low input impedance in terms of power transfer.

According to [34] mismatch gives rise to two problems, reflected power, measured by return loss, and loss of power transfer, measured by mismatch loss. As we know return loss is the ratio between the power reflected from a load to the power incident on that load. Thus, a return loss of - 10 dB means that the reflected power from a mismatched load is 10 dB below the power incident on that load.

The loss of power transfer, measured by mismatch loss can be calculated as:

$$\sigma = \frac{1 + \dfrac{E_r}{E_i}}{1 - \dfrac{E_r}{E_i}} = \frac{1 + \Gamma}{1 - \Gamma} \qquad \textbf{Eqn. 2-1}$$

$$\Gamma = \frac{\sigma - 1}{\sigma + 1} = \frac{Z_L - Z_0}{Z_L + Z_0} \qquad \textbf{Eqn. 2-2}$$

$$\text{Return Loss} = -20 \log_{10}(|\Gamma|) \qquad \textbf{Eqn. 2-3}$$

$$\text{Mismatch Loss} = -10 \log_{10}(1 - |\Gamma|^2) \qquad \textbf{Eqn. 2-4}$$

With a well matched antenna the impedance values at the connector dictate that current will only flow on the antenna and the inner and outer conductors of the coaxial feed. However, under certain conditions of mismatch the current on the antenna sees a lower impedance path of the outside of the outer conductor. This current may re-radiate or cause frequency pulling of the generator. Upon measurement this can be seen as perturbations or the filling in of nulls on the far-field pattern. These losses can be lowered by the use of ferrite beads [35], the purpose of which is to stop the surface currents due to the reflection from the antenna because of impedance mismatch. Authors of [35] has investigated the functionality of ferrite beads to minimize the radiation effects of the coaxial cable using FDTD method and found that lossless ferrite beads on the outer conductor of a coaxial cable reflect the currents which flow on the outer conductor. The position of the ferrite bead plays and important part in the radiation characteristics of the antenna, Maximum radiation efficiency was achieved

by the authors of [35] when a ferrite bead was placed at $\lambda/4$ from the end of the outer conductor. However, according to [36], ferrites typically work well as chokes up to 1GHz, e.g. in EMC measurements [35]. Since mobile communication systems are now popular up to several GHz, ferrites are not thought to perform well for wearable antennas. The authors of [36] have given an alternative method to reduce the reflected wave propagation on the surface of the cable by using a cap to simulate an open termination for the energy propagating on the surface of the feed cable. The size of the cap was about quarter of the wavelength, which formed a trap for the currents travelling on the cable. The end of the cap towards the antenna was open, designated as "a" in the figure 1.3 and the far end was short circuited designated as "b" in figure 1.3 to the cable surface. The cup acts as a quarter wave open circuit. This means that any current on the outer of the outer conductor of the coaxial cable sees very high impedance. Therefore currents of this type are choked off.
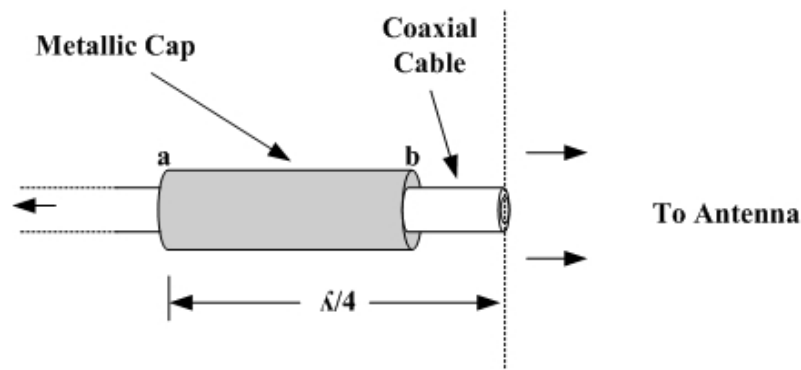
Figure 2-3: Reducing the surface waves on coaxial cable by using a metallic cap.

2.5 Complex Permittivity and Equivalent Conductivity of the Medium

Having discussed the systematic errors in measurements due to cabling, we now move onto losses due to absorption in biological tissue. The assumption has been made in this research that radiofrequency radiation associated with wearable antennas is non-ionising and complies with current safety guidelines in terms of power levels. In

the tissue of the body power radiated from wearable antennas is turned into heat. To understand the mechanism we need to first discuss the properties of body tissue. There are no metals normally present in the body except those inserted during surgery. Assuming non-magnetic materials the media through which electromagnetic waves pass has the same permeability as free space but may have different permittivity which is complex.

When an electric field is applied across a given material, the electrons will naturally want to move due to applied field. The conduction electric current density (a measure of the flow of the electrons) is directly proportional to the strength of the electric field. So:

$$\overline{J}_c = \sigma_s \overline{E}$$
<div align="right">**Eqn. 2-5**</div>

Where σ_s is the conductivity which gives a measure of how fast the electrons move through the material.

Similarly the electric flux density also varies proportionally with electric field and is given by:

$$\overline{D} = \varepsilon \overline{E}$$
<div align="right">**Eqn. 2-6**</div>

Here ε is called permittivity of the material.

According to the time harmonic form of the Maxwell's equation

$$\nabla \times \overline{H} = \overline{J} + j\omega \overline{D}$$
<div align="right">**Eqn. 2-7**</div>

$\overline{J}$ is the electric current density and has two parts. The impressed electric current density, $\overline{J}_i$ (an excitation to the system by an outside source) and the second part is conduction current density $\overline{J}_c$ defined in equation 2.5, which is due to external electric field. We now can write equation 2.7 as,

$$\nabla \times \overline{H} = \overline{J}_i + \overline{J}_c + j\omega \overline{D}$$
<div align="right">**Eqn. 2-8**</div>

Putting equation 2.5 and equation 2.6 in equation (2.8) we get,

$$\nabla \times \overline{H} = \overline{J}_i + \sigma_s \overline{E} + j\omega\varepsilon\overline{E} \qquad \text{Eqn. 2-9}$$

The absolute permittivity is given by:

$$\varepsilon = \varepsilon_0\varepsilon_R \qquad \text{Eqn. 2-10}$$

Here ε_0 is the permittivity of free space which is equal to $8.85 \times 10^{-12} \ s^4 A^2/m^3 kg$ and ε_R is the relative permittivity of the medium, in our case its human body tissue, which is a complex quantity. When an alternating electric field is applied to the medium the dipole inside the material aligns itself with the applied electric field. In the next half cycle, the electric field changes its direction, so the dipole moves again to align itself with the new direction of the field. As it rotates it losses in the form of heat (friction) as well as the acceleration and deceleration of the rotational motion of the dipole. The imaginary part of the permittivity is determined by the degree to which it is out of phase with the field and losses produced in the material and is a function of the material and frequency. So a larger imaginary part means more energy is being dissipated through the motion and less amount of energy is propagated through the dipole. This is more obvious at high frequencies since the time for polarisation is smaller per half circle[37, 38].

The real and imaginary part of absolute permittivity is given by:

$$\varepsilon_0\varepsilon_R = \varepsilon' - j\varepsilon'' \qquad \text{Eqn. 2-11}$$

Equation 2.9 can be written as:

$$\nabla \times \overline{H} = \overline{J}_i + \sigma_s \overline{E} + j\omega(\varepsilon' - j\varepsilon'')\overline{E} \qquad \text{Eqn. 2-12}$$

Re-arranging equation 2.12, we get:

$$\nabla \times \overline{H} = \overline{J}_i + (\sigma_s + \omega\varepsilon'')\overline{E} + j\omega\varepsilon'\overline{E}$$

$$\nabla \times \overline{H} = \overline{J}_i + \sigma_e \overline{E} + j\omega\varepsilon'\overline{E} \qquad \text{Eqn. 2-13}$$

In equation 2.13 we have defined another term known as effective conductivity, which is:

$$\sigma_e = \sigma_s + \omega\varepsilon''$$

<div align="right">Eqn. 2-14</div>

The first term in the right hand side of the equation 2.14 is the static conductivity and we can define the last term as conductivity due to alternating electric field. Thus

$$\sigma_e = \sigma_s + \sigma_a$$

<div align="right">Eqn. 2-15</div>

Re-arranging equation 2-13 we get:

$$\nabla \times \overline{H} = \overline{J_i} + j\omega\varepsilon'\left(1 - j\frac{\sigma_e}{\omega\varepsilon'}\right)\overline{E}$$

<div align="right">Eqn. 2-16</div>

Putting equation 2-11 in equation 2-16, we get:

$$\nabla \times \overline{H} = \overline{J_i} + j\omega\varepsilon'\left(1 - j\frac{\sigma_s}{\omega\varepsilon'} - j\frac{\varepsilon''}{\varepsilon'}\right)\overline{E}$$

<div align="right">Eqn. 2-17</div>

The term $\dfrac{\varepsilon''}{\varepsilon'}$ in equation 2.17 shows how much of the supplied energy is being lost as motion and heat in the tissue. This term dominates in the dielectrics (low conductors) than the metals (highly conductive), so Maxwell's equation for dielectric material like human tissue will be:

$$\nabla \times \overline{H} \approx \overline{J_i} + j\omega\varepsilon'\left(1 - j\frac{\varepsilon''}{\varepsilon'}\right)\overline{E}$$

<div align="right">Eqn. 2-18</div>

We turn now to find out how much energy is dissipated in biological matter.

2.5.1 Energy loss in biological tissue

In Equation 2.16 we were able to combine σ_s and σ_a into the effective conductivity. Using this parameter along with the knowledge of the electric field, the energy loss in biological tissue can be defined as:

$$P_d \quad = \frac{1}{2} \iiint_v \overline{J}.\overline{E^*} dv$$

$$= \frac{1}{2} \iiint_v \sigma_e \overline{E}.\overline{E^*} dv$$

$$= \frac{1}{2} \iiint_v \sigma_e |\overline{E}|^2 dv$$

$$= \frac{1}{2} \iiint_v \frac{|\overline{J}|^2}{\sigma_e} dv \qquad \textbf{Eqn. 2-19}$$

In essence energy from the electromagnetic wave becomes heat in the tissue and therefore constitutes a loss. The loss in the tissue depends on the distance of antenna from the tissue, as more energy will be absorbed by the tissue for a closely placed antenna than a farther one. Reducing such losses can be achieved in several ways and these are discussed at length in subsequent chapters. However all of these methods conclude to ways to reduce electric field density in biological tissue.

2.6   Conclusion

The purpose of this chapter was to discuss the most common kinds of errors which are associated with wearable antennas measurements and to give suggestions for their reduction. The last section in this chapter was concerned with the electrical properties of human tissue and losses in the body when electromagnetic waves pass through it.

Chapter 3:
Electromagnetic waves Propagation Trends around the Human Body

3.1 Introduction

WBAN is an acronym for **Wireless Body Area Networks** and in its simplest form it consists of a set of antennas either inside or upon the body. As of March 2010 there have been few propagation studies for communication channel around the surface of humans. Without a description of the channel degradation, it is impossible to identify optimal RF solutions. Therefore, one of the principal goals of this chapter is to discuss electromagnetic wave propagation on the human body, section 3.2. A brief discussion of interaction of human body with electromagnetic waves propagation and their effects on wearable antenna parameters is given in section 3.3.

3.2 Properties of Human Body Tissues and Electromagnetic Propagation Trends in Body Area Networks

Propagation around the body is complex and depends on a number of factors some of which are, the environment near the user, the electrical properties of human tissue, the geometry of the body and the type of source. Before discussing propagation trends near the body, it will be helpful to summarise the electrical properties of human tissue.

According to [39] and [40] either free charges or dipolar molecules like water, are responsible for energy exchange in the biological tissue. When rapidly alternating field is applied, free charges are accelerated to produce current which will result in some resistive losses. This resistive loss depends on material conductivity. Some frictional loss will arise due to reorientation of dipolar molecules which depends on

material permittivity.

In general it can be seen that dielectric permittivity of human tissue goes down with frequency and conductivity of human tissue goes up with frequency rise. This trend can be found in figure 3.1 and figure 3.2 and also in table 3.1 and table 3.2. Figure 3.1 and Figure 3.2 gives the graphical representation of fact stated before, these figures are constructed after taking data from [38].
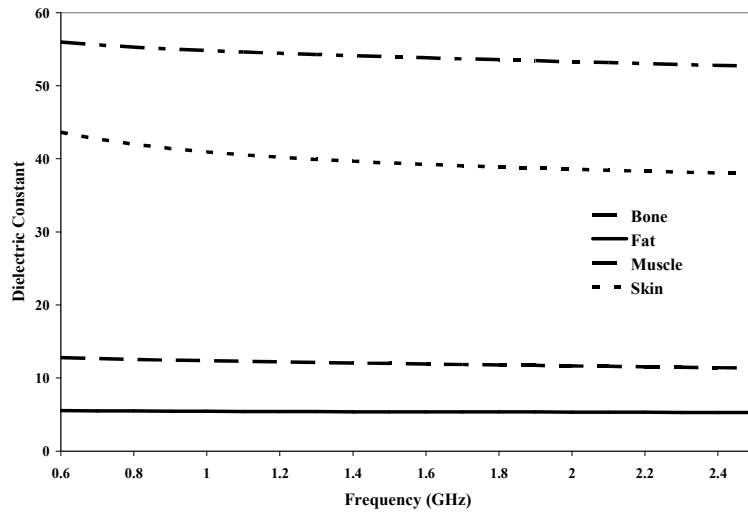
Figure 3-1: Dielectric Constant versus frequency for body tissues
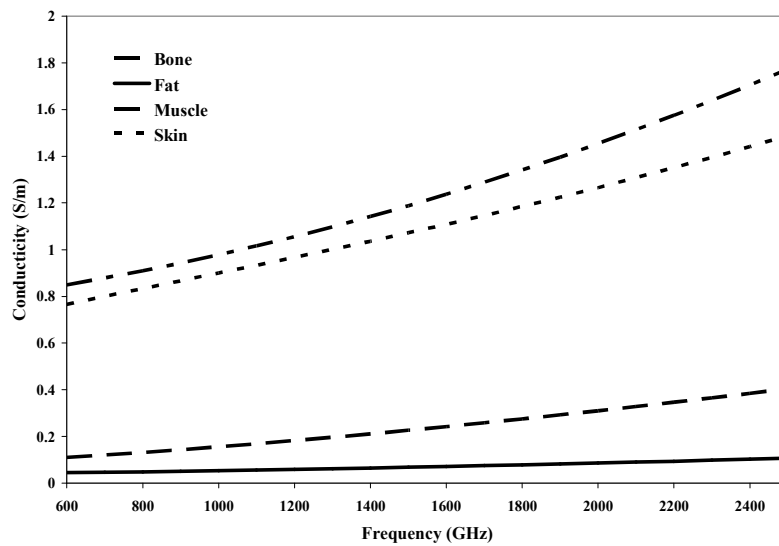
Figure 3-2: Conductivity versus frequency for body tissues

In general it can be seen that the body's tissues have dielectric constant values greater than free space. Fat is found to have values close to free space at all frequencies.

3.2.1 Wave Speed in Human Tissue

When an electromagnetic wave propagates through a dielectric material its wave speed will be reduced which eventually will decrease its wavelength.

$$\lambda = \frac{\lambda_0}{\sqrt{\varepsilon_R}}$$

Equn. 3-1

where λ_0 is the wavelength in free space, ε_R is the relative permittivity of the material. The complex permittivity of a material can be found using a relation given by the authors of [39] as:

$$\varepsilon = \varepsilon_R \varepsilon_0 + j\frac{\sigma}{\omega}$$

Equn. 3-2

Where ε_0 is the permittivity of free space, ε_R ε_r is the relative permittivity, σ is the conductance and ω is the angular frequency.

Table 3-1: Electric properties of human tissues with high water content like muscle and skin [40].

Frequency (MHz)	Wavelength in free space(cm)	Relative permittivity (ε_R)	Conductivity $\sigma(moh/m)$ (σ)	Wavelength λ (cm)
915	32.8	55	0.94	4.4
1800	16.67	53	1.34	2.3
2450	12.2	52	1.74	1.7

Table 3-2: Electric properties of human tissues with low water content such as fat and bone [40].

Frequency (MHz)	Wavelength in free space(cm)	Relative permittivity (ε_R)	Conductivity $\sigma(moh/m)$	Wavelength λ (cm)
915	32.8	5.5	0.05	13.9
1800	16.67	5.4	0.07	7.2
2450	12.2	5.3	0.10	5.3

A half-wave dipole at a frequency of 2.45GHz in free space will nearly be eight times larger than a half-wave dipole in human skin.

3.2.2 Propagation of Power through Human Tissue

It is well understood that electromagnetic waves support the movement of energy. A vector that shows the direction of propagation is called the Poynting vector. The Poynting vector $\overline{S}$ can be defined as

$$\overline{S} = \overline{E} \times \overline{H} \quad (Watt/m^2)$$
Eqn. 3-3

This vector gives the instantaneous power per unit area carried by an electromagnetic wave. The direction of the Poynting vector is the direction of propagation. The time average power density is given by

$$S_{av} = \frac{1}{2}\text{Re}\left\{\overline{E} \times \overline{H}^*\right\}$$
Eqn. 3-4

For an electromagnetic wave in the $\hat{z}$ direction in a lossless medium

$$S_{av} = \frac{\hat{z}\left|\overline{E}\right|^2}{2\eta} = \frac{\left|E_{x0}\right|^2 + \left|E_{y0}\right|^2}{2\eta}\hat{z}$$
Eqn. 3-5

Where η is the intrinsic impedance of the free space. However, biological tissue as we have seen in previous sections is lossy so that for an electromagnetic wave in the $\hat{z}$ direction

$$S_{av} = \hat{z}\frac{\left|\overline{E}_{z=0}\right|^2}{2|\eta|}\cos\theta_\eta e^{-2k''z}$$
Eqn. 3-6

Where k'' is the imaginary part of complex wave number which determines the attenuation in the medium and η is the intrinsic impedance of the medium.

When a wave is propagated through a lossy medium, it will be attenuated according to the electrical properties of the medium, and the ratio of the average power density at $z = z'$, $S_{av(z')}$ to the average power density at $z = 0$, $S_{av(0)}$ is given by [41]

$$\frac{S_{av(z')}}{S_{av(0)}} = e^{-\alpha_d z'}$$

Eqn. 3-7

Where z' is the thickness of the medium through which wave is propagating and α_d is the dielectric attenuation constant, which depends on the chosen frequency and permittivity of the medium. This is given by

$$\alpha_d = \frac{\pi}{\lambda} \sqrt{\varepsilon_R} \tan \delta$$

Eqn. 3-8

Here $\tan \delta$ is the loss tangent of the material and is given by

$$\tan \delta = \left(\frac{\sigma}{\omega \varepsilon_R \varepsilon_o} \right)$$

Eqn.3-9

So for example if a wave of power density of 1 watt/m^2 is passed through a cube of blood with relative permittivity of 61.36 and skin with relative permittivity of 41.4 having dimensions of 1m^3, then due to attenuation the signal power at the other side will roughly be -160 dB and -110db down respectively for the frequency of 900 MHz.

So it can be concluded from the above discussion that in body area networks, where both antennas are placed on the surface of human body, and since losses inside the human body are so substantial that most of the communication takes place around and along the surface of human body.

So up till now we have looked at the propagation in the tissue, now we look at propagation on the tissue.

3.2.3 Propagation on the Body- A Mechanism Illustrated Using a Lossy Cylinder.

Having considered the way an electromagnetic wave is both absorbed and slowed by tissue the way the wave behaves in and close to the body will now be discussed. To understand the propagation trends in a body area network, a comprehensive amount of work was done by G. Roqueta, et al. [42] by taking a lossy cylinder representing a human torso. This cylinder had a radius of 15cm which is reasonable for the dimensions of a torso. The material properties of the lossy cylinder were set according to the high water content tissue as given in Table 3.1. An antenna was modeled by line charge source of arbitrary polarity 1cm away and parallel with the cylinder. The purpose of this work was to find the phenomenon of diffraction around the curved lossy medium, reflection from the surface and penetration into the human body. The geometry in Figure 3.3 gives an idea of the measurement setup.
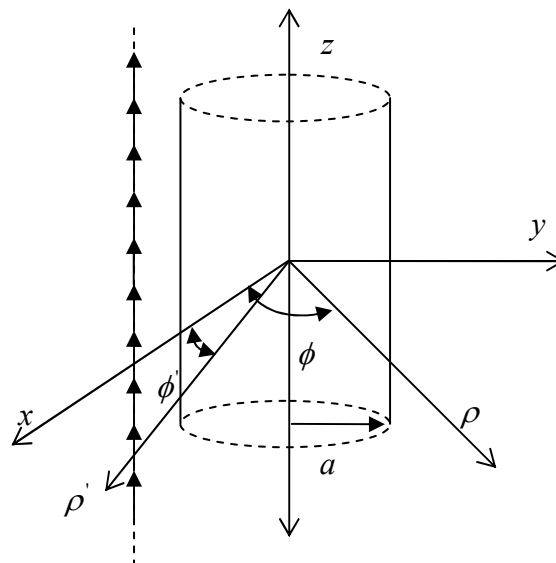
Figure 3-3: Geometry and co-ordinates system for the measurement

The magnitude of electric field strength was calculated as a function of observation distance from the source outside the lossy cylinder shown in figure 3.4. The properties of the cylinder were set according to high water content tissues given in table 3.1.

They identified three zones. Propagation away from the cylinder (Free Space), propagation through the cylinder and propagation behind the cylinder. The interfaces and field values are shown Figure 3-4.

Electric field away from the cylinder follows the trend of free space propagation; A free space path model will have the form:

$$PL_{free\,space} = \left(\frac{\lambda}{4\pi d}\right)^2$$

Eqn. 3-10

Where λ is wavelength of signal and d is the distance from the transmitter. Here the rate of decay is controlled by a path loss exponent of 2 and is independent of frequency. The paper [43] shows us how the field decays away from the human torso simulating cylinder. Inside the cylinder the electric field decays exponentially [43] and this variation in path loss was found to be frequency dependent. This trend is shown between the dash lines representing the lossy cylinder. Here an important concept of skin depth (a property of a medium which accounts for the attenuation) can also be explained. As skin depth of the medium is proportional to wavelength [43], so attenuation inside the cylinder would be more for 2.45GHz than 400MHz.
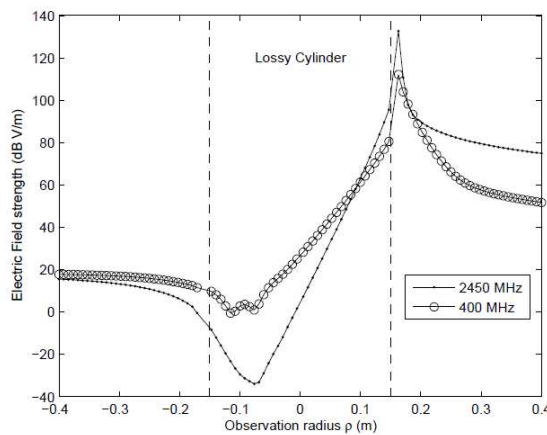
Figure 3-4: Electric field as a function of observation radius for a point source just outside a lossy cylinder, the lossy cylinder is shown with dashed lines [42].

The propagation trend behind the cylinder and away the dashed line in the figure 3.4 was again in free space, so path loss will follow the same law given in equation 3.10. The field values on this side of cylinder are shadowed by the lossy cylinder and consequently are lower.

A tangential decay in the field can also be found on the left side of the cylinder, showing a more rapid decay in field on the left edge of the figure than the field next to the cylinder. According to the authors of [42] this fact was associated with the conducting nature of the cylinder. If the cylinder was a perfect conductor then according to Maxwell's equation the field would have vanished on the surface of the perfect conductor.

The propagation trend along the surface of the cylinder was explained by the authors of [42] by representing electric field strength along and around the lossy cylinder compared with free space propagation shown Figure 3.5.
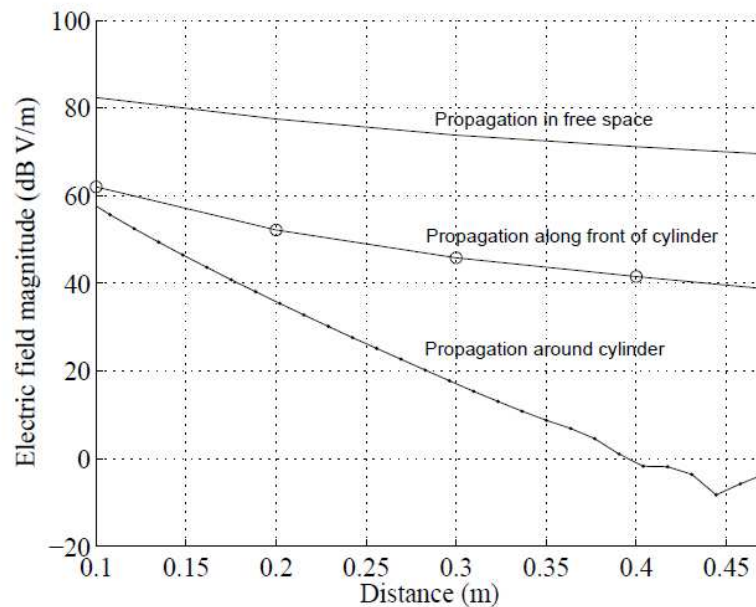
Figure 3-5: Electric field as a function of distance through free-space, along the length of the cylinder, and around the cylinder for a frequency of 2.45 GHz [42].

The top curve in Figure 3.5 shows the electric field versus distance for a point source in free space, the middle curve shows the electric field versus distance along the front surface of a lossy cylinder and the bottom curve shows the electric field versus distance around the surface of the cylinder.

As expected, the curves showing propagation along and around the cylinder are shifted down when compared to the curve of free space propagation. This is due to losses in the field near the lossy cylinder and is shown in figure 3.5. Also propagation around the cylinder was found lossier than the propagation along the front of the body due to line of sight situations for propagation along the front of the body. In relation to propagation around the cylinder the results seemingly show an inconsistency at maximal distance (0.45m) around the lossy cylinder. It is reasonable to assume that this is an artfact   of distance on the surface versus distance to the antenna which at some point benefits from a shorter tangent.

According the authors of [42] the middle curve decayed faster than the free space with the pathloss exponent of about 3-3.5 depending on frequency and radii. The third curve which was showing the propagation trend around the cylinder was also found to be exponentially decaying on log-linear scale as $(|E|^2 \propto \exp(-\alpha d))$. According to the authors, exponential decay can be interpreted as creeping waves around the curved surfaces. For creeping wave propagation, the rapid attenuation around the body was related to the continuous shedding of energy tangent to the cylinder as a wave rotates around the surface into the shadowed region[44]. Thus, energy radiated away from the body during the diffraction process, resulted in a faster pathloss versus distance trend close to the surface of the body.

From the above discussion we can conclude some important facts like, the electric field (E) is inversely proportional to the distance away from the body in free space however, the field has a much more rapid exponential decay into and around the body.

The exponential decay into the body is expected in a lossy medium while the exponential decay around the body is typical of creeping wave propagation around conducting surfaces. Along the front of the body, the field decay rate α is lower than the decay rate for propagation around the body. The decay rate, α depend on several factors including the tissue properties, frequency, polarity, and proximity to the body [45].

Similarly pathloss trends will vary considerably depending on the body area propagation scenario we consider. Thus, we will not be able to define a single pathloss law that will be appropriate for all body area communication scenarios and applications. In general, on-body and in-body propagation scenarios can have surprisingly high pathloss despite the close proximity of the two antennas. In fact, in some situations it may be easier to communicate to a remote device located off the body and across a room than it is to communicate to a device just 10+ centimeters away but worn directly against the body [46].

3.3 Interaction of Electromagnetic waves with Biological Matter:

It is clear that antenna away from and close to the human body may behave in very different ways. Therefore an understanding of how the energy output from an antenna couples with the body is important to facilitate reliable on-body antenna measurement techniques. In the section that follows these interactions are discussed.

3.3.1 Interaction of Electromagnetic field with Human Body at Mobile Communication Frequencies:

In this thesis the range of frequencies over which mobile communications is popular has been assumed to be 1GHz to 6GHz. It turns out that the human body is more sensitive to higher frequencies. Therefore in general it can be stated that as a proportion, more radio frequency radiation will be turned into heat inside the body at 6GHz than at 1GHz [47, 48]. The heating effect is directly related with the amount of

power absorbed by the human body. The authors of [34] provide a method of predicting the amount of power being absorbed by tissue. According to them when a human body is exposed to radio frequency radiation it acts as non-perfectly conduction wire antenna. The antenna fields and currents are solved for using Pocklington's integral equation and the electrical properties of the body. Pocklington's integral is a popular electric field integral equation (EFIE), for thin wires and was solved using boundary element method (BEM) based procedure.

The induced current density, the electric field, the total power absorbed, and the average specific absorption rate (SAR) for the whole body can be calculated from the electric field. The authors of [49]were able to evaluate a tissue related impedance per unit length Z_L and thus calculate current density $J_z(\rho, z)$, SAR and power.

3.3.2   Effects of the Human Body on the properties of Wearable Antennas:

Unlike the usual communication through constant air, the various tissues and organs of the body have their own unique conductivity, dielectric constant and characteristic impedance, so the signal level and propagation through a human body is not a simple thing to predict. In the case of in-body communication losses arise from attenuation due to conductive tissues. According to [50] such losses are typically of the order of 20dB. On related point an important factor put forward by the authors of [51], that attenuation in the electric field never coincides with the attenuation in magnetic field at particular frequency, so both fields should be measured simultaneously. By doing so, the risk of underestimating the field exposure for almost all directions of incidence and polarisation can be eliminated.

According to [52] the effect of human body on the input impedance of an antenna is equivalent to adding a series inductance L and a shunt conductance G to antenna. This means there will be a reduction of input impedance due to the human body. The resonance frequency of the antenna will also tend to decrease. The average reduction

in gain because of the human body was found to be more than 10 dB.

Several research works have been published at the human body effects on wearable antennas or antennas near a human body. Many useful results have come out of these publications. For example authors of [3] concluded that human body effects on antennas depend on age, sex, personal characteristics and environmental conditions. These results can be useful for the analysis of the electromagnetic waves in space and for the investigation of the surface of the human body.

In [4] electromagnetic energy absorption in the homogeneous and layered human body models due to body-worn UWB antennas, at frequencies of 3, 6 and 8 GHz was presented. Typical small planar UWB antennas were used in that study. Distances of 2, 5 and 10mm between antennas and human body were chosen, approximating realistic scenarios of operation in Wireless Body Area Networks. To approximate different parts of the human body, the authors of [4] compared results obtained for the planar homogeneous (muscle) model with those for three-layer body models (skin, fat and muscle tissues). For these body models they investigated the electromagnetic energy absorption mechanism by examining the peak 1g SAR and peak SAR. According to them results disclosed the increased peak SAR in all layered models, compared to the homogeneous body model.

In [5] the coupling effects of human body on radiation characteristics of superquadric loop antennas for pagers' application were discussed. The authors examined the 3-D and 2-D Patterns of antenna in free space and in front pocket of human. The imaginary part of input impedance remained same but the real part reduced due to human body and according to them 53.2% of the power was absorbed by the human chest tissue.

Effects of human head on small planar antenna were observed in [9], according to the authors of this publication, impedance matching was slightly affected but there was a

significant change in gain and radiation pattern of the antenna. Gain reduced for lower frequencies and increased for higher frequencies due to reflections from the human head while the radiation pattern becomes more directive due to blockage, reflection and absorption effects of human head.

In [10] the effects of human body on impedance bandwidth were observed and it was found that impedance bandwidth is almost double due to the presence of lossy material near the antennas.

3.4   Conclusions:

The purpose of this chapter was to give a detailed view of electromagnetic waves propagation trends in, away, along and around the human body in Body Area Networks (BAN) because without a description of the channel degradation, it is impossible to identify optimal RF solutions. At the end an interaction of human body with wearable antenna was explained with the possible effects of human body on antenna parameters.

Chapter 4:
Literature Review of Experimental Techniques for On-Body Measurements

4.1 Introduction:

As has been discussed in the previous two chapters an ongoing trend in communications is the incorporation of technology both onto and into the human body. However, humans are not an ideal medium for radio wave frequency propagation. Human tissue is a partially conductive medium that consists of approximately thirty different tissues types each of which has its own different electrical properties. The dispersive and lossy nature of humans means that resonance and absorption can quickly lead to far field pattern distortion [53, 54].

These factors and the absence of a convenient on-body power supply combined with the relatively high power requirements of mobile communications devices make on-body systems an interesting area of research. So many researchers all over the world have tried to characterise the on-body channels using their own ways of experimental techniques. Many of those experimental techniques have been summarised in the section 4.2 which is followed by a section about how propagation models are developed by different scholars, section 4.3.

4.2 A Review of On-Body Measurements: Procedure and Setups

This section contains a short review of the techniques and parameters that have been used by and are of interest to other researchers in the field of on body measurements. On–body channel characteristics were outlined by the authors of [55, 56] by examining the electromagnetic wave propagation around the torso of human body. Their experimental setup included a human volunteer wearing two antennas on

different positions on it, front, sides and back of the volunteer torso. These two antennas were connected to a vector network analyser via properly calibrated cables. The transmission coefficient (S_{21} dB) was measured for the frequency range of 3-6GHz. A large empty room was selected for the measurements. The researchers reasoned that any wave propagating upon the surface of a body would dominate reflections arriving via multipath if the room was large in terms of wavelengths. According to the authors of [55, 56] the multi-path components of the surface wave upon the body reached the receiver in 0.5-2 ns and the reflections from the ground and the walls were found to be later, which were easily separated from the diffracting multi-path components. The same small, low profile Skycross [57] UWB antennas were used for all measurements. The antennas were 16 by 13.6 by 3 mm in size and weigh only 0.3grams. One significant influence on path-loss was found to be the distance of the antennas from the surface of the body's skin. It can be rationalised by an antenna that is insulated by distance from the body working in a more efficient way. Therefore a 5mm thick dielectric wafer made of plastic was placed between the antenna and the skin and was held against the body through an elastic band. The experimental setup used in this paper [55, 56] has been reproduced in figure 4.1.
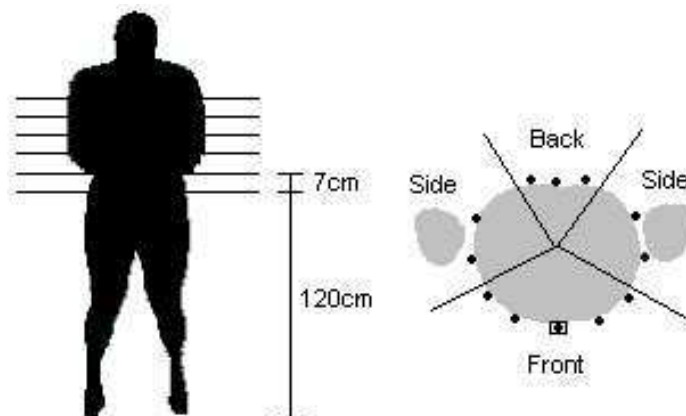
Figure 4-1: Measurement Locations on the Body (around the torso) [55, 56]

The channel parameters were calculated in six horizontal planes separated by 7cm along the vertical axis of torso. The receiver positions are shown as small circles and

the transmitter is shown as a box on the torso in figure 4.1. The transmitter was always placed on the front of the body, and the receiver was placed at various positions on the torso at distances of 10 cm, 15 cm, 20 cm, 25 cm, 40 cm, and 45 cm measured around the perimeter of the body. The authors of this research considered that 144 measurements were enough to define the channel. The path loss of waves diffracting around the body was found to be much higher than waves travelling along the front of the body. The reference path loss near the antenna depended on the separation between the antenna and the body due to antenna mismatch. Arm movements gave a pronounced effect on the path loss when the arm was in between the antennas and was disturbing the line of sight.

According to authors of [58] MicaZ boards [59], which operate at the 2.4 GHz ISM frequency band and adopt the IEEE 802.15.4 communication protocol, were used to measure the path loss between two receivers and a transmitter. These MicaZ modules were placed at a distance of 1cm from the body surface of a volunteer. The transmitter position was kept constant and the two receivers which were 2cm apart from one another were moved along two different paths. The first path was along a straight arm and the second path was along the waist. The amplitude of received power was recorded for each position of receiver and plotted against distance. The simulated model was a two layer cylinder having 10mm thick fat surface over 60mm diameter of muscle. The electrical properties of the simulated muscle were ε_r= 10.84, σ= 0.26 S/m for the fat layer, and ε_r= 53.64 and σ= 1.77 S/m for the muscle tissue. The experimental setup showing the radios, the arm of a volunteer and the model is shown in figure 4.2.
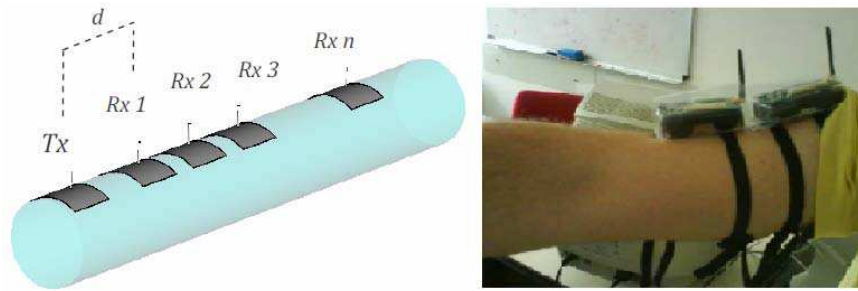
Figure 4-2: The cylindrical model used to study the path loss between two antennas located at different distances along a human arm (left) and the photo of the practical experiment during data acquisition (right) [58]**.**

P. S. Hall and his co-authors have written several papers containing experiments to characterise the on-body channel [60-67]. They have used a similar procedure to that of [61], A portable vector analyser was connected to antennas through flexible and calibrated co-axial cables. The path loss measurements were performed both inside and outside of an anechoic chamber and S_{21}(dB) response was measured in each of these experiments for volunteers who changed their postures every 20 sec whilst wearing a pair of antennas. The different body postures were standing, turning left, turning right, body bending forward, standing head bending forward, standing head turn left, standing head turning right, arms held sideways, arms above head, arm forward, forearm forward, standing and moving, sitting etc. All these postures were maintained for 20 sec and whole period of the experiment was 360 sec. The transmitting antenna was placed at a fixed position on belt at the front while the receiving antennas were placed at different positions on head, chest, arms, back, knees and legs. All of these positions are shown in figure 4.3.
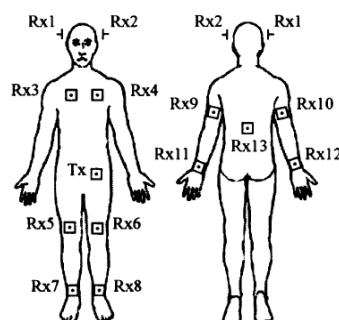
Figure 4-3: Antenna locations on human body for the paper referenced as [64]

Different types of antennas were used in these experiments. In[60-62] patch antennas were used, in [63-65] monopole antennas, [66]used a monopole on a circular ground plane and a loop antenna. In [67] both monopole and patch antennas were used for the comparison purposes.

A comprehensive study of on-body channel characterisation at 400 MHz, 600 MHz, 900 MHz, 2.4 GHz and at UWB frequency band was done by the authors of [68]. The measurements were taken inside an anechoic chamber and in a room of a hospital. The measurement positions and layout of the hospital room are shown in figure 4.4 and figure 4.5.
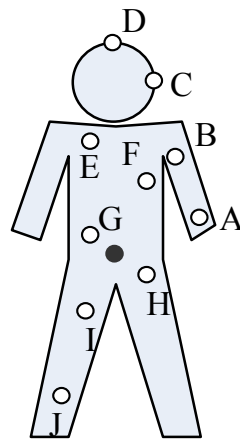
Figure 4-4: Measurement positions on the human body [68]
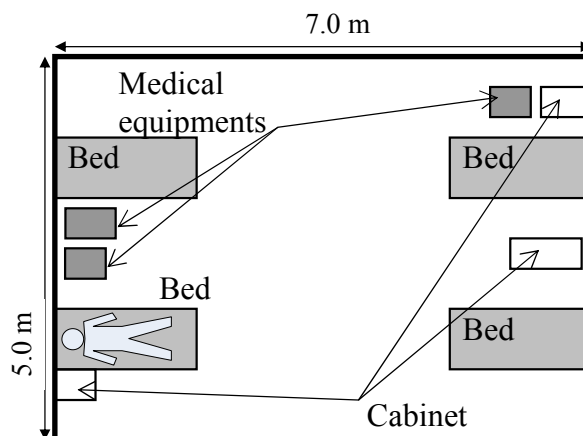
Figure 4-5: Layout of the measurement room (a hospital room) [68]
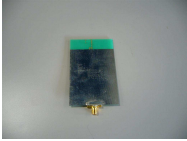
Photographs were taken during the measurements as shown in figure 4.6.

Figure 4-6: Photographs taken during the Measurements

The frequency band and the layout of the antennas used are shown in table 4.1.

Table 4-1: Frequency band and types of Antennas used

Frequency band	Frequency range	Antenna
900 MHz	950 - 956 MHz	Chip antenna
2400 MHz	2400 - 2500 MHz	Chip antenna

Chip antennas were used for 400, 600, 900MHz and 2.4GHz and for UWB measurements a Skycross antenna was used. Different antenna positions and frequency bands were chosen so as to cover most wearable applications. The separation of the antennas from the body surface is summarised in Table 4.2, given below.

Table 4-2: Distances between the two body-worn antennas in both measurement sites

Position Index	Position	900 MHz	2.4 GHz
		Distance (mm)	
A-1	Left hand	424	428
A-2	Left hand	400	422
B	Left upper arm	354	372
C	Left ear	588	578
D	Head	746	740
E	Shoulder	384	384
F	Chest	242	224
G	Right rib	146	148
H	Left waist	186	176
I	Thigh	404	404
J	Ankle	982	972

(b) Hospital room

Position Index	Position	900 MHz	2.4 GHz
		Distance (mm)	
A-1	Left hand	410	408
A-2	Left hand	388	386
B	Left upper arm	424	414
C	Left ear	578	562
D	Head	742	734
E	Shoulder	400	392
F	Chest	266	248
G	Right rib	174	170
H	Left waist	164	174
I	Thigh	388	402
J	Ankle	980	998

The difference in the distance for the same location was due to the different sizes of antennas at different frequencies and a 15mm distance between body and antennas was always maintained in all cases. The height and weight of the volunteer participating in this experiment were 173 cm and 64 kg, respectively. S_{21}(dB) was measured 10 times at each position and each frequency band.

M. I. Khattak et al. [32] has also done some work related to the on-body channel but in the case the work was concerned with the effects of wet clothing on the propagation channel and the techniques used. A portable network analyser was connected to quarter-wave on-body monopoles through calibrated flexible co-axial cables. Four body postures were used. S_{21}(dB)measurements were recorded inside the anechoic chamber and outside in the open area. The antenna layout, position and postures positions are shown in the figures 4.7, 4.8 and 4.9.
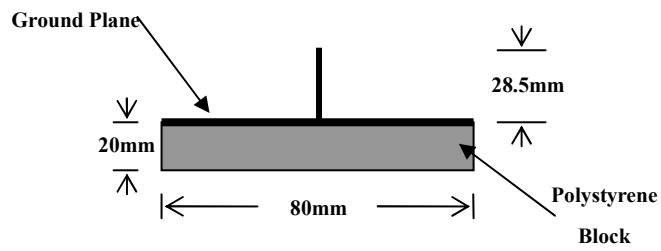
Figure 4-7: Antenna Layout
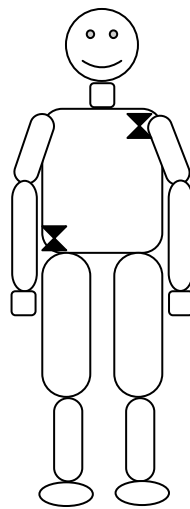
Figure 4-8: The Placement of Antennas in Chest to Waist link
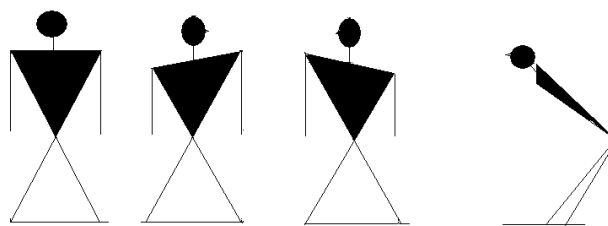
Figure 4-9: Different Body Postures during the experiment (a) Standing, (b) Turning Left, (c) Turning Right and (d) Bending.

After assessing the risks of using fluids inside the anechoic chamber, it was decided that experiment to be performed outside in an open area. To minimize reflections a large open field was chosen which is shown in the figure 4.10. The nearest source of

interference was more than 100m away from the point of measurement, for which the free space pathloss was nearly -150dB, which is less than the noise floor for 802.11b (-85dBm). So it was reasonably assumed that interference from the nearest source is too low to effect the measurements.
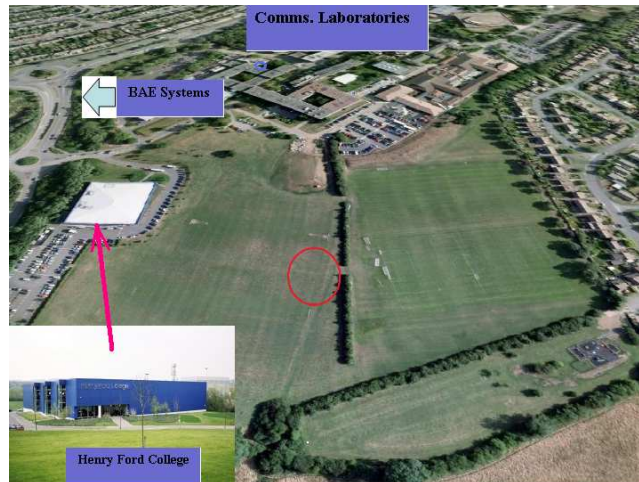
Figure 4-10: Open area chosen for performing the on-body measurements for wet and dry clothing of human male at frequency of 2.5GHz.

4.3 A survey of On-body Propagation Models:

This section provides a short review of theoretical models used to predict the properties of a radio wave travelling on the surface of the body. This may be considered useful since the scattered wave may be blocked and any propagation through the tissue of the body will be severely attenuated, thus the surface wave may be the most reliable form of propagation. Although as has been discussed in chapter 2 work regarding the human body's influence on antenna parameters began in the late 90s, major contributions regarding on-body propagations began to appear in 2002-2003, [69, 70]. In Europe key research on the on-body channel has been provided by ETH Zurich [71], IMEC (NL), ULB (Brussels) and UCL (Louvain) [45, 72-75]. More specifically in the UK contributions home come from the University of Birmingham [76], Queen Mary University of London [61, 64], and Queen's University of Belfast [77][78].

The different electrical properties of tissues of the human body make it difficult to derive a simple path loss model for Body-Area-Network (BAN). Since the antennas in BANs lie close to the body, a BAN channel model has to take into account the influence of the human body.

Previously nodes in on-body communication systems have been divided into three groups, namely: Implant Node: Nodes placed inside the human body under the skin; On-body Node: Nodes placed on the surface of the human body; External Node: Nodes which are not in direct contact with the human body surface.

When the transmitter and receiver nodes are not in line of sight with one another then the distance between them will be the distance around the body and creeping wave diffraction will need to be taken account of in any model. Body movement can be quite dynamic. Typical postures are sitting and standing, bending and twisting. However all of these postures may change slowly as in a social environment or quickly as in a sporting environment [64]. Most changes in posture will change the distance between nodes as well as the propagation path. Thus the characterisation of radio wave propagation needs to not only to account for those movements but also the location of the nodes on the body surface. According to the Hall et. al. changes in the local geometry of the environment will also affect the antenna parameters such as input match and radiation pattern, so the design of wearable transceivers should consider changes in the antenna and propagation loss to enable maximum channel capacity and minimum power consumption. This comment is important for it implies that the same type of antenna will behave differently according to its position on the body. Further it can be inferred that different antennas may suit different parts of the body.

The on-body propagation channel around the human body is a combination of free space propagation, diffraction (creeping wave) and reflections from the environment. As radio wave propagation in free space is characterised by Frii's formula, which is

$$P_r = \frac{P_t G_r G_t \lambda^2}{16\pi^2 d^2}$$

Eqn. 4-1

Where G_r and G_t are gain of receiving and transmitting antennas, d is the separation between them and λ is wavelength in meters. In some case equation (4-1) also includes a system loss factor which does not depend on the propagation. It is clear from equation (4-1) that this path loss model does not hold for $d = 0$.

According to the authors of [45, 55, 79-81] the path loss model in dB between transmitting and receiving antenna is given by

$$PL(d) = PL_0 + 10n\log_{10}(\frac{d}{d_0})$$

Eqn. 4-2

Where d_0 is the reference distance which is taken as 1m for on-body measurements by most of the researchers, PL_0 is the path loss at some reference distance and n is the path loss exponent. Now depending upon the environment, antenna positions on the body, antenna type and frequency, different authors have given different values for path loss exponents. Fort et al. found path loss exponents of 7.5 and 3.1 for different scenarios (around and front of torso that is NLOS and LOS respectively) while authors of [80] gave a value of 4.4 for horizontal, vertical and diagonal propagation on the body. Similarly A. Alomainy et al. has found $n = 3.9$ and 2.6 for Horn Shaped self-complementary antenna (HSCA) and Planar inverted cone antenna (PICA) respectively.

The power received by the receiving antenna will be different from equation (4-2) due to the changes in the environment around the human body and also due to the body movement, shadowing, which reflects the path loss variation around the mean. Path loss will then be equal to

$$PL = PL(d) + S \qquad \text{Eqn. 4-3}$$

Where S is the shadowing component. The shadowing here means the obstruction of the line if sight by the human body parts, antenna alignment, pattern distortion and impedance mismatch which are related to installation of antennas.

Path Loss models for the mobile communication frequencies of 900MHz and ISM band 2.4GHz were presented by the authors of [68, 82, 83]. According to the authors of [68]whose measurements were done inside an anechoic chamber and a hospital room can be fitted to an on-body propagation model given by

$$PL(d)_{dB} = a.\log_{10}(d) + b + c + N \qquad \text{Eqn. 4-4}$$

Where a and b are the coefficients of linear fitting (which were different for both environments and were frequency dependent), d was the distance between transmitter and receiver, N was a normally distributed variable with a standard deviation of σ_N. Also in their equation c was difference in the signal level for the different types of antennas that were used. In this case a dipole and a chip antenna were measured.   As a result of the On-body measurements done by the authors of [82]it was concluded that concluded that the path loss model around the human body follows an exponential decay that can be modeled by and proposed following relation.

$$PL(d)_{dB} = -10\log_{10}(P_0 e^{-m_0 d} + P_1) + \sigma_p n_p \qquad \text{Eqn. 4-5}$$

where m_0 is the average decay rate in dB/cm for the surface wave travelling around the perimeter of the body. This rate was found to be approximately 2.1 dB/cm. P_1 is the average attenuation of the scattered components in an indoor environment radiated away from the body and reflected back towards the receiving antenna. σ_p is the log-normal variance in dB around the mean, representing the variations measured at different body and room locations. This parameter will depend on variations in the body curvature, tissue properties and antenna radiation properties at different body locations.

Many on-body measurements were performed by the authors of [83]. Their method involved locating the transmitting antenna on different locations on the human body and fixing the receiver antenna at chest and right hip. Three different postures were examined in this study; these were standing, walking and running. The main factors which caused variation in the path loss were found to be human body movements. The path loss was found to be:

$$PL_{dB} = P_{tx} - P_{rx} + G_{amplifiers} - L_{cable} \qquad \text{Eqn. 4-6}$$

Where P_{tx} was the transmitted power, P_{rx} was The RMS received power, $G_{amplifiers}$ was the amplifier gain and L_{cable} were cable losses. Note that unlike other papers that have been discussed so far this model has in it some of the systematic losses mentioned in Section 2.2. In general for scenarios in which the subject is moving it is not yet possible to calibrate out systematic errors due to cabling. Systematic errors due to cabling are discussed in Section 2.2.

Values for the different parameters used in equation (4-4), (4-5) and (4-6) were found to be different for different frequencies and can be found in the literature of [68, 82, 83].

Hall et al. [64] performed many on-body measurements for the modeling of path loss for different situations such as line of sight (LOS) and non-line of sight (NLOS) at 2.45GHz. A Path loss model for the LOS case using transmitter and receiver at the front of the body was found to be

$$PL(d)_{dB} = -5.33 - 20\log_{10} d_{cm} \qquad \text{Eqn. 4-7}$$

which the authors point out indicates a decay rate on the body nearly 5dB more than that for air.

Path loss model for NLOS case using a transmitter and receiver at front and back of the human body respectively for the approximation of exponential decay using a linear regression formula was

$$PL(d)_{dB} = -0.36d_{cm} - 35$$

This gave a decay of 0.36 dB/cm. Finally for this section according to Fort et al. [45] when the distance between the transceivers is less than 25cm, that is line of sight conditions, the distribution is Rician[84] but for non line of sight situation the distribution is mainly Rayleigh[84]. In this case the authors made their measurements at mobile communications frequency of 2.45GHz.

4.4 Conclusion:

The purpose of this chapter has been to review the work of several leading authors who made significant contributions to the area of on body antenna measurements. In particular techniques used to propose propagation models for the on-body surface wave have been discussed. Three points would seem to be common. Firstly on body channels are highly dynamic. This will be confirmed in the experiments written up in Chapter 6. Secondly, ground planes and insulation layers between antennas and supporting tissue are particularly important. Lastly, many on body measurements can be done in quiet areas outside of an anechoic chamber.

Chapter 5:

Evaluation of Loughborough University Anechoic Chamber for Wearable Antenna Measurements

5.1 Introduction:

In common with several UK Universities the communications group has the use of several anechoic chambers. This chapter contains the experimental procedure required to ensure confidence in results of measurements at typical mobile communications frequencies. Since they are not commercial facilities such chambers are not calibrated and are mainly bespoke in design. Therefore, in order to accurately carry out the measurements necessary for this research an appraisal of the reliability of chamber measurements at Loughborough was undertaken.

The rest of this chapter is structured as follows. In section 5.2 details of the wiring and dimensions of the anechoic chamber are given along with the details of a procedure for testing the range of frequencies for which the chamber can be relied upon to make accurate measurements within a tolerance. In section 5.3 the radio frequency absorber used in the chamber is discussed in relation to the orientation of the cones upon the floor of the chamber. Recollect that there are essentially three ways in which the chamber assists in the measurement of antennas. Firstly the room is made to be a closed metal box which prevents (severely attenuates), radio wave energy from sources outside of the chamber. The chamber is also lined on the inside with absorber that has two main properties. The absorber is foam impregnated with a carbon like substance and therefore absorbs radio frequency energy. The shape of the absorber

(pyramidal), also helps to break up any standing waves present inside the chamber. The effects of introducing a walkway made of polystyrene blocks are written up in section 5.4. Finally included in section 5.5 are details of a technique to consider the perturbations on an antenna close to a lossy body. This procedure is new to Loughborough and is likely to be used extensively at a future date for on-body antenna measurements.

5.2 Application of the Normalised Site Attenuation (NSA) method to the Loughborough EEE Anechoic Chamber.

In this research the range of frequencies from 900MHz to 2500MHz was of particular interest. A standard that covers this range was found to be ANSI C63.4-1992 [85]. Other standard can be seen in [86]. The wiring diagram of anechoic chamber in Loughborough University is shown in the diagram given below in the figure 5.1.
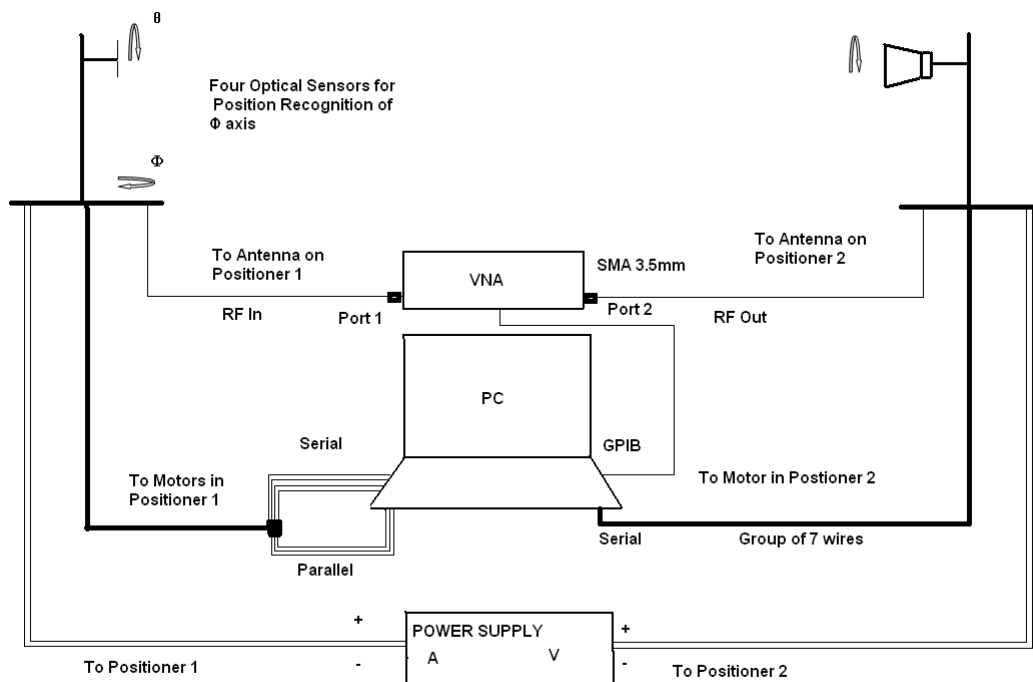
Figure 5-1: Wiring Diagram of Loughborough University Anechoic Chamber

5.2.1 Normalised Site Attenuation (NSA) Calculation of an Anechoic Chamber

The NSA (dB) parameter is a frequency response characteristic of a test site which has been derived by the authors of [87-92], using a similar procedure to that explained in the ANSI C63.4-1992 standard. The protocol involves taking measurements in the chamber under test (CUT), to produce an NSA(dB) figure of merit. The measured value of NSA(dB) was then compared with the theoretical (Ideal) model developed by Smith *et al.*[93] to determine a deviation from a benchmark test site. In the case of ANSI C63.4 the standard specifies a maximum allowable deviation of $\pm$4dB over the frequency range of 600-6000 MHz for our chamber.

The procedure followed here for the calculation of Normalised Site Attenuation (NSA) was taken from [85].

5.2.2 Experimental Setup:

The Loughborough University anechoic chamber has dimensions of 7 x 3 x 3 m^3. The two antenna positioners are so made that the distance between antennas becomes approximately 3.9m. Transmitting end positioner is fixed and can only rotate the antenna in elevation (θ) plane and is connected to port 1 of the vector network analyser (VNA), while the receiving end positioner can be rotated in both directions that's azimuth (ϕ) and elevation(θ) planes and is connected to port 2 of VNA. This setup is also explained in figure 5.1.

To perform this experiment we needed a positioner which should have the facility of moving the antenna up and down, so a temporary positioner was set having this facility. This new positioner had the ability to move the antenna up and down by approximately 1m. The VNA range is up to 6GHz and so was the expected range of anechoic chamber. The experimental setup illustrated above is shown in Figure 5.2. The simulation software helped in controlling the rotation of the positioners,

downloading the data from VNA to the computer and making appropriate graphs.

Measurement of V$_{site}$:

After connecting transmitting and receiving antennas to Vector Network Analyser (VNA), maximum signal strength was achieved by varying the height of receiving antenna.   This quantity which has the units of dB represents the maximum available signal at that frequency using the two reference antennas, is known in the standard as V$_{site}$.
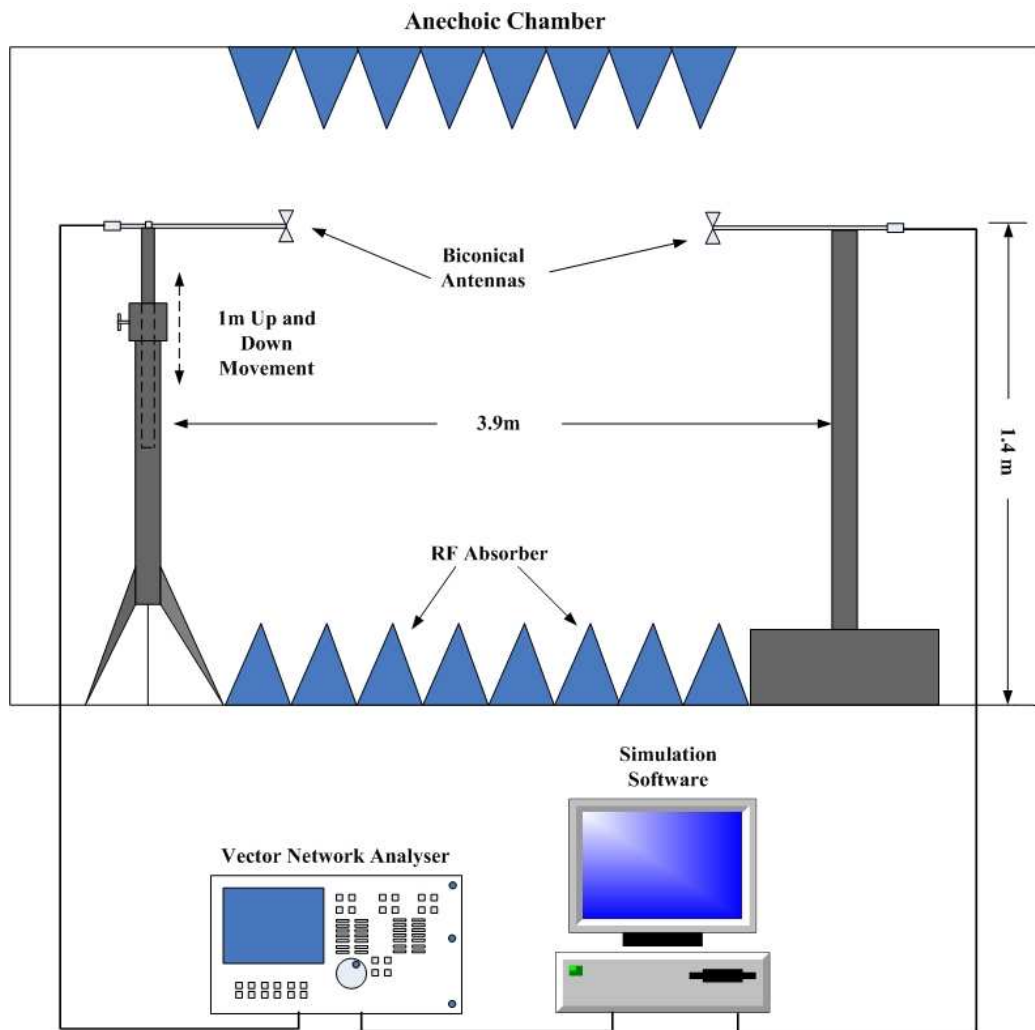
Figure 5-2: : Experimental Setup for Normalized Site Attenuation Measurement.

Measurement of V_{direct}:

The transmitting antenna and receiving antenna were disconnected and replaced with a through link shown in figure 5.3.The signal readout in this case was V_{direct}.

The values of Normalised Site Attenuation (NSA) was then calculated using formula given below.

$$NSA_{dB} = V_{direct} - V_{site} - AF_r - AF_t - \Delta AF_{Total} \qquad \textbf{Eqn. 5-1}$$

Where AF_r and AF_t are antenna factors of receiving and transmitting antennas respectively, which are given in the manual for the broadband biconical antenna and is given in the Appendix D. ΔAF_{Total} is mutual impedance correction factor, this factor accounts for nonlinearities of attenuation versus distance for resonant dipoles in close proximity but according to ANSI C63.4-1992 standard ΔAF_{Total} is equal to zero for broadband antennas.
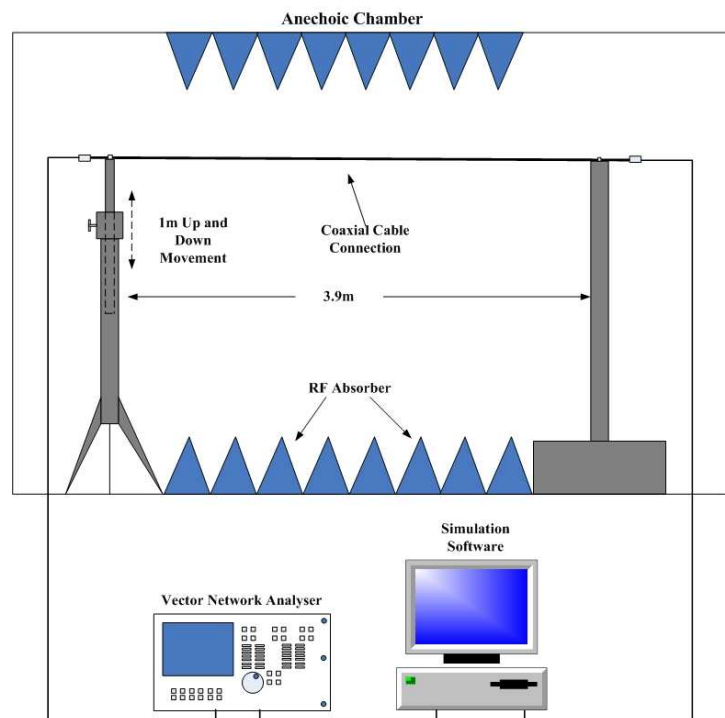
Figure 5-3: Direct coupling through coaxial cable.

Theoretical NSA:

Smith's equation [93] for theoretical NSA calculation is:

$$NSA_{Th} = 20\log\left(\frac{39.76d}{f_{MHz}}\right)$$ **Eqn. 5-2**

Where d is the distance between the two antennas and f is the frequency in MHz.

5.2.3   Calculations and Results:

Measurements were done for horizontal (HH) and vertical polarisation (VV) of biconical broadband antennas and are shown in the chart 5.4 and 5.5.
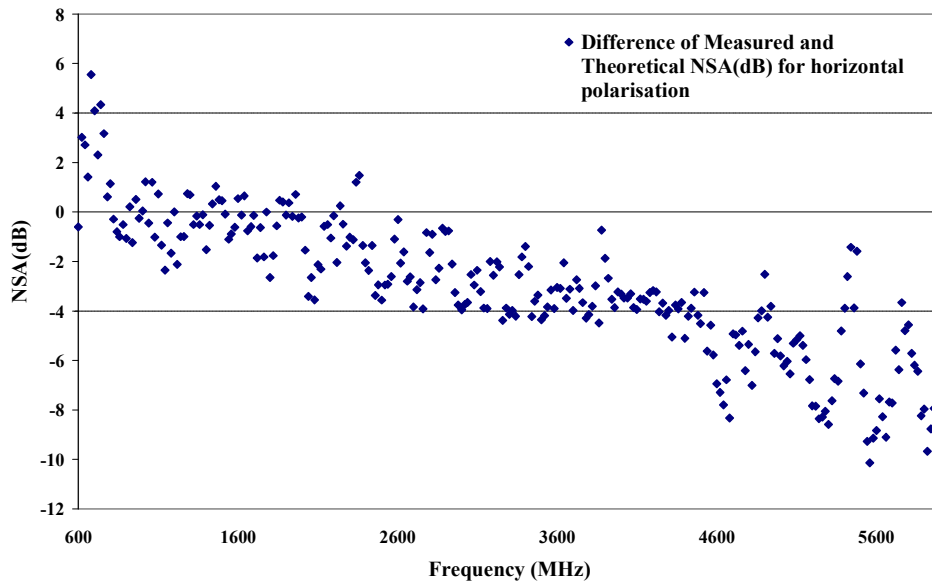
Figure 5-4: Normalised Site Attenuation measurements for horizontal polarisation of biconical antennas
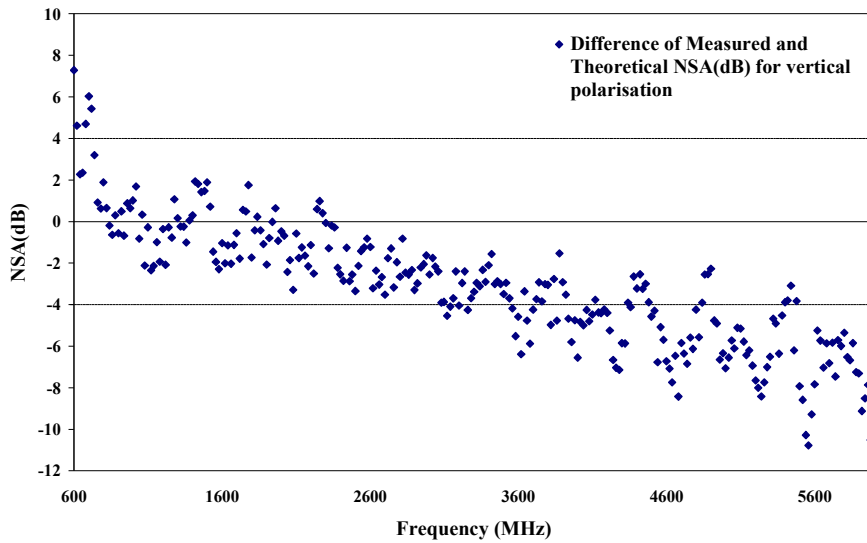
Figure 5-5: Normalised Site Attenuation measurements for vertical polarisation of biconical antennas

5.2.4 Conclusions:

The purpose of this experiment was to measure and benchmark the performance of the anechoic chamber that was used in our experiments. Broadband biconical antennas (1-6GHz) [94] were used in these measurements. The charts 5-4 and 5-5 give some important results about the chamber and first obvious one is that horizontal polarisation of antennas gives more appropriate results than vertical polarisation of antennas. Looking at charts 5-4 and 5-5, the frequency range in which difference between measured and theoretical NSA(dB) remained in between ±4dB was nearly 0.6-4.5GHz for horizontal polarisation, while for vertical polarisation the range we found was nearly 0.6-3.6GHz.

For the three mobile frequencies of 0.9, 1.8 and 2.4GHz, where most of the measurements were done, the anechoic chamber was found to be within the limits suggested by ANSI C63.4-1992.

5.3 The Effects of alignment of pyramidal RF Absorbers in the Anechoic Chamber at Mobile Communication Frequencies

5.3.1 Aim:

The purpose of anechoic chambers is to provide a low noise free space environment for antenna measurements. Chambers are screened by metal to prevent energy from outside being significant. Energy from the source impacting upon the radio frequency absorber is severely attenuated so little can be reflected. This means that the receive antenna sees only the direct wave. In addition to this the shape of the absorber is designed to break up any standing waves that form in the chamber. Since this property of the absorber depends on the electrical size and shape of the blocks they must also have a better or worse effect due to polarisation. Polarisation of the absorbers was therefore also investigated.

The material used in absorbers and its effectiveness over frequency range is explained in appendix B.

5.3.2 Procedure:

The two positions for the absorber are shown in figure 5.6. S_{21}(dB) was measured by connecting horns [95]to both receiver and transmitter.
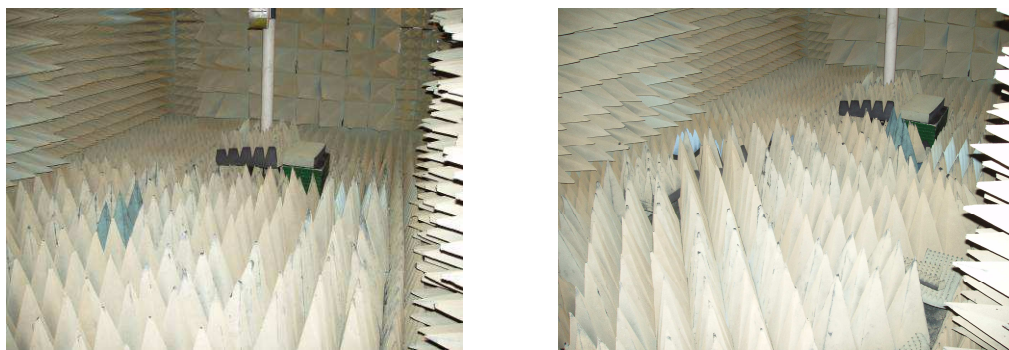
Figure 5-6: (a) Normal and (b) Crossed position of RF absorbers inside the anechoic chamber

5.3.3 Results:

Two measurements were performed for horizontal and vertical polarisation of horn antennas and their difference are shown in the figure 5.7 given below.
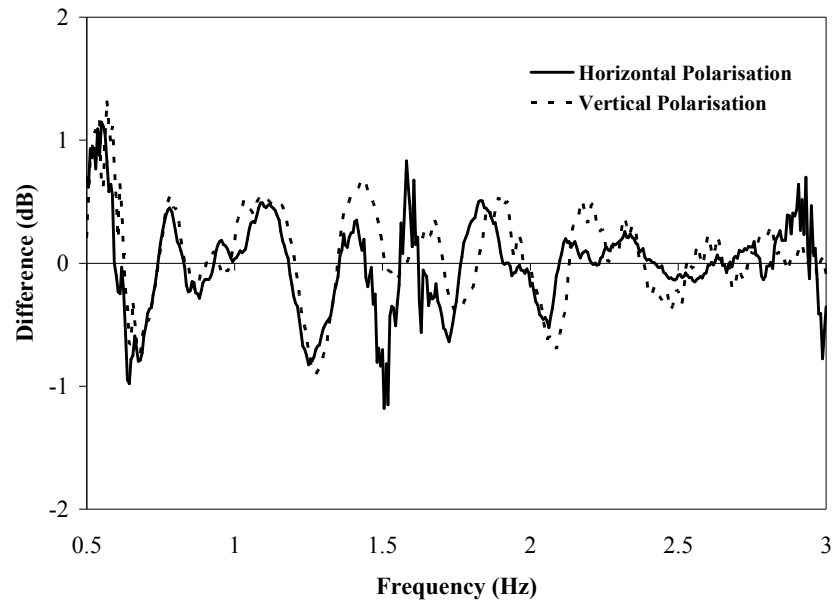
Figure 5-7: Difference of the S_{21}(dB) measurements for both positions of RF absorbers.

5.3.4 Conclusions:

Therefore looking at these results it was subsequently assumed that across the range of frequencies of interest the orientation of the absorber had no significant effect.

5.4 Effects of Introducing a Polystyrene Walkway into an Anechoic Chamber.

5.4.1 Aim:

In the group's anechoic chamber the distance between the source and the receiver is typically approximately 3.9 meters plus or minus an adjustment range of 22cm. Access to the far end of the chamber was found to be required with much greater

frequency during wearable antenna experiments than had previously been the case. Typically the absorber on the floor of the chamber would be removed and then replaced after any adjustments had been to the antenna on the far end positioner. Therefore this section looks at the effect of replacing a section of the absorber and replacing it with a polystyrene walkway. The walkway which neither absorbs energy nor negates the standing waves was to make up approximately 20 percent of the floor area and approximately 10 percent of the whole area of absorber surface in the chamber.

5.4.2 Procedure:

Far-field radiation patterns were obtained with and without the walkway inside the chamber.
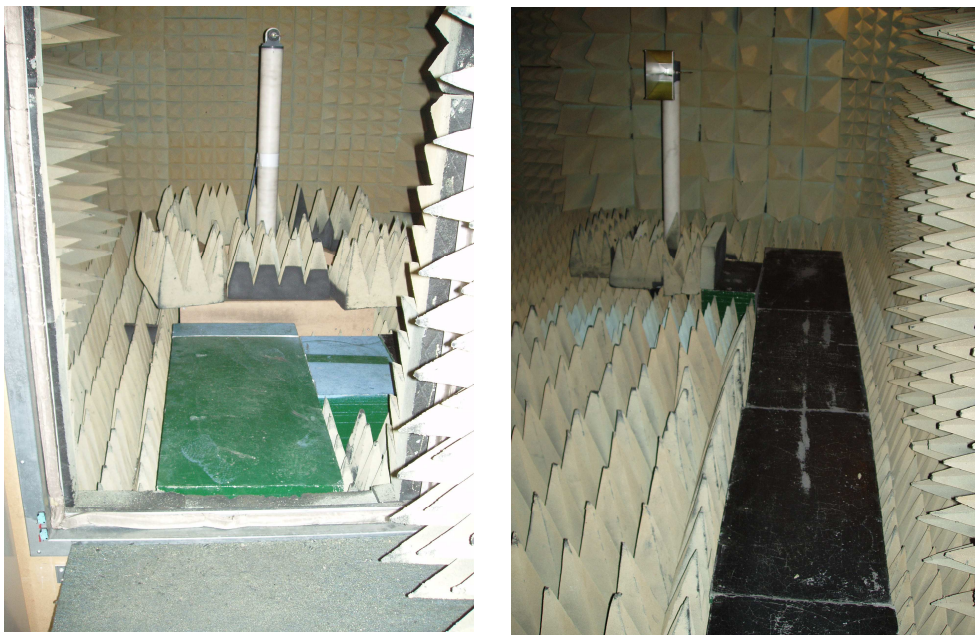
Figure 5-8: Introduction of walkway inside the anechoic chamber.

5.4.3 Results:
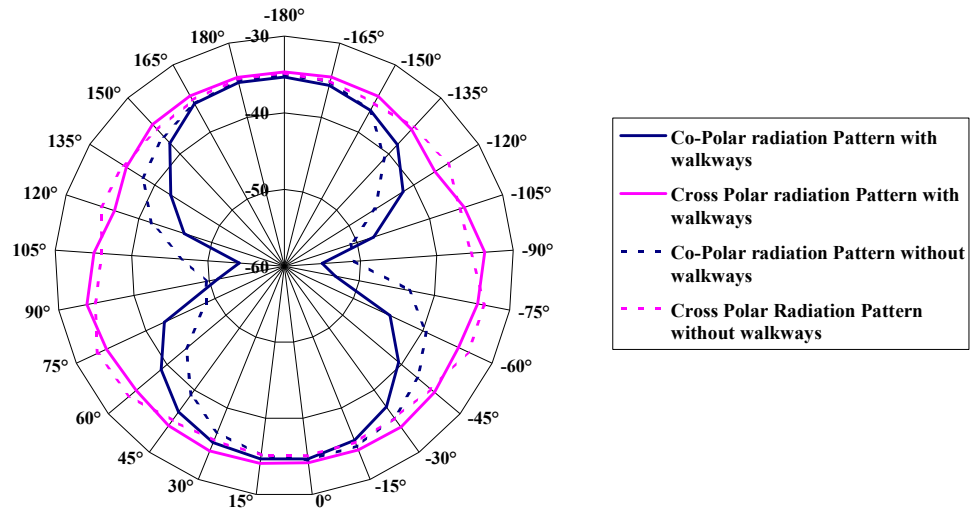
Figure 5-9: Radiation Pattern of a Dipole at 900 MHz with and without Walkways inside the
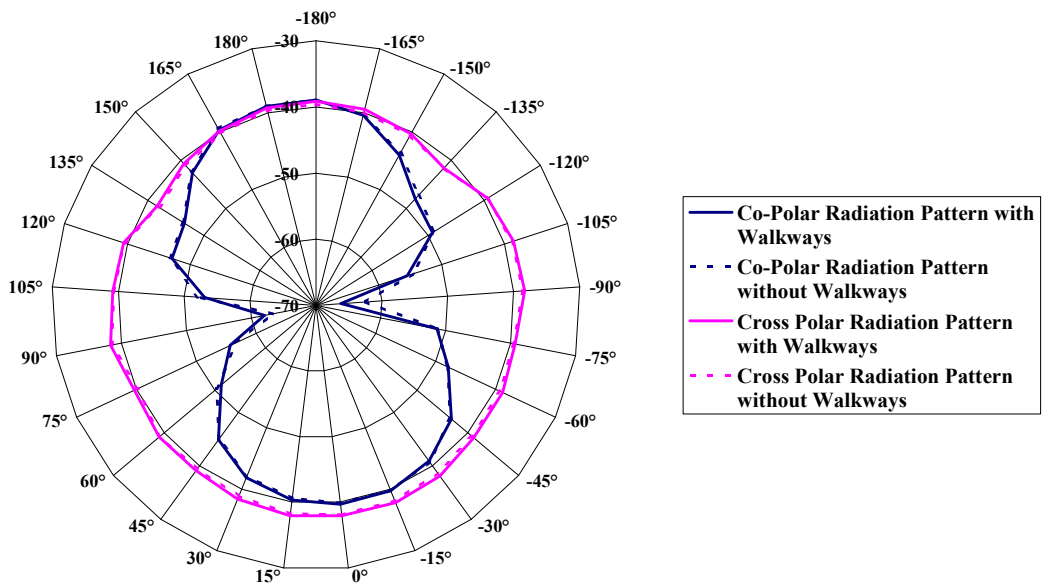
Anechoic Chamber

Figure 5-10: Radiation Pattern of a Dipole at 1.8GHz with and without Walkways inside the
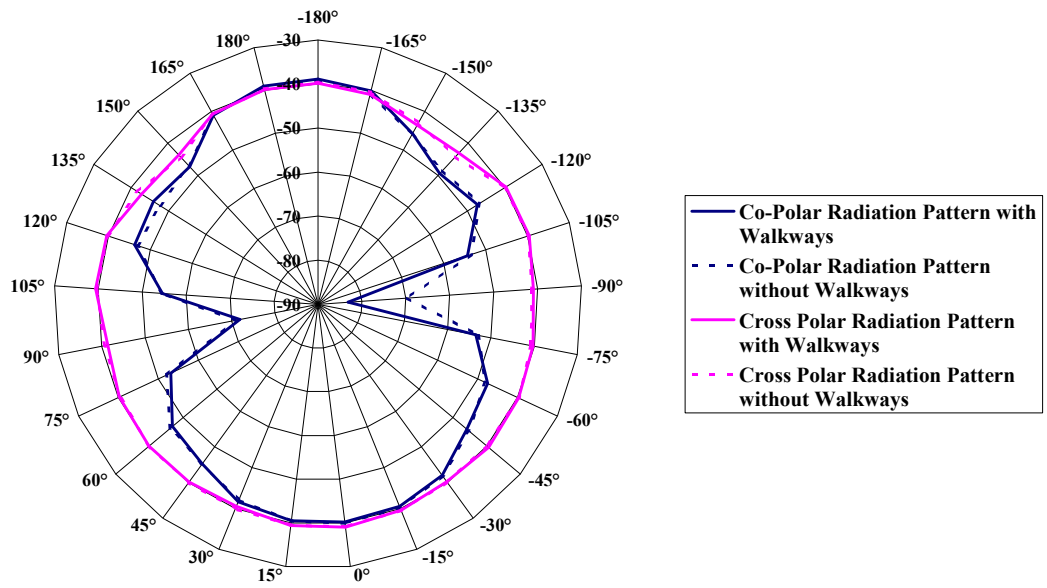
Anechoic Chamber

Figure 5-11: Radiation Pattern of a Dipole at 2.45GHz with and without Walkways inside the
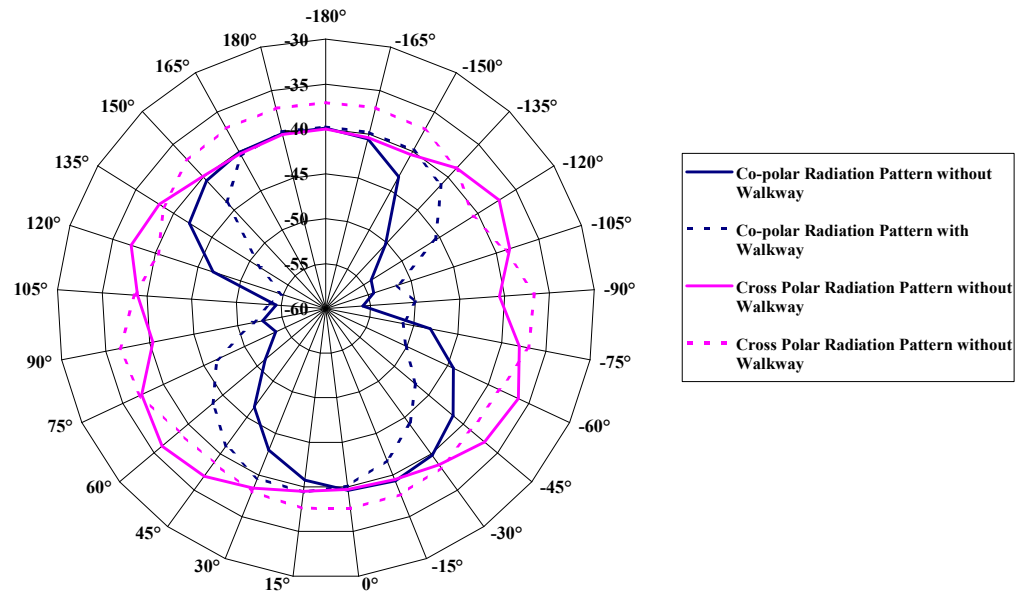
Anechoic Chamber

Figure 5-12: Radiation Pattern of a Dipole at 4.5 GHz with and without Walkways inside the

Anechoic Chamber

5.4.4   Conclusion:

Radiation patterns of dipole were measured in this experiment to find out the effect of walkways inside an anechoic chamber at mobile communication frequencies. The results suggest that the effect of introducing walkway in to the chamber had only a small effect on patterns and therefore the walkway was used during later experiments. Figure 5.12 shows some of the deviation in the results for the radiation pattern of a dipole at 4.5GHz. So it was concluded that walkway does not have any significant effect on the antenna measurements upto approximately 4.5 GHz but after that walkway seem to be deviating the results by approximately $\pm3dB$.

5.5 Measured Results for the Perturbations of hand-held Cellular Antenna due to the Proximity of a Tissue Simulating Phantom at GSM 900

The user experience of a mobile handset system mainly depends on the performance of the bi-directional link between the base station and the handset [96]. Due to rapid developments in the field of mobile communications, there is a strong need for fast and reliable evaluation methods for estimating the performance of the handsets. The performance of the handset here refers to evaluation of the performance under actual conditions such as speech/data as well as in free-space. In addition the latest mobile handsets must operate in multiple bands to enhance the radio network capacity. An antenna in the mobile handset is extremely important as they serve to establish the link between the base station and the equipment [96].

For this reason, CTIA (The Wireless Association, representing all sectors of wireless communications that is cellular, personal communication services and enhanced specialized mobile radio) and 3GPP (The 3rd Generation Partnership Project (3GPP)

unites telecommunications standards bodies to produce Technical Specifications and Technical Reports for a 3G Mobile System based on evolved GSM core networks and the radio access technologies that they support Universal Terrestrial Radio Access (UTRA) both Frequency Division Duplex (FDD) and Time Division Duplex (TDD) modes)) have made efforts to set-up formal specifications to test the radio performance of mobile terminal in active mode, including antenna. This is known as Over-the-air (OTA) Measurements.

With regard to the research undertaken for this thesis a method was needed to reliably assess the stability of on body antennas whilst in use on an actual network such as Orange or Vodaphone. With this motivation, sensitivity measurements for the GSM phones at 900 MHz were performed in free space and near a human head phantom. The experimental setup can be seen in figure 5.15. The equipments used consisted of anechoic chamber for free space and isolation, multi-axis positioning system for spherical measurements, Base station simulator (BSS), wideband horn, mobile handsets, test SIM card and human head phantom.

5.5.1   Anechoic Chamber

The anechoic chamber is the main facility required to perform our measurements, the chamber proposed to carry out the tests should be large enough to allow measurement antenna to be at considerable distance from the device under test (Mobile handset) and the site should be interference free. In addition, the chamber should be supported by a Multi-axis Positioning system and a standard gain horn antenna range of 2.5 GHz.

5.5.2   Base Station Simulator

A   Base Station Simulator (BSS) is a sophisticated device required for Sensitivity measurements. The base station simulator provides a network connection to the mobile phone. The BSS used is shown in the figure 5.13.

Figure 5-13: Front panel of HP/AGILENT 8922 M/S Base station simulator

5.5.3 Mobile Handset and Test SIM

A mobile handset (DUT) is required for the measurements. In this research the effect of a lossy body on the phone antenna was of interest and therefore the mobile initially used was chosen arbitrarily. In this case a Nokia 2610 phone was used whose internal antenna was investigated. A test SIM was fitted in the mobile handset during the measurements.

A fixture of non–conductive Polyvinyl Chloride (PVC) was fabricated. This apparatus, which is shown in figure 5.14 has three main parts. Firstly, there is a clamp to affix the device to the positioner, secondly there is a hollow container which can be filled with 2kg of tissue simulating liquid and thirdly there is a clamp to hold the mobile phone. The constituents and preparation procedure of tissue simulating liquid can be found in [97].

Figure 5-14: DUT and Phantom fixture

Figure 5.15 shows the test set-up for sensitivity measurements of GSM Phones. Via a

standard horn antenna the BSS was used to generate a link inside the anechoic chamber. The orientation of the phone in relation to the BSS was swept in azimuth and elevation using control software on a PC. Note that the BSS was not interpreted into the positioner control program and therefore angles were selected manually.
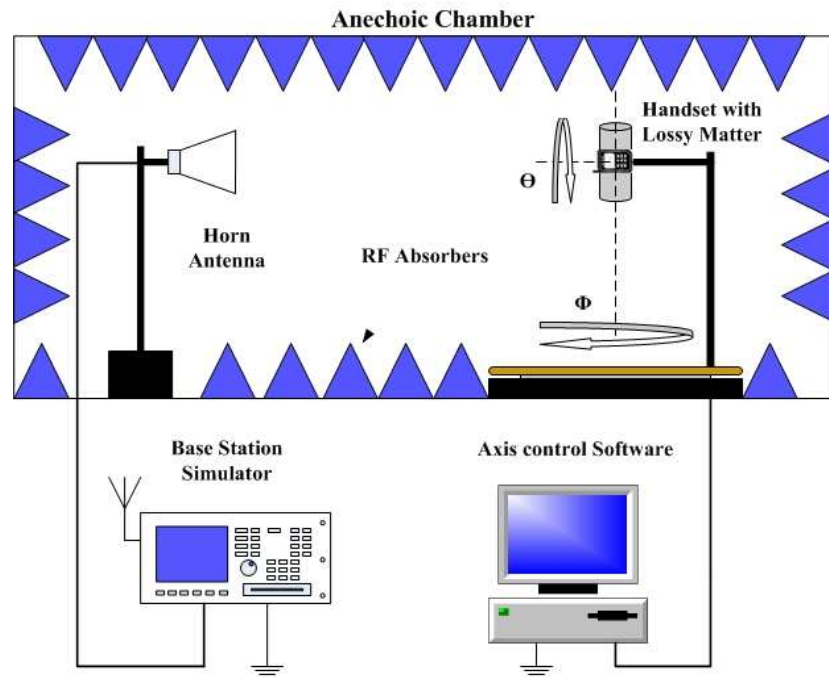
Figure 5-15: Test setup for sensitivity measurement for GSM mobile phone.

This measurement was an iterative process which varied the base station simulator output power at the phone while measuring the Bit-error-rate (BER). When the target BER was achieved, the iteration was stopped and the received power at the phone was recorded as sensitivity (that is the minimum power required to maintain specific BER, 2.44% for GSM).
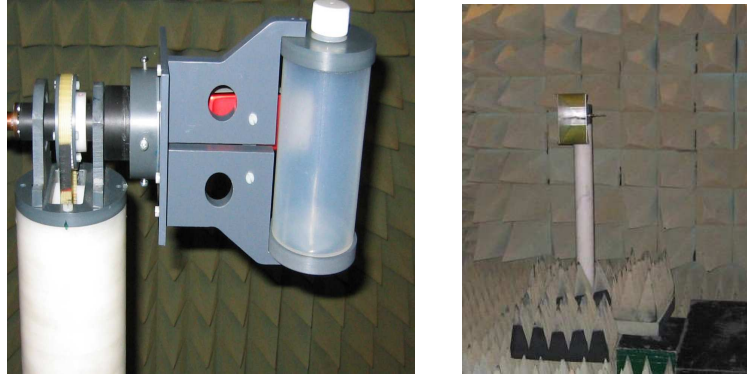
Figure 5-16: Actual set-ups at Loughborough University Anechoic Chamber.

The step by step procedure of the experiment and the BER measurement steps are given in appendix C. A code was generated in Matlab for the calculation of TIS whose code and snapshots are given in appendix D.

5.5.4 Modified Total Isotropic Sensitivity (TIS):

In order to quantify the performance of the receiver, the sensitivity is measured on the spherical surface surrounding the mobile phone. The sensitivity is defined as the received power level at which the mobile station (MS) exceeds a specific digital error limit, Bit-error-rate (BER) in our case. Sensitivity is measured by lowering the base station amplitude Traffic Channel (TCH) power level until the specified digital error limits is exceeded. The TCH power that required obtaining the error limit is the sensitivity value [98].

According to [98] and [99] Total Isotropic Sensitivity (TIS) can be calculated as follows:

$$TIS = \frac{2NM}{\pi \sum_{i=1}^{N-1} \sum_{j=0}^{M-1} \left[\frac{1}{EIS_\theta(\theta_i, \phi_j)} + \frac{1}{EIS_\phi(\theta_i, \phi_j)} \right] \sin(\theta_i)} \qquad \textbf{Eqn. 5-3}$$

Where N is the number of θ intervals, M is the number of ϕ intervals, $EIS_\theta(\theta, \phi)$ represents power available from an ideal isotropic, theta polarised antenna generated by the theta-polarised plane wave incident from direction (θ, ϕ) which, when

incident on the device under test DUT, yields the threshold of sensitivity performance and $EIS_\phi(\theta,\phi)$ represents power available from an ideal isotropic, phi-polarised antenna generated by a phi-polarised plane wave incident from direction (θ,ϕ) which, when incident on the DUT, yields the threshold of the sensitivity performance [100]. The receiver performance of the device under test (DUT) is measured utilising the bit error rate (BER). (The ratio of received bits that are in error relative to the total number of bits received in a bit stream.)

Data points are taken every 30˚ in the theta (θ) and in the phi (ϕ) axes are sufficient to fully characterise the DUT's receiver sensitivity. This account for a total of 60 measurements all together.

All of the measured sensitivity values for each DUT test condition will be integrated to give a single figure of merit referred to as Total Isotropic Sensitivity (TIS).

5.5.5 Test Results for Total Isotropic Sensitivity without Head Phantom:

Table 5-1: Total Isotropic Sensitivity (dBm) in free space for ϕ Polarisation

θ^o / ϕ^o	30	60	90	120	150
30	-100	-102	-99	-100	-98
60	-105	-97	-98	-103	-100
90	-94	-95	-98	-102	-105
120	-90	-88	-92	-98	-99
150	-97	-93	-99	-100	-105
180	-101	-97	-96	-104	-102
210	-99	-98	-98	-86	-102
240	-102	-93	-94	-87	-103
270	-89	-90	-103	-91	-102
300	-88	-94	-103	-86	-99
330	-100	-102	-102	-98	-106

Table 5-2: Total Isotropic Sensitivity (dBm) in free space for θ Polarisation

θ^o ϕ^o	30	60	90	120	150
30	-110	-105	-106	-108	-105
60	-106	-102	-98	-108	-103
90	-106	-100	-102	-110	-110
120	-107	-98	-109	-110	-107
150	-103	-99	-101	-107	-102
180	-109	-97	-103	-102	-104
210	-110	-104	-100	-110	-103
240	-105	-107	-109	-104	-100
270	-103	-109	-105	-100	-108
300	-110	-100	-102	-99	-103
330	-104	-110	-99	-107	-100

5.5.6 Sensitivity Measurements with Phantom for GSM 900

Table 5-3: Total Isotropic Sensitivity (dBm) near the head phantom for θ Polarisation

θ^o / ϕ^o	30	60	90	120	150
30	-107	-99	-102	-106	-101
60	-103	-96	-94	-106	-99
90	-103	-94	-98	-108	-106
120	-104	-92	-105	-108	-103
150	-100	-93	-97	-105	-98
180	-106	-91	-99	-100	-100
210	-107	-98	-96	-108	-99
240	-102	-101	-105	-102	-96
270	-100	-103	-101	-98	-104
300	-107	-94	-98	-97	-99
330	-101	-104	-95	-105	-96

Table 5-4: Total Isotropic Sensitivity (dBm) near the head phantom for ϕ Polarisation

θ^o / ϕ^o	30	60	90	120	150
30	-98	-97	-96	-97	-94
60	-103	-92	-95	-100	-96
90	-92	-90	-95	-99	-101
120	-88	-83	-89	-95	-95
150	-95	-88	-96	-97	-101
180	-99	-92	-93	-101	-98
210	-97	-93	-95	-83	-98
240	-100	-88	-91	-84	-99
270	-87	-85	-100	-88	-98
300	-86	-89	-100	-83	-95
330	-98	-97	-99	-95	-102

5.5.7 Results and Conclusions:

At GSM900 the modified total isotropic sensitivity of mobile phone under test in free space and near the dielectric filled phantom were found to be -65 dBm and -62.6 dBm respectively. This shows that the tissue simulating liquid absorbs more than 2 dB of the power that would normally be available to the phone. Note that since the phantom and the phone were rotated in space together (same bracket), then this test is slightly unlike that performed in [98, 99] in which a phantom orientation would have been fixed relative to the chamber and the phone moved in increments of azimuth and elevation. As in [101] power available to the mobile phones drops with the presence of a lossy body.

5.6 Conclusion

This chapter has discussed the application of techniques used in the measurement of wearable antennas. Normalised Site Attenuation measurements in anechoic chamber used to check performance have also been discussed. It was found that the available chamber performs within recommended limits across the range of frequencies that hove been used in this work. Complimentary research was also undertaken to access the impact of absorber orientation and the addition of a polystyrene walkway. A novel phone mount and tissue simulating liquid phantom was also presented.

Chapter 6:
Experimental Results Germane to On-Body Measurements

6.1 Introduction:

A probable trend in communications is the incorporation of technology into clothing. The twin factors of the absence of a convenient on-body power supply and the relatively high power requirements of mobile communications devices combined with the lossy properties of biological tissue make on-body systems an interesting area of research. In wearables, radiation efficiency of an antenna, its resonant frequency and input impedance, and its radiation pattern are all to some extent dependent on the dielectric properties of human body tissues [5, 9]. It is therefore important to assess the relevant power budgets and a key component of this is the on-body channel.

On-body channels exist whenever there is a need of communication between two terminals on or within the human body. In view of authors of [76] the communication channel in body area network (BAN) will be a combination of different effects and the propagated ray will be a grouping of rays reflecting from different parts of human body and also from the surroundings like walls, ground etc. As well as this there is an on-body surface wave component.

The dynamic nature of these on-body channels has been looked at by the authors of [102] in and outside anechoic chamber at 2.4 GHz, with various locations of antennas on the human body, with different body postures. In the view of author of [103] channel conditions in body area networks are not as benign as the short distance between the transmitter and receiver may suggests. When signal attenuation due to

body blocking is a factor then for the most part the link relies on the multipath propagation. This concludes to the user actions [32] causing the channel characteristics to vary greatly over short periods of time.

In the next section (section 6.2) measurements to characterize the on-body communication channel are presented. This type of experiments set was performed on a human male with wet and dry clothing. The next section (6.3) explains the perturbation in wearable antennas due to their proximity with lossy biological matter such as the body. The topics of measurement setup, antenna design and synthesis, phantom design and human body simulation using CST Microstripes are also covered in this chapter.

6.2 Measured and Simulated Results for the Characterisation of the on-body Channel Creeping Wave with Wet and Dry Clothing:

Our intention during these experiments was to deduce by experiment an indicative figure for the difference in the on-body component of the propagation path between a dry subject and the same subject who was wet.

6.2.1   Methodology:

The antennas used were $\lambda/4$ monopoles located over a square ground plane. The monopoles were l = 27mm, d = 0.9 mm copper wire over a ground plane of 80x80 mm^2. For 0.9GHz and 1.8GHz monopole length of l = 80mm and l = 40mm respectively were used with ground plane size of 120x120mm^2 and were attached onto chest and hip of a human volunteer and were isolated from body by using a 20mm thick expanded polystyrene tile. One of the two identical antennas at 2.5GHz is shown in figure 6.1. The positions and placement of antennas on human body are shown in the figure 6.2. The return loss of the antennas is shown in figure 6.4. In free space the simulated gain of the antenna for 2.5GHz was 1.36dBi, antenna efficiency of

approximately 91% and radiation efficiency of approximately 99%, while gain for 1.8GHz antenna was 1.9dBi having antenna efficiency of approximately 94% and radiation efficiency of 99% and for 900 MHz antenna 1.1Bi, 90% and 99% gain, antenna and radiation efficiency respectively.

The antennas were then connected through calibrated flexible co-axial cables to portable vector network analyser. Over intervals of approximately 30 seconds the S_{21}(dB) response was measured while a volunteer was wearing the antennas. Four indicative positions were used, standing upright, standing with the torso twisted to the left, standing with the torso twisted to the right and bending these positions are shown in figure 6.3. The majority of the measurements were carried out on a sports field with possible spurious sources greater than 0.5 mile away. For comparison some measurements were performed inside the anechoic chamber. The distance between antennas when the volunteer was standing was approximately 55cm, turning left and right changed this distance by approximately 10cm, making the distance between antennas 65cm and 45cm respectively.
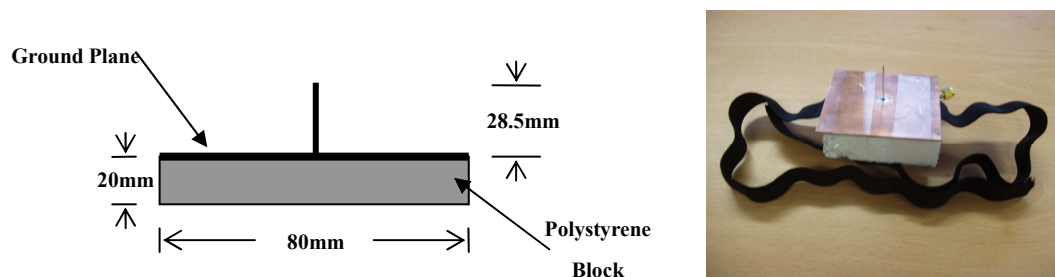
Figure 6-1: Design of the on-body monopoles used. Left shows the 2.5 GHz version with a tuned probe. The right hand picture shows the antenna with its polystyrene insulator and elastic body strap.
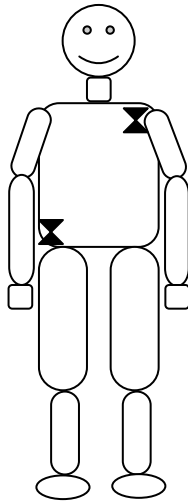
Figure 6-2: Graphic of placement of antennas on the torso.
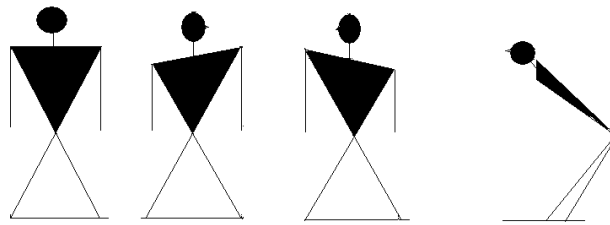
Figure 6-3: Different Body Postures during the experiment (a) Standing, (b) Turning Left, (c)

Turning Right and (d) Bending.
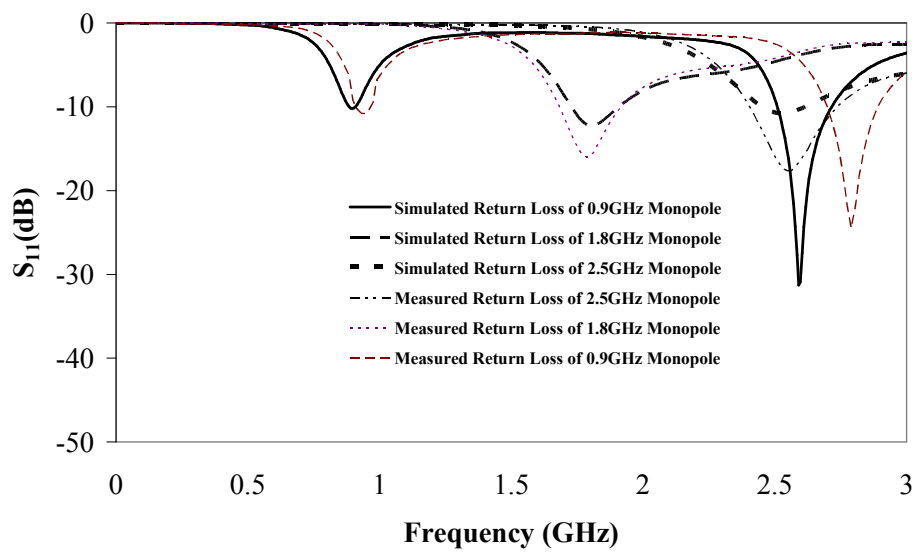
Figure 6-4: Simulated and Measured return losses of all three monopole antennas used in the

experiment.

Due to the difficulty of using fluids inside the anechoic chamber, it was decided that these experiments, which involve both fresh and rain water, to be performed outside in an open area. To minimize the multipath component of the signal in the channel a playing field was chosen. This field is shown in the figure 6.5. The nearest source of interference was always more than 100m away from the point of measurement. A source at this point was calculated to have to undergo a free space pathloss of -150dB. So it was assumed that interference from the nearest source was not significant.

Figure 6-5: Open area chosen for performing the on-body measurements for wet and dry clothing of human male at frequency of 2.5GHz.

The variation in the cable loss due to body movements were measured and were not more than ±0.1 dB. In these experiments the choke shown in Figure 6.6 was used to prevent mismatch at the antenna cable junction causing stray current on the coaxial outer surface. The samples of water which were used were normal tap water and rain water. Rain water was collected in a vessel left outside for one week. However it turned out that rain water and tap water was so similar in their electrical properties that it was reasonable to use tap water in all experiments. The permittivity of the water samples used was measured as 73 with a conductivity of 23 μS/cm. Note that no correction factor was added for the temperature of the water. Also in salty environments it is likely that rain water and tap water will have significantly different conductivities.

Figure 6-6: Ferrite chokes used on coaxial cables during on-body channel characterisation measurements.

The maximum orientation mismatch of the monopoles between wet and dry tests was nearly ± 5 to ± 10 degrees. The Polarisation Loss Factor (PLF) of orientation mismatch was nearly 0.96, which contributed an error of nearly -0.13 dB to the final results. The T-Shirts which were used in the experiment were 99.9% cotton with dielectric permittivity of 1.54 having a Loss Tangent of 5.8×10^{-2}.

An ISM band for frequency of operation was chosen for the measurements of transmission co-efficient. We rationalise that this band is sufficiently close to typical 802.11b and UWB radio as to be usefully representative.

6.2.2 Simulated Human Torso Model:

A simple 4 layer model was created in CST. These kind of layered models are common in practice [104-107]. The simulated model contained layers of muscle, dry skin, wet skin and cotton T-shirt. The properties of human body tissues can be found on the website of Federal Communication Commission and are also given in CST Microstripes, while the dielectric properties of the cotton T-shirt were measured in our laboratory using a Split Post Dielectric Resonator. The dimensions of the cylindrical model in CST Microstripes approximated the human torso, 290mm from stomach to back, 418mm from shoulder to shoulder and 450mm for vertical height from shoulder

to waist. The CST model with monopole antennas at front and back is shown in Figure 6.7. Simulated results of S_{21} (dB) for the model explained above at 2.5GHz is shown in Figure 6.9.
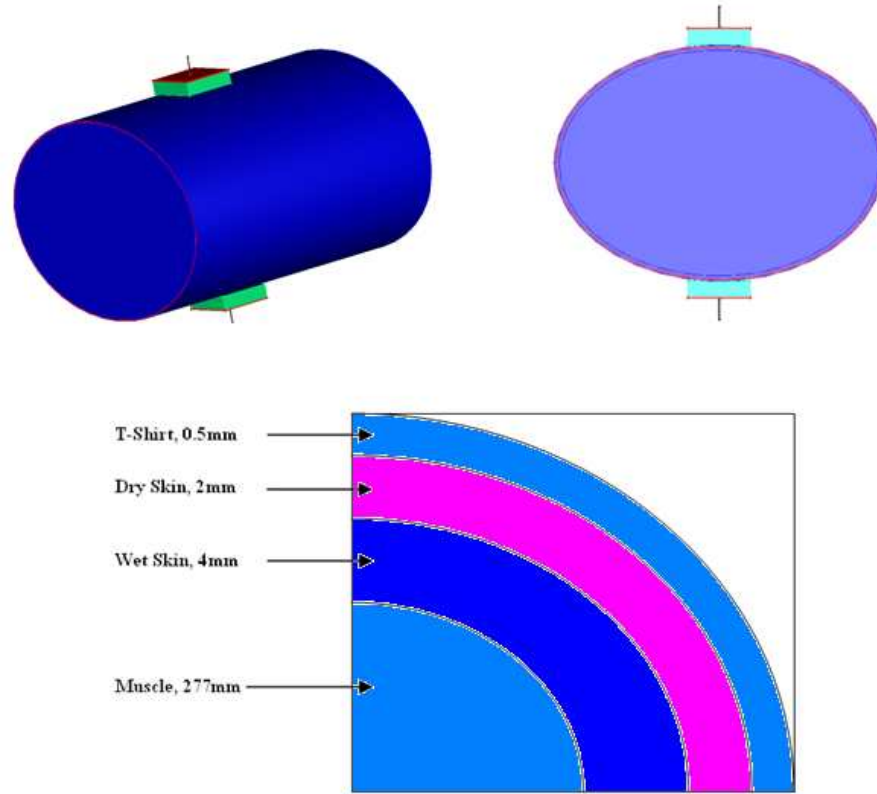
Figure 6-7: 4-layer (T-Shirt, dry skin, wet skin and muscle) human torso simulated model with their thickness and antennas placement setup.

Another simulation was also performed in which antennas were placed in line of site condition which resembled the standing straight posture of the volunteer in out experiments with antennas placed at his chest and hip and is shown in figure 6.8. the results are shown in figure 6.10.

The extents of mesh around the model were increased to 30% around the model. The size of the largest and smallest cells in the mesh have a significant effect on the accuracy and speed of the simulation, and deserve careful consideration. The smaller the cell size is the more accurate the results will be but the run time and memory requirements will also be increased. It was for this reason that a 64-bit operating system with 64-bit version of CST Microstripes was used to perform the simulation to

over come the memory shortage in 32-bit system. The size of smallest cell was chosen to be 1/30 of the wavelength in free space at requested maximum model frequency. The run time for these conditions and for every simulation was approximately 10 hours.
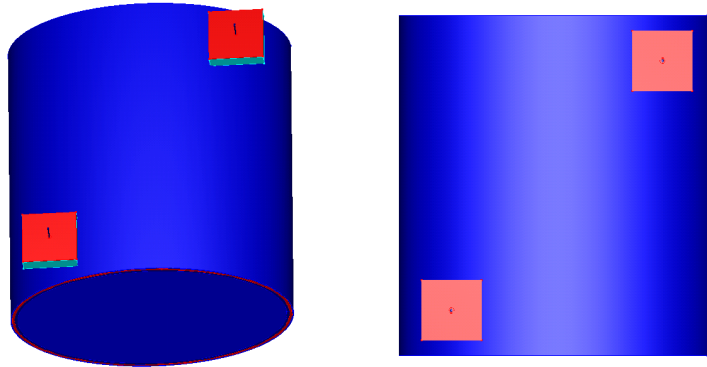
Figure 6-8: 4-layer (T-Shirt, dry skin, wet skin and muscle) human torso simulated model with antennas in line of site situation setup.
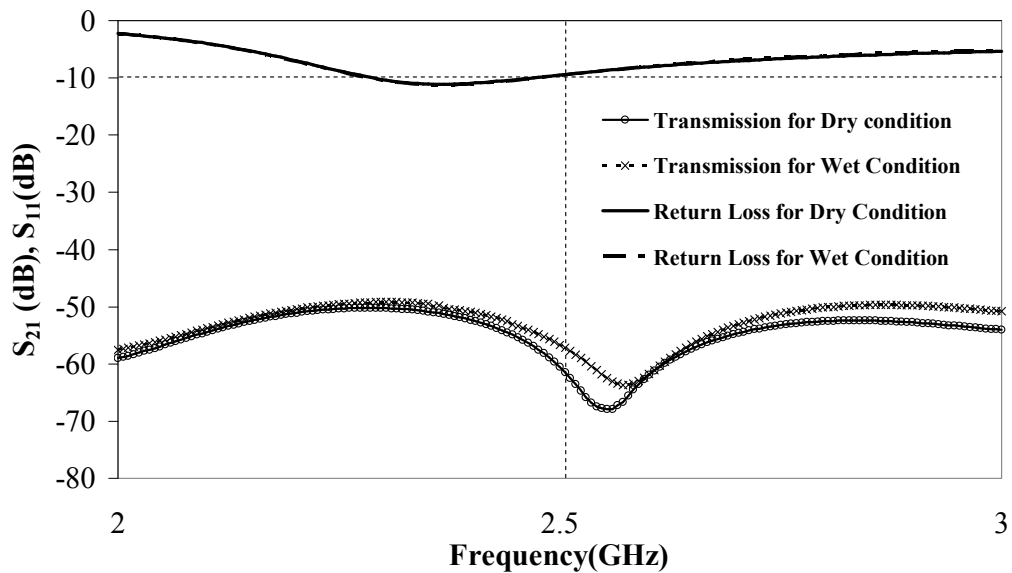
Figure 6-9: Simulated S$_{21}$ (dB) and S$_{11}$(dB) results for the 4-layered Human torso model with antennas at front and back at 2.5 GHz
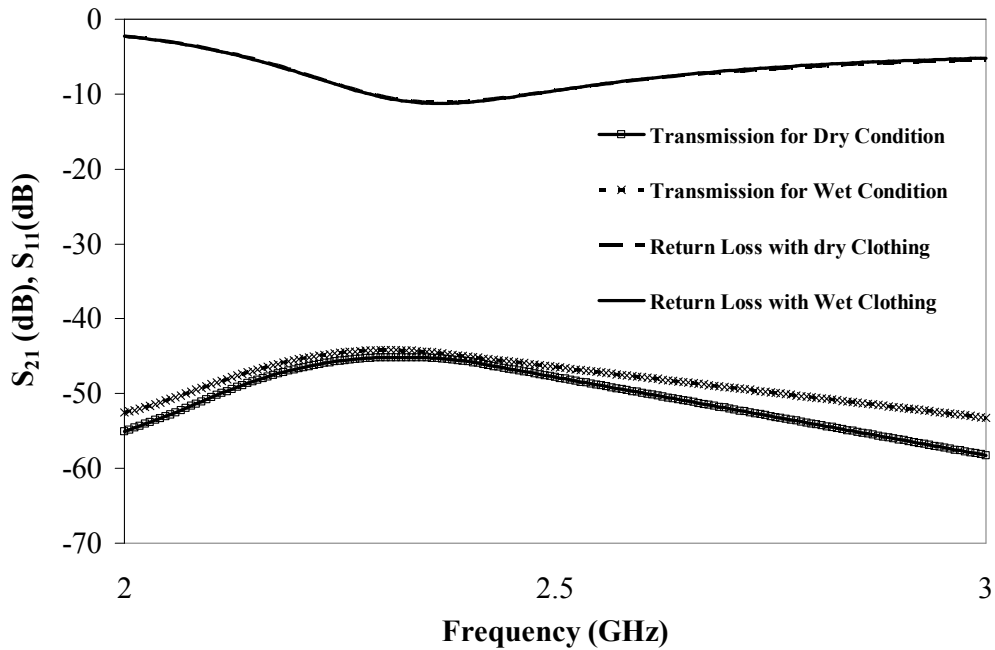
Figure 6-10: Simulated S$_{21}$ (dB) and S$_{11}$(dB) results for the 4-layered Human torso model with both antennas at front at 2.5 GHz

6.2.3   Results:

Figures 6.11 shows the results for measured path loss between waist-to-chest worn antennas on human body located inside the anechoic chamber at 900MHz. The results have four periods for changes in postures (0-30s standing straight, 30-60s torso left, 60-90s torso right and 90-120s bending forward). It can be seen that in general the wet clothing improves transmission. The transmission is improved in all postures. Transmission is worse for a volunteer who is bending forward due to body blocking. The most marked improvement in transmission between wet and dry was seen in the first three postures. Over the thirty second interval the measurements remained relatively stable. The most perturbed results were in the bent forward posture. We rationalise that this is due to breathing and it's leading to changes in the degree of body blocking.

The next set of results is shown in Figure 6.12 with the same experiment but this time performed at 1.8GHz. It can be seen that in all cases propagation in the on body channel is improved in wet clothing versus dry. However, the transmission coefficient in the postures has changed significantly. A point to note here is that the bent forward position was highly variable due to the varying degree of body blocking between volunteers and even between repetitive measurements on the same volunteer on different days. Therefore these results do not reliably infer that prorogation is better or worse in the bent forward posture at any frequency but do reasonably support the hypothesis of better propagation due to water by a relative comparison.

Figure 6.13 is at 2.5 GHz but this time with a slightly different experiment. Here two sets were achieved in the outdoor site shown in Figure 6.5, one wet and one dry whilst another one dry measurement was performed in the chamber. These results show several important characteristics. Firstly there is little difference between the chamber and open area for a dry volunteer. In postures one and three although wet clothing tends to better propagation the dynamic nature of the channel supports the hypothesis made previously that only relative degrees of propagation can be relied upon. Finally for this set in posture four we see the most marked improvement in propagation of approximately l0 dBs.

In Figure 6.14 are the results for the experiments in the open area but with different volunteer. The trend between wet and dry is the same. In posture three the results show an aberration in the wet set. This experiment was not repeated since it seems to be at a single point of thirty measurements. The results shown in Figure 6.15 are for a third volunteer and also show the same properties as mentioned earlier in this discussion. There is variation in the degree of difference between wet and dry in figures 6.14 and 6.15. For example the difference in the two sets for posture two is significant. However, the trend of wet having better propagation is maintained.

A test for finding the effect of number of clothes on the body was also performed inside the anechoic chamber and the results are shown in figure 6.16. The results suggest that on-body propagation is improved with wet clothing but the the number of layers has only a small effect. Note that this aspect would require further investigation.

One measurement with the volunteer standing inside the anechoic chamber with his arms stretching outwards parallel to the floor was also performed. In this measurement both antennas were put on the hip of the human male and with non line of sight conditions, results are shown in figure 6.17. The results show the same property as before and we can reasonably conclude that the position of the arms of the volunteers do not alter this.

Initially it was thought that one reason for the improved propagation between the antennas was that water in some way improved the match of the antennas. Figure 6.18 shows the return loss of quarter wave monopole with dry and wet clothing on the human body respectively. It is clear from figure 6.18 that the resonant frequency has reduced with human body but wetting the cloth does not have any noticeable effect on the return loss of the antenna and same fact is clear in figure 6.9, which shows the simulated results of the antennas placed on the human body model. Figure 6.19 represents all on-body propagation models presented by different researchers and location of our data in that.
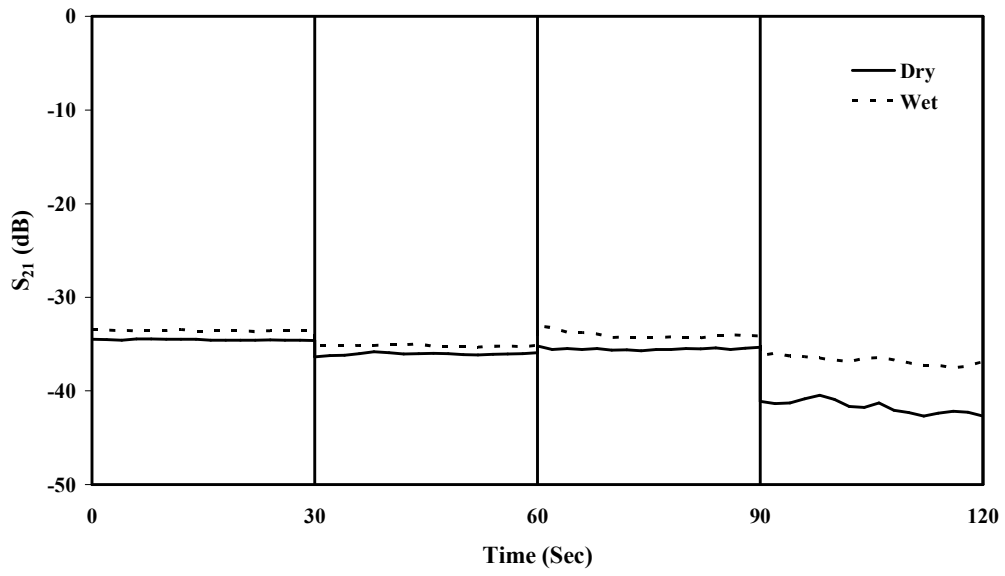
Figure 6-11: Measured Path Loss Between Waist-to-Chest worn antennas on human body located inside the Anechoic Chamber with changes in postures (Frequency 0.9GHz, 0-30s Standing Straight, 30-60s Torso Left, 60-90s Torso Right, 90-120s Bending Forward)
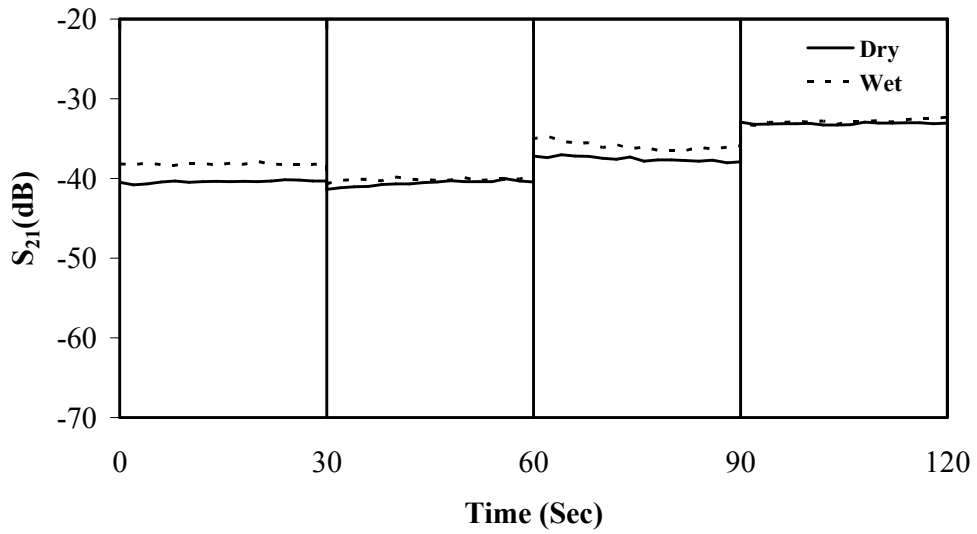
Figure 6-12: Measured Path Loss Between Waist-to-Chest worn antennas on human body located inside the Anechoic Chamber with changes in postures (Frequency 1.8GHz, 0-30s Standing Straight, 30-60s Torso Left, 60-90s Torso Right, 90-120s Bending Forward)
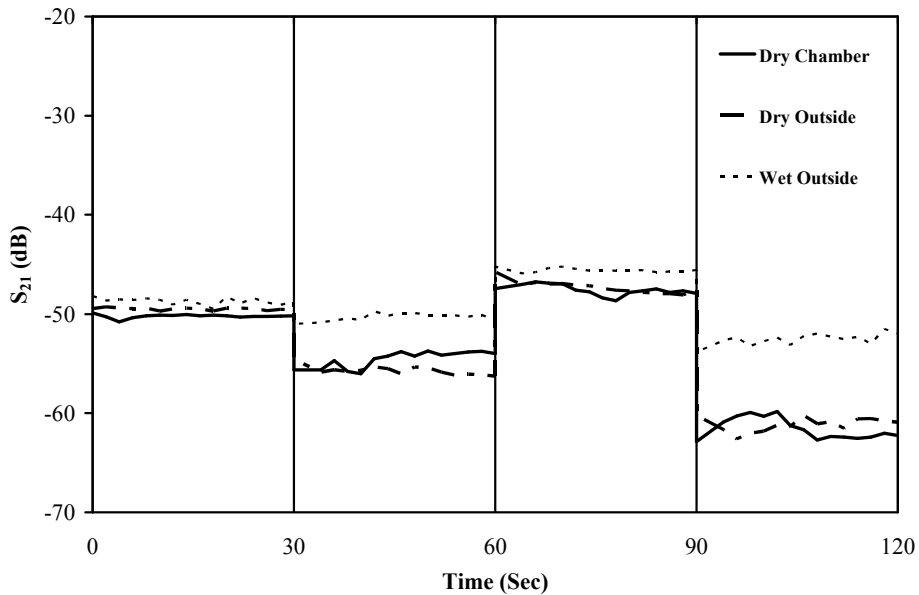
Figure 6-13: Measured Path Loss Between Waist-to-Chest worn antennas on human body located outside the Anechoic Chamber with changes in postures (Frequency 2.5 GHz, 0-30s Standing Straight, 30-60s Torso Left, 60-90s Torso Right, 90-120s Bending Forward)
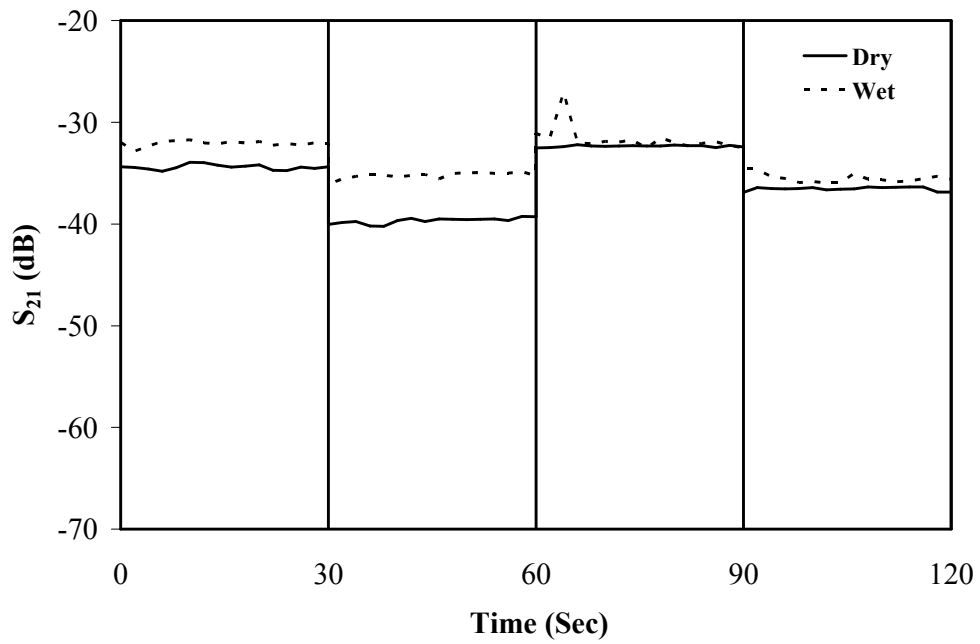
Figure 6-14: DRY and WET measurement outside on another human male with different size and weight at 2.5GHz.
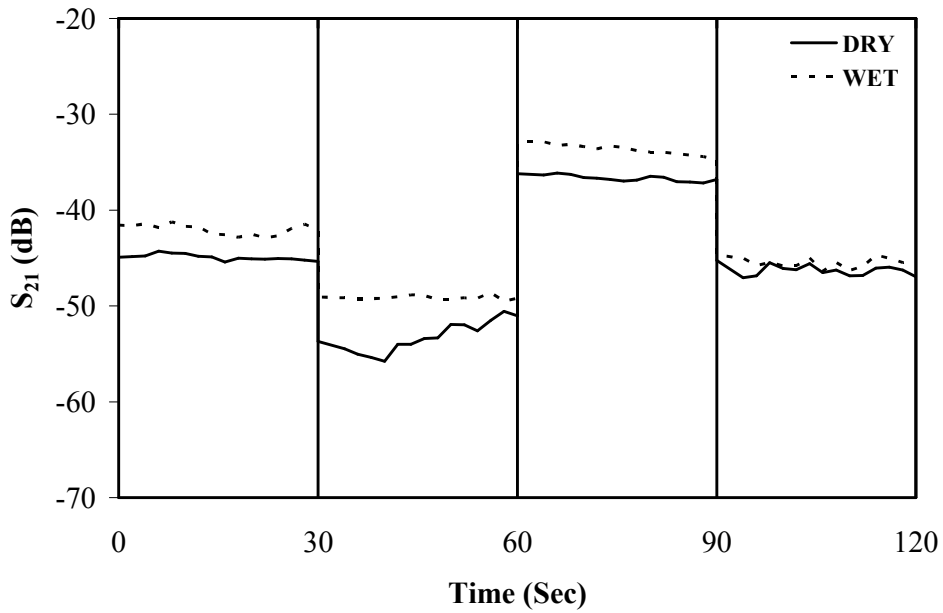
Figure 6-15: DRY and WET measurement outside on another human male with different size and weight at 2.5GHz.
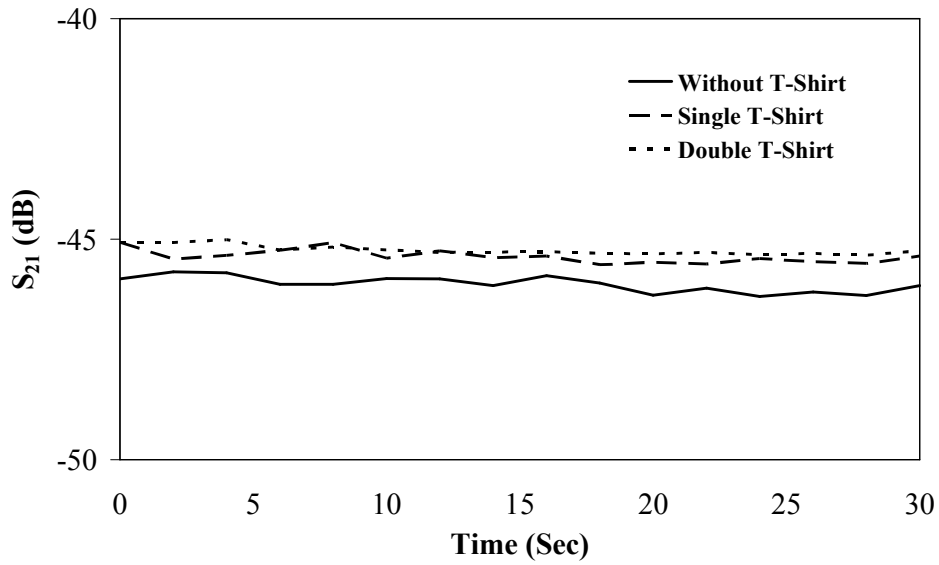
Figure 6-16: Comparison of S$_{21}$(dB) Measurements for Different number of Clothing on Human Body Inside the Chamber at 1.8GHz
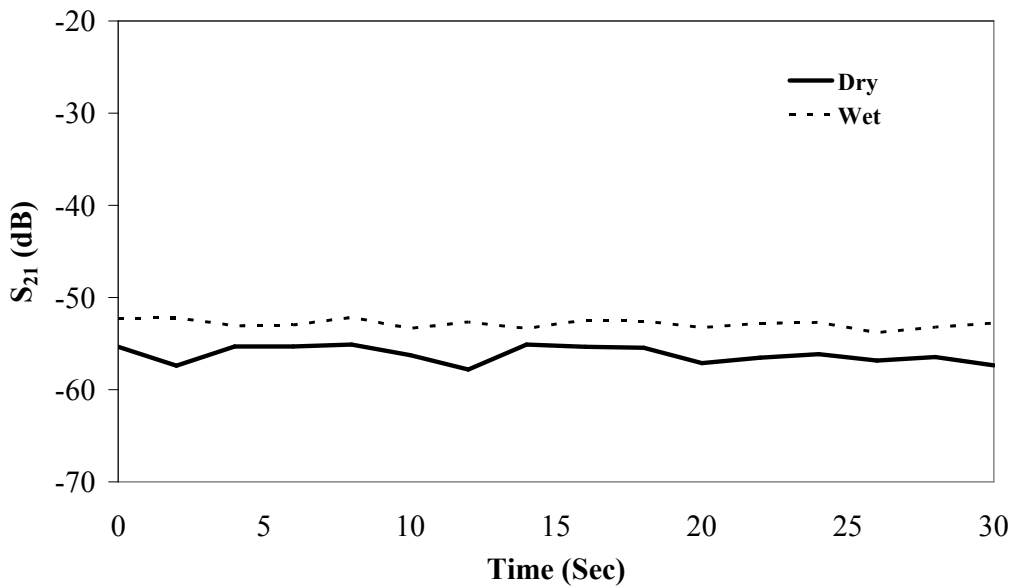
Figure 6-17: S$_{21}$(dB) Measurements for Antennas located on the waist of Human Body with arm stretching outwards, Non Line of Sight condition at 2.5GHz.
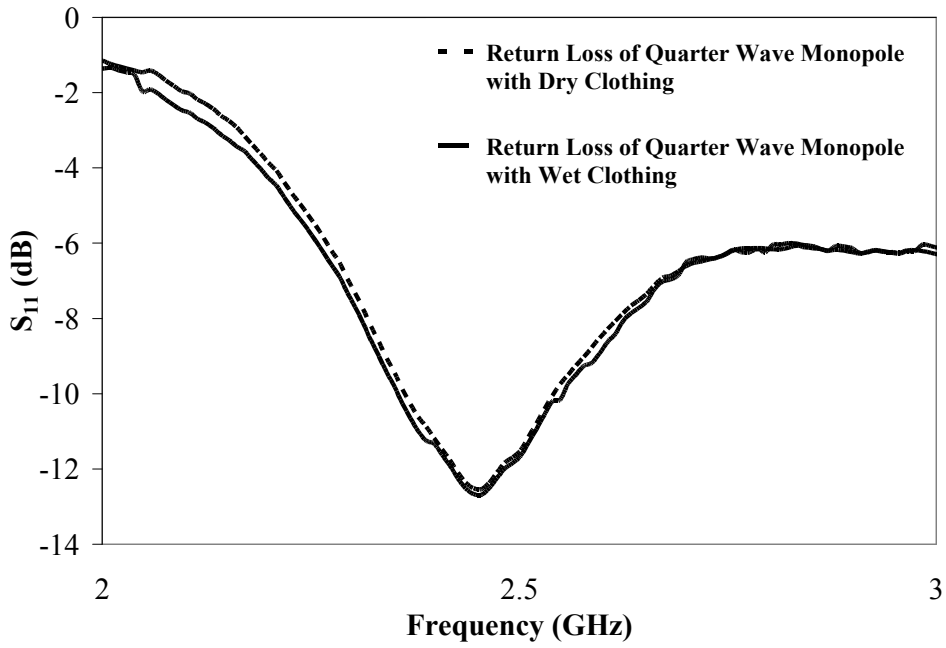
Figure 6-18: Measured return loss of quarter wave monopole with dry and Wet clothing on the human body at 2.5GHz respectively.
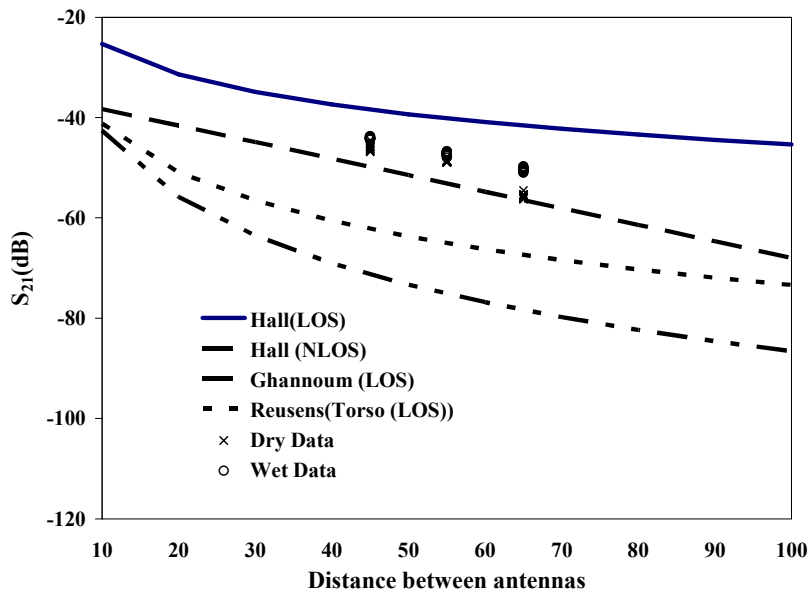
Figure 6-19: Comparison of On-body Propagation Models at 2.45 GHz on and around the Human Torso and placement of our data on them.

It was known that a monopole above a ground plane tends to a linear vertical polarised and to check the response for horizontal polarisation a square loop antenna was also used in the same experiment. The square loop antenna on an 80mm^2 ground plane at 2.5GHz is shown in figure 6.18.
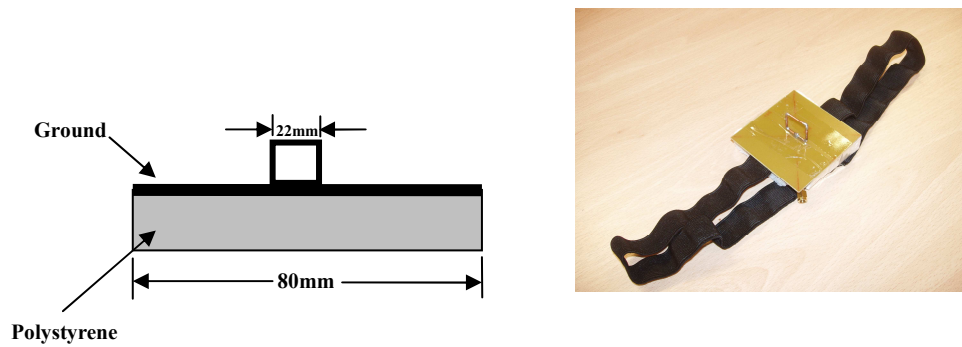
Figure 6-20: Layout of the square loop antennas

The simulated and measured return loss of the square loop antenna is given in figure 6.19 below.
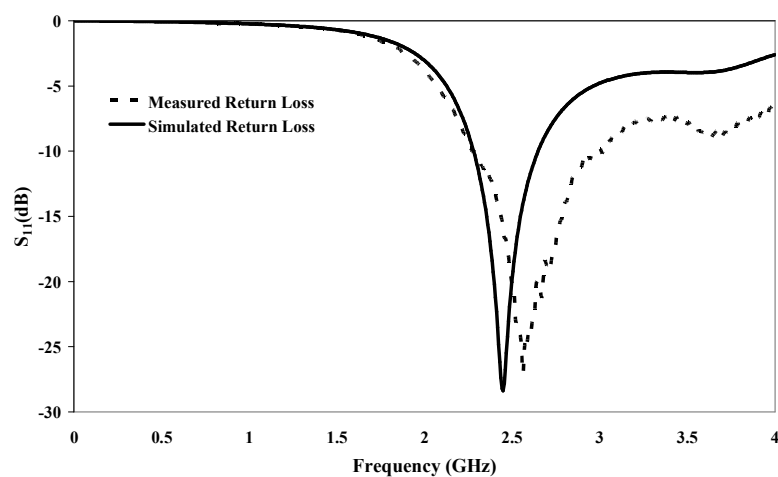
Figure 6-21: Measured and simulated return loss of square loop antenna

The S$_{21}$(dB) response of loop antennas on the human torso is given below in Figure 6.20.
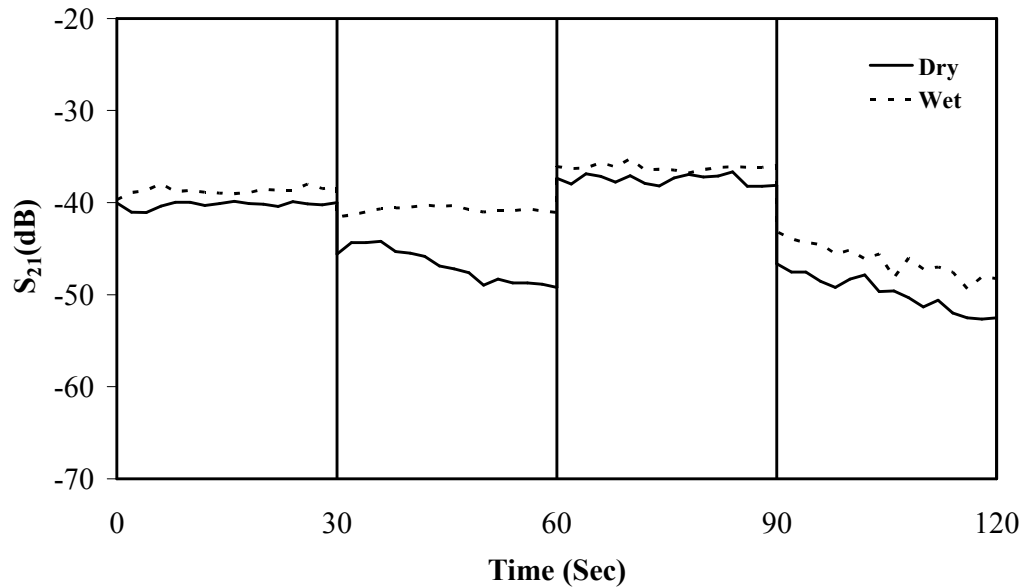
Figure 6-22: Measured Path Loss Between Waist-to-Chest worn square loop antennas on human body located inside the Anechoic Chamber with changes in postures (Frequency 2.5 GHz, 0-30s Standing Straight, 30-60s Torso Left, 60-90s Torso Right, 90-120s Bending Forward)

6.2.4 Conclusions:

Based on the results we achieved for finding the effects of wet clothes on on-body channels at mobile communication frequencies, the main conclusion reached was that wet clothing tends to improve propagation by between 1 and 3 dBs. This effect was independent of posture, of matching, of environment of body shape, of volume and of antenna coupling dominant field. Lastly that clothing layers may improve propagation.

6.3 Measured and Simulated Results for the Perturbation of the Input Impedance of Wearable Antennas due to Close Proximity with Humans and Tissue Simulating Liquid Filled Phantoms for Circularly and Linearly Polarised Antennas

6.3.1   Aim:

It turns out that to be effective in the context of cellular a wearable antenna currently requires a degree of isolation from the body upon which it is to be used. In essence as the flux density in the biological matter increases the efficiency of the antenna is reduced. There are currently three popular techniques to reduce the flux density in a body close to an antenna. Firstly ground planes can be used to reflect energy away from the skin. This method is effective but to be maximal requires an infinite ground plane which is impractical. Secondly the antenna can be designed to have a closely coupled near field. Dielectric resonator antennas are a good example of this. However such antennas require a high dielectric constant material and these tend to be ceramics which, since they are hard and brittle, are not best suited to wearable antennas. Thirdly a distance between the antenna and the body can be maintained using an insulating layer such as clothing. In common with method two this reduces the density of flux in the skin thereby reducing losses and hence increasing efficiency. At this time most antennas for wearable applications use methods one and three but not exclusively so. It is method three, the optimal separation distance between the body's surface and the antenna, which this section is concerned with.

Wearable antennas are best designed with a body perturbation in place and therefore need to be tuned on the body. However for a number of reasons humans are far from uniform in their tissue proportion. Fat, thin, tall and short are collective terms however age, race and sex may also be important.

The use of consistent human body phantoms has been thought to be a reliable alternative for measurements.

In this experiment we measure the effects of a simple tissue simulating liquid filled fibre glass phantom on the input impedance of an antenna and compare these results with measurements using the same antenna on the back and chest of several male volunteers. The objective of these experiments is the correction factor needed when using a phantom as opposed to a volunteer while considering isolation distance from the body for antennas.

6.3.2 Description of Experiment, Antennas, Phantom, Volunteers and Equipment

Antenna Design:

The antenna selected was a microstrip patch antenna built on common 1.6mm thick FR4 board. The tuned rectangular patch was probe fed via an SMA connection. All dimensions are shown in Figure 6.21. Initial design was reached using Balanis [108], and refined using the EM simulator Microstripes. The reason that most wearable antennas are currently planar and that this linearly polarised patch is therefore representative. Spacers were then used (4 off), also shown in figure 6.21, to position the antenna's ground plane above first the phantom and then above the chest and back of our volunteers.

Care was taken to ensure accurate calibration and minimise cable disturbance. Ferrite beads were used to choke off currents on the outer of the coaxial cable due to impedance mismatch at the feed. Note that since confidence in the ferrites maintaining their properties at these frequencies was low and so a choke balun was also used. The experiments were repeated over several days to assess repeatability. It was noted

that slightly flexing the coaxial cable gave results of ±(0.5-to-1dB) in S_{11}. The measurement instrument was an Anritsu Portable Network An

alyser which is portable and operated on batteries.
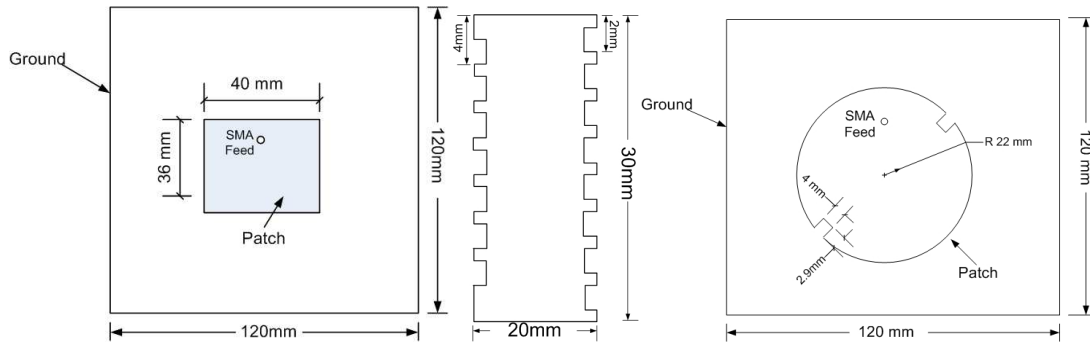
Figure 6-23: A line drawing of a linearly and circularly polarised patch antenna and an experimental spacer (Not to Scale).

Torso Phantom with a Tissue Simulating Liquid:

A rectangular phantom was made from 2mm thick glass fibre with the dimensions approximately 400mm long, 320mm wide and 210mm high shown in figure 6.22. These dimensions were chosen to be closely representative of the volume of the torso of a male. Note that the use of glass fibre phantoms in microwave measurements is now accepted practice [109]. The dielectric properties of the phantom and the muscle simulating liquid are shown in table 6.1. A recipe for the filling substance is given in [97]. When full the phantom holds approximately 10litres of liquid and was designed in such a way as to minimise air pockets on filling. However, slow filling and settling are advised to avoid air pockets. A picture of the torso phantom is shown in figure 6.22. When full this phantom weighs 26.8kg and is therefore portable but not unduly so.

	ε_r	$\sigma\,(S/m)$
Muscle Simulating Liquid	55.16	1.46
FR4 Board	4.5	0
PVC (Spacer Material)	4.0	10e(-6)

Table 6-1: Dielectric properties of muscle simulating liquid and FR4 board.
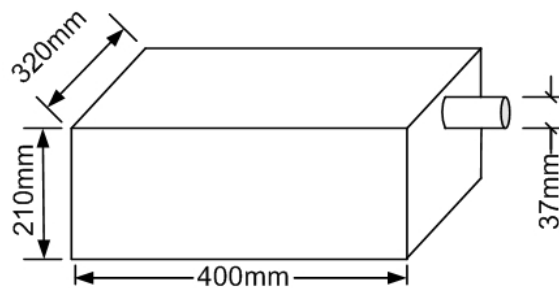
Figure 6-24: A Line drawing of Torso Simulating Phantom (Not to Scale).

6.3.3   Experimental Method:

For practically it was assumed that the range of measurements should be within 3cm of the surface of the body. This equates to several layers of clothing including an outer garment such as a coat. Previous work at Loughborough University had suggested that most garments have dielectric constants real of between 1 and 2.5 and are low loss. An exception is neoprene with a dielectric constant of 6 but this is still rare in clothing. Therefore we consider it reasonable to neglect clothing by making the assumption that the two major contributors to changes in antenna parameters when closed up to the body are the reflection at the air phantom/body interface and the loss in the tissue simulating liquid and the skin and muscle and blood of the torso.

After calibration the antennas return loss was measured at intervals of approximately 2mm over the range 2 to 30mm. An on surface measurement was not taken since the conductivity of skin at 1.8GHz (1.2 S/m), effectively shorts out the antenna and

prevents conducting surfaces pooling charge in the intended way. At 2mm intervals the S_{11} was recorded for phantom, human back and human chest. The abstracted drawings of figure 6.23 show the experiment in progress. Note that the phantom is truly planar whilst the human mid top back is reasonable planar and the mid top chest is a little less so. Our four volunteers were all male in their mid twenties. The first series of experiments used three volunteers and a phantom over the range 2 to 20mm. Subsequently it was decided to investigate the null in match for the human measurement and therefore the range was extended to 30mm for phantom and chest and back for a 4th volunteer.
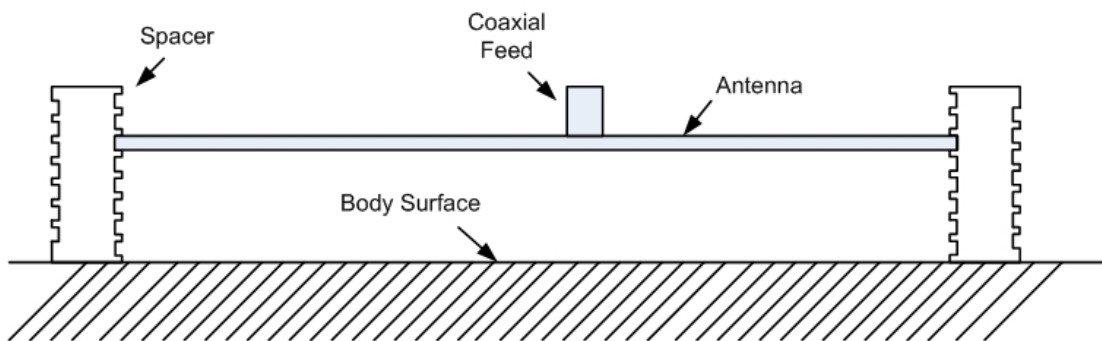
Figure 6-25: Placement of Antenna on the surface of Human Body and Phantom.

6.3.4 Results:

In Figures 6.24 and 6.25 results are plotted for return loss versus distance from surface for the chest of one volunteer and the back of two volunteers at 1.8GHz. It can be seen that in the presence of the phantom the match is generally better close in to the phantom when compared to the body. The rates of change of the responses are roughly the same however the effects due to the body occur right shifted in that they happen to the same degree at a greater distance. In both experiments the null of the phantom occurs at 16mm out which implies repeatability. All three volunteers give rise to similar responses however there is a difference in the body match beyond

16mm between the back and the chest. Nevertheless all of the body match profiles show a distinct right shift. The figure 6.26 shows the results we achieved for larger distance of 30mm from the surface of the body.
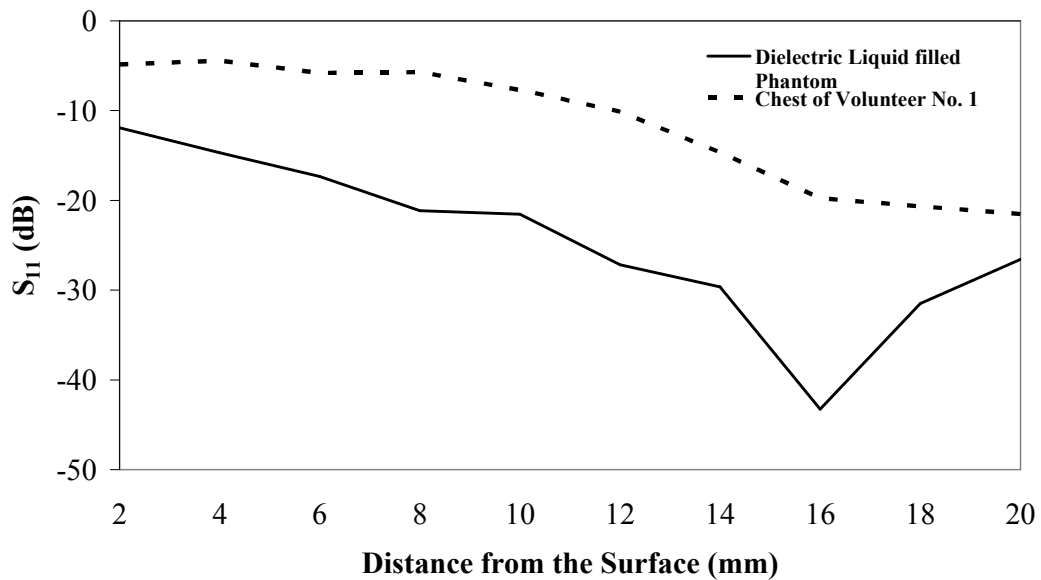
Figure 6-26: Comparison of S$_{11}$(dB) Measurements for Dielectric Liquid filled Phantom and Chest of a Human Body at 1.8GHz
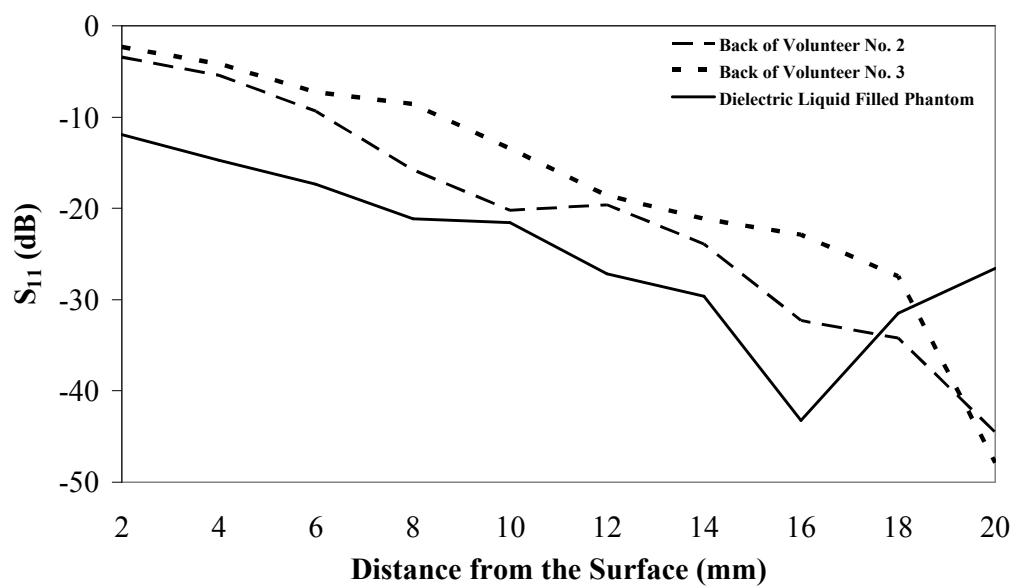
Figure 6-27: Comparison of S$_{11}$(dB) Measurement for Dielectric Liquid filled Phantom and Back of Human body at 1.8 GHz
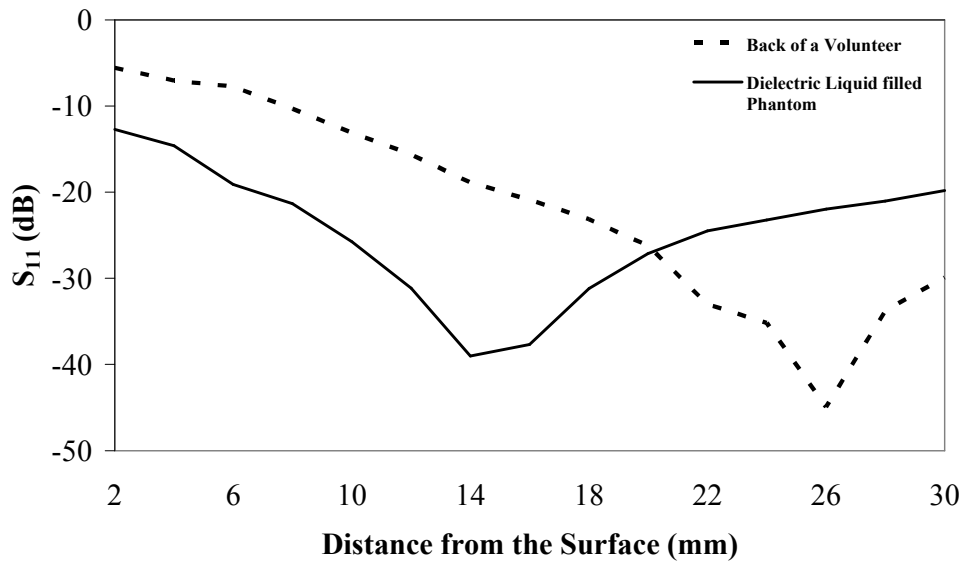
Figure 6-28: Comparison of S_{11} (dB) Measurements between Dielectric Liquid filled Phantom and

Human Body at 1.8 GHz

Another setup was designed in anechoic chamber for more accuracy as shown in the figure 6.27. In this setup the phantom and the antenna was masked with RF absorber so that any reflections from the floor could be attenuated. Another concept of putting a cap at the end of the coaxial cable was also adopted in these measurements, which results in improved readings to reduce the mismatch when antenna was brought close to the lossy biological matter. This trend can be seen in figure 6.28 named as measurement 2. The results of linearly polarised antenna near the dielectric filled phantom and human body is shown in figure 6.29.
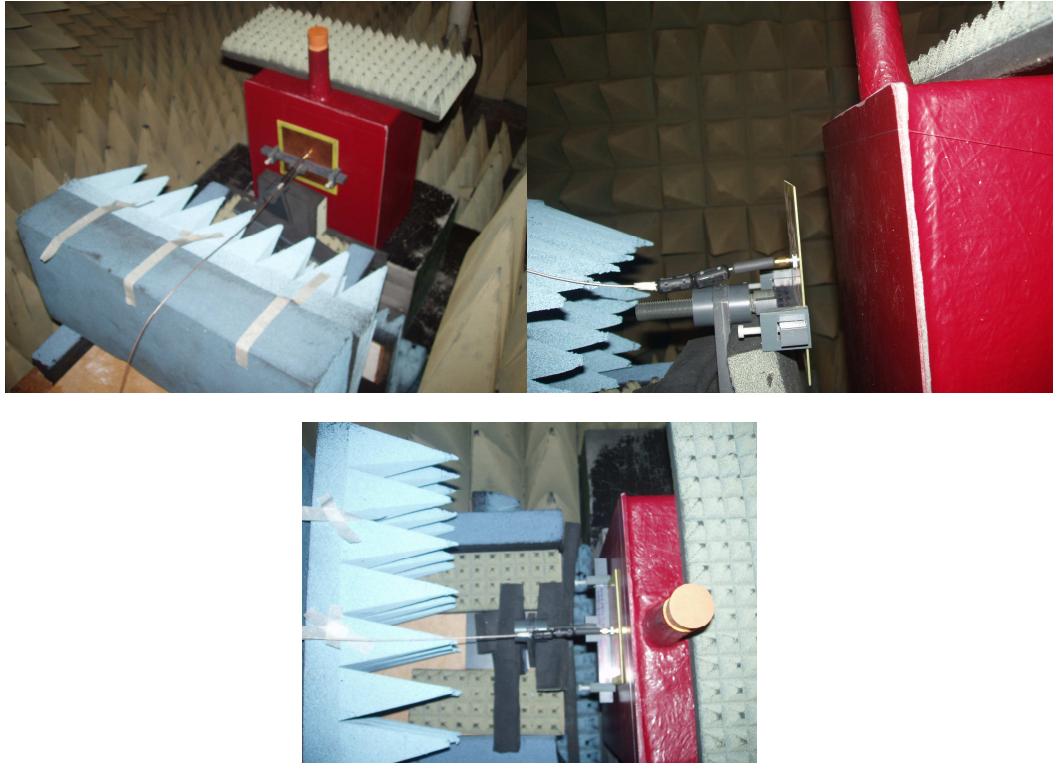
Figure 6-29: Measurement setup inside the anechoic chamber with floor covered with RF absorber.
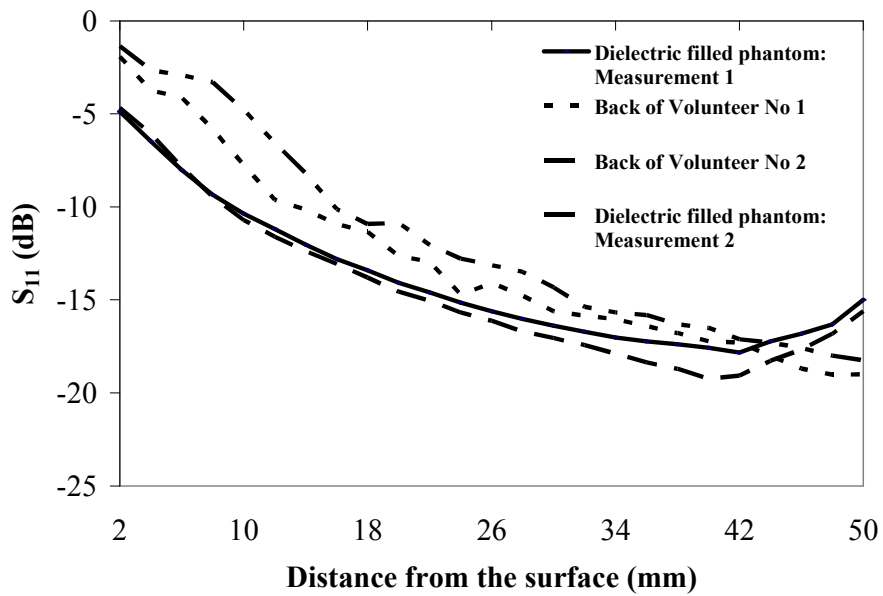
Figure 6-30: Comparison of S$_{11}$ (dB) between Dielectric Filled Phantom and Human Body for Circular Polarised Antenna at 1.8 GHz
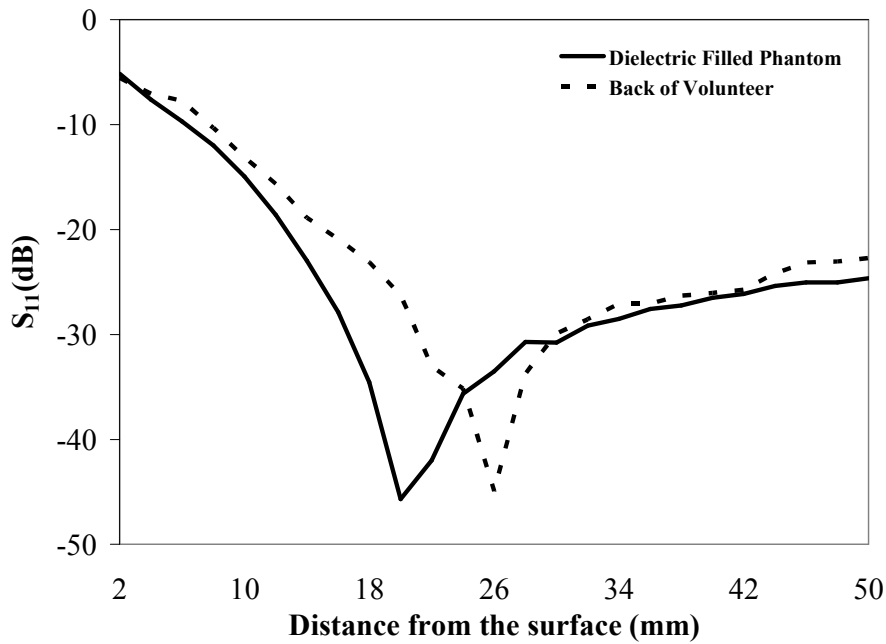
Figure 6-31: Comparison of S_{11} (dB) between Dielectric Filled Phantom and Human Body for Linearly Polarised Antenna at 1.8 GHz

To test the behaviour of an antenna with its main beam directed away from the surface a microstrip line linear polarised [108] and circular polarised [110] patch antennas shown in figure 6.30 were used to gather the results for return loss presented in Figure 6.31 and Figure 6.32. Since only the reduced back lobe of the antenna now interacts with the surface of the body or the phantom the rate of change of mismatch is now reduced and therefore the knee of the response is not as clear. However, the conclusions gained from the first set of experiments are still seen.
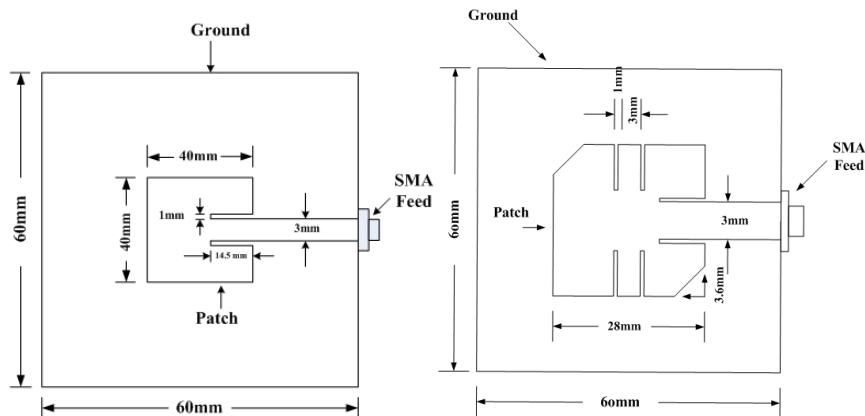
Figure 6-32: A line drawing of microstrip line linear and circular polarised patch antennas (Not to Scale).
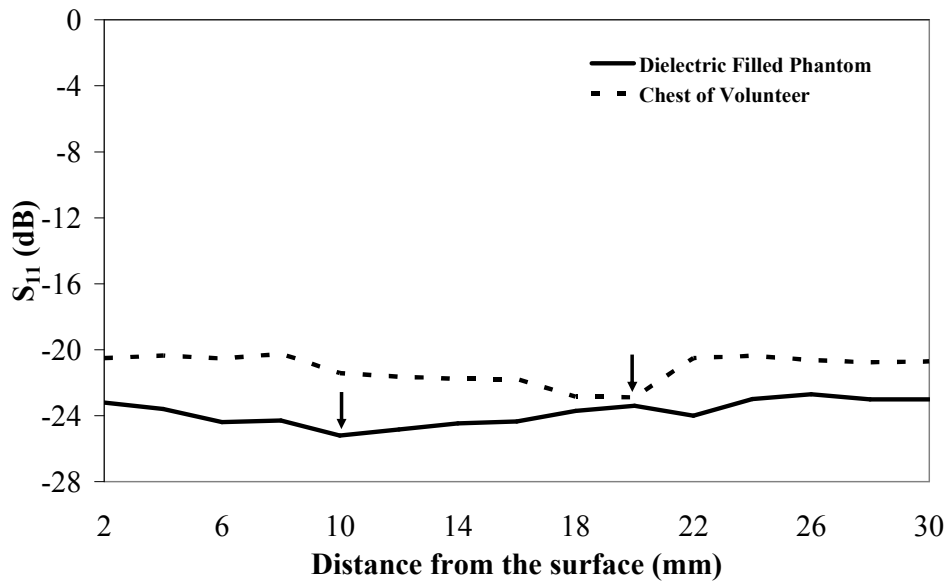
Figure 6-33: Comparison of S$_{11}$(dB) Measurements for Dielectric Liquid filled Phantom and Back of a Human Body for Microstrip line fed Linear Polarised Antenna at 1.8GHz
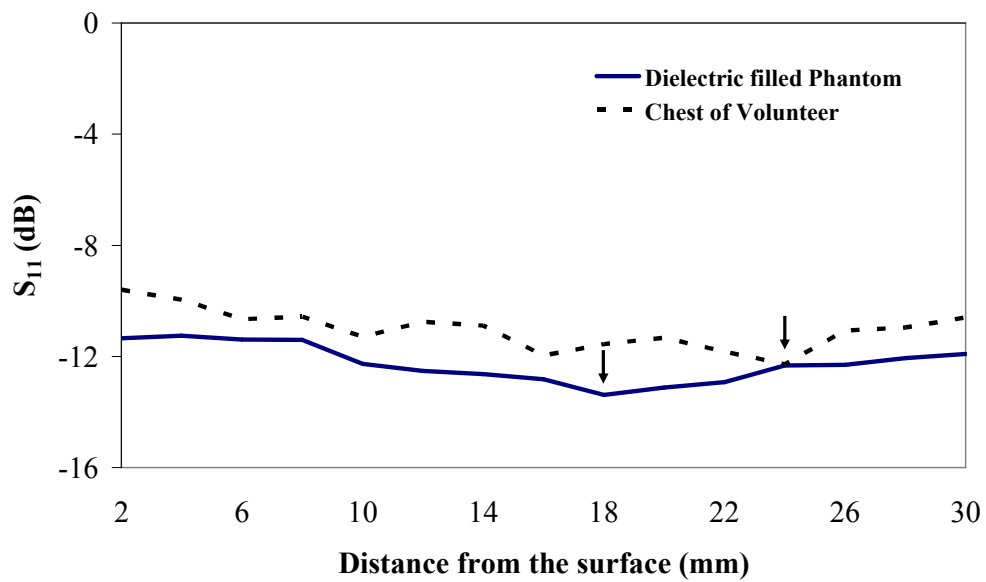
Figure 6-34: Comparison of S$_{11}$(dB) Measurements for Dielectric Liquid filled Phantom and Back of a Human Body for Microstrip line fed Circular Polarised Antenna at 1.8GHz

6.3.5 Conclusions:

It should also be noted that in use a patch antenna would normally have its main beam directed away from the body although not always. The body and the phantom also detune the patch to a lower operating frequency of resonance (the body more than the phantom) and that both have produced a broad-banding effect on the resonant curve. No correction has been made for this. It is also likely that since the phantom and body are finite and rectangular some effects due to polarisation and edges will be apparent between types of wearable antennas.

However we can reasonably draw the following general conclusions:-

The phantom changes the match of the antenna in a similar way to a human torso. Isolation distance should be increased when considering insulating layers of clothing for on body antennas if using a phantom of this type for tuning. Similarly considering the linear and circular polarization of the antenna, results suggest that the best match for circularly polarized antennas comes nearly at double the distance as of linearly polarised antenna.

6.4 Conclusion

This chapter gave an insight into on-body channels and effects of wetting the cloths have been investigated on on-body propagation channels by using quarter wave monopole and square loop antennas. The results showed that wet cloths gave a better propagation channel than dry cloths. The later section explains how Specific Anthropomorphic Mannequin (SAM) can deviate the final results from real human body measurements. The results showed that optimum return loss for SAM occurred before the one which occurred for real human body. Results presented here are useful in assessing optimal antenna/body separation for wearable antennas in Body Area Networks using both intra and inter wireless connectivity.

Chapter 7:
Conclusions and Future Work

7.1 Summary of Research

This thesis has covered the relevant material for on-body channel characterisation of antennas at microwave frequencies across the range 900MHz to 6GHz. This has included cabling errors associated with on-body measurements; on-body channel characterisation procedures and on-body propagation models. The novel part of this thesis has been concerned with the on-body channel characterisation for dry and wet clothing on a human body inside and outside of an anechoic chamber, the perturbation of patch antennas near a human body and dielectric filled human body simulating phantom and the effects of antenna polarisation on these perturbations at mobile communication frequencies.

A literature review of wearable antennas was given in Chapter 1 of wearable antenna design and applications. It was determined that wearable antennas have recently received growing interest due to the introduction of personal communications technology which provides momentum to make mobile phones smaller and simpler to carry and use. Clothing may now have a variety of consumer electronics incorporated into it and antennas are key components to such technology. So it was concluded to plan some on-body experiments to find out the effects of human body and SAM on antenna parameters and to characterise the on-body propagation channel for different conditions (Dry and Wet clothing) around a human volunteer wearing the antennas. These experiments were explained in Chapter 6.

Due to the flexible nature of coaxial cables in wearable antenna measurements, on-body measurements are always vulnerable to cabling errors, so the idea behind Chapter 2 was to introduce different types of cabling errors associated with on-body

measurements. Chapter 2 includes an introduction to the cabling errors that are connected with on-body measurements for wearable antennas, in which phase and amplitude errors linked with the surface currents on the coaxial cables, bending of the cables, mismatch losses and systematic errors are explained and possible solutions were also proposed. Later on this chapter also explained the permittivity and conductivity of a medium (biological matter) whose knowledge was necessary in order to find out the energy losses in human body.

In Chapter 3 some electrical properties of human body that is dielectric constant and conductivity, wave speed in human tissue, propagation of power through the human tissues and propagation trends around the human body were highlighted. The propagation trend of electromagnetic waves around the human body was explained by a lossy cylinder near an antenna. At the end of the chapter the interaction of human body with electromagnetic waves was explained and a review of human body effects on wearable antenna parameters were summarised.

The purpose of Chapter 4 has been to review the work of several leading authors who made significant contributions to the area of on body antenna measurements. In particular techniques used to propose propagation models for the on-body surface wave have been discussed. Three points would seem to be common. Firstly on body channels are highly dynamic. Secondly, ground planes and insulation layers between antennas and supporting tissue are particularly important. Lastly, many on body measurements can be done in quiet areas outside of an anechoic chamber.

Chapter 5 has discussed the application of techniques used in the measurement of wearable antennas. Normalised Site Attenuation measurements in anechoic chamber used to check performance have also been discussed. It was found that the available chamber performs within recommended limits across the range of frequencies that have been used in this work. Complimentary research was also undertaken to access the impact of absorber orientation and the addition of a polystyrene walkway. A novel

phone mount and tissue simulating liquid phantom, over the air (OTA) measurement to check the sensitivity of mobile phone, was also presented.

Chapter 6 gave an insight into on-body channels and effects of wetting the cloths have been investigated on on-body propagation channels by using quarter wave monopole and square loop antennas. The results showed that wet cloths gave a better propagation channel than dry cloths. The later section explain how Specific Anthropomorphic Mannequin (SAM) can deviated the final results from real human body measurements. The results showed that optimum return loss for SAM occurred before the one which occurred for real human body. Results presented here are useful in assessing optimal antenna/body separation for wearable antennas in Body Area Networks using both intra and inter wireless connectivity. Similarly considering the linear and circular polarization of the antenna, results suggest that the best match for circularly polarized antennas comes nearly at double the distance as of linearly polarised antenna.

7.2 Future Work Suggestions

This thesis has investigated the characterisation of on-body channel for dry and wet clothing at mobile communication frequencies using monopole and square loop antenna. Here in this thesis the effects of close proximity of human body and SAM has also been investigated linearly and circularly polarised patch antennas on FR4 substrate at 1.8GHz only. There are still more possibilities of performing all these measurements in different ways, which will help to quantify the results a bit more.

Firstly the on-body propagation channel can be characterised for MIMO (Multiple In Multiple Out) systems containing more than two antennas. MIMO systems are gaining popularity due the reason that in mobile radio channel suffers from the effects of multi path fading which contributes to inter signal interference and poor signal to noise ratio (SNR). To improve the quality of received signal, it is suggested that the

receiver should receive multiple copies of the transmitted signal which is the basic purpose of MIMO.

Secondly the antennas used in this research are rigid and not flexible, as we have designed one on high impedance surface, our next aim is to perform the experiments using flexible antennas.

Thirdly the effects of close proximity of human body and SAM has been investigated only at 1.8GHz due to the lack of body simulating liquid for 0.9 and 2.45GHz, so the solution for these frequencies can be made locally at Loughborough University and experiments can be re-performed to derive a comparison between different frequencies.

Fourthly dielectric resonator antennas (DRAs) can be used to find out the effects of the close proximity of human body to these antennas. The purpose of these antennas is that they low backlobes and provide with lesser interaction of human body with the antenna.

Lastly on-body channel characterisations can also be performed for different varieties of clothing and different races of human, which might be dependent on on-body propagation models.

Appendix A:

Select the Measurement

The Measurement Menu can be accessed by pressing the **Measurement** function hard key below the display. All VNA Master measurements can be found in the Measurement Menu. For S_{11} Log Magnitude and S_{21} Log Magnitude measurements, the Measurement Menu can be changed from the Field Menu to the VNA Menu by pressing the **Shift** key followed by the **System** (8) key, and selecting Applications Options. Press the Meas Menu soft key to select either Field or VNA.

Set the Frequency Range

Regardless of what measurement is being made, the frequency range for the desired measurement must be set before calibrating the VNA Master. Changing the frequency after calibration is performed will invalidate the calibration. Press the **Freq/Dist** function hard key below the display to bring up the Freq menu.

Setting the Start and Stop Frequencies

Set the Start Frequency by pressing Start Freq soft key and entering the desired frequency in Hz, kHz, MHz, or GHz using the keypad, the arrow keys, or the rotary knob. Set the Stop Frequency by pressing the Stop Freq soft key and entering the desired frequency in Hz, kHz, MHz, or GHz using the keypad, the arrow keys, or the rotary knob. The frequency range can also be set using the Center Freq and Freq Span soft keys. For example, to set a frequency range of 1850 to 1990 MHz, set the Center Frequency to 1920 MHz and the Frequency Span to 140 MHz.

Setting the Signal Standard

The Signal Standard list contains common frequency standards and displays the standard name, frequency of operation, and channel number. Selecting the Signal Standard soft key will display the list. Use the rotary knob or Up/Down arrow keys to highlight the desired signal standard. Once highlighted, press **Enter** to select the highlighted standard. The Center Frequency and Span will automatically tune to the first channel of the selected standard. Press Channel to enter the Channel number for

the selected Frequency Standard.

NOTE: The Start Frequency MUST be lower than the Stop Frequency.

Calibration

For accurate results, the VNA Master must be calibrated at the ambient temperature after allowing for warm up time and before making any measurements. The VNA Master must be re-calibrated whenever the setup frequency changes or when a test port extension cable is added, removed or replaced. The 1-port calibration is an OSL-calibration removing source match, directivity, and frequency response errors. The 2-port calibration is a 1-path 2-port calibration and removes transmission response errors and transmission source match errors in addition to reflection error terms.

1-Port Calibration Procedure (OSL)

Step 1. If a test port extension cable is to be used, connect the cable to the RF Out connector on the VNA Master. The calibration components will be connected at the end of the cable.

Step 2. Set the frequency range as described in the earlier section.

Step 3. Press the **Shift** key and then the **Calibrate** (2) key.

Step 4. Press the Start Cal soft key.

Step 5. Connect the Open to the RF Out port (or to the end of the test port extension cable) and press the **Enter** key.

Step 6. When prompted, connect the short to the RF Out port (or to the end of the test port extension cable) and press the **Enter** key.

Step 7. When prompted, connect the Load to the RF Out port (or to the end of the test port extension cable) and press the **Enter** key.

Step 8. Verify that calibration has been performed properly by checking that the Cal Status On message is now displayed at the top of the status window.

2-Port Calibration Procedure (OSLIT)

Step 1. If a test port extension cable is to be used, connect the cable to the RF Out

and/or RF In connector on the VNA Master. The calibration components will be connected at the end of the cable.

Step 2. Set the frequency range as described in the earlier section.

Step 3. Press the **Shift** key and then the **Calibrate** (2) key.

Step 4. Press the Cal Power soft key to set the power level to Low (-35 dBm) or High (0dBm).

Step 5. Press the Start Cal soft key.

Step 6. Connect the Open to the RF Out port (or to the end of the test port extension cable) and press the **Enter** key.

Step 7. When prompted, connect the short to the RF Out port (or to the end of the test port extension cable) and press the **Enter** key.

Step 8. When prompted, connect the Loads to the RF Out port (or to the end of the test port extension cable) and to the RF In port (or to the end of the test port extension cable) and press the **Enter** key.

Step 9. Connect the RF Out port to the RF In port, including any test port extension cables used in the prior steps, and press the **Enter** key.

Step 10. Verify that calibration has been performed properly by checking that the Cal Status On message is now displayed at the top of the status window.

Appendix B

Radio Frequency (RF) Absorbers

Objects that can absorb incident EM wave and convert these into a heat or which can cancel out the phase of the incident wave. They are also known as RAM (Radiation Absorbent Material).

The effectiveness of RAM is determined by the level of reflected waves form it that is for a good quality absorber the level of any reflected wave will be much smaller than the wave which is incident on it. Pyramidal shaped absorbers are commonly used which are made up of suitable lossy material. For a chamber to work effectively, all internal surfaces of the chamber must be covered with RAM. To be sufficiently lossy, RAM can neither be a good electrical conductor nor a good electrical insulator as neither type actually absorbs any power. It has to be an intermediate grade of material which absorbs power gradually in a controlled way as the incident wave penetrates it. Typically pyramidal RAM will comprise a rubberised foam material impregnated with controlled mixtures of carbon and iron [111].

Pyramidal-shaped absorber material is usually used for the frequency range from 1 GHz to 40 GHz. By adjusting the percentage of carbon loading of the foam a reflectivity of less than -60 dB can be obtained for normal incidence. For frequencies below 1 GHz, the required taper length of the pyramid becomes too bulky and difficult to be installed in an anechoic chamber. To achieve small reflectivity using electrically thin absorber material, a different carbon loading for the foam pyramids must be used. This can give a reflectivity of -20dB for the 200-1000MHz range, but this may not work for higher frequencies where more quietness is required [112].

On the other hand, ferrite tiles or grids, with thicknesses of about 6 mm, perform very well from 30 to 600 MHz, but their reflectivity go down as the frequency goes higher. In order to obtain an extremely wide operating frequency range - from 30MHz to 1 GHz - a combination of a pyramidal foam absorber on a ferrite tile is necessary. This configuration is called a hybrid absorber. The reflectivity of RF absorbers can also be improved by adding dielectric material between the ferrite and metal wall [112].

urethane

Ferrite Tiles

Metal wall
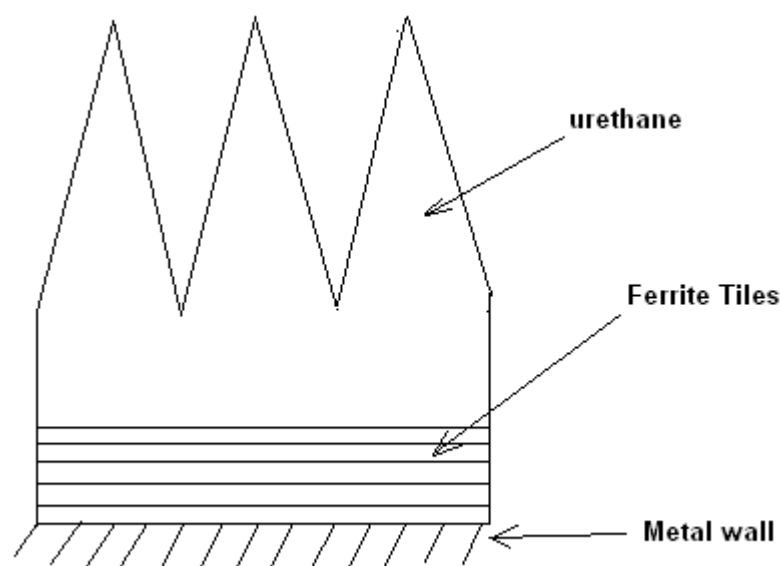
Ferrite Tile absorber

Effectiveness of RF Absorbers over Frequency

The performance quality of an RF anechoic chamber is determined at its lowest frequency of operation where the measured reflection inside the chamber are most significant compared to higher frequencies. Pyramidal RF absorbers are at their best when incident wave strikes it at right angle with its pyramid height equal to $\lambda / 4$, where λ is the free space wavelength. Increasing the size of pyramid beyond $\lambda / 4$ could improve its performance at low frequencies but it results in increase of cost and reduced unobstructed working volume [111].

At higher frequencies, where the wavelengths of electromagnetic waves are smaller compared to the dimensions of RF absorber and the wave sees a structure of pyramid, the incident wave undergoes several reflections with tapered side of the pyramids resulting in huge loss of energy. Similar reductions occur for the remaining (transmitted) wave which is then reflected from the metal wall. The overall reflection coefficient is then very low, since very little energy is left to re-emerge from the pyramids [111].

In order to apply the same arguments at low frequencies (or long wavelengths), the length of the pyramidal taper must be correspondingly increased. This leads to very large pyramids, which use excessive amounts of space in chambers. For example, at 30 MHz the pyramids would need to be 30 feet long. Fortunately, typical materials in absorbers have skin depths, which allow the wave to penetrate the absorber and can be dissipated at these frequencies [111].

Appendix C

Procedure of making call from Base Station Simulator (BSS):

1. Connect the supplied power cord to the **AGILENT 8922M/S TEST SET** and power up the instrument or select Preset Button.

2. Use the key '' **SHIFT**'' and '' **CELL CONFIGURE**'' and set the following fields.

3. SET ''**PAGING IMSI"—8010123456043**

4. SET'' **IMSI ATTACH AND DETACH – ON**.

5. Press '' **CELL CNTL**''

6. SET'' **OPERATING MODE"**

7. SELECT '' **CONFIG**'' Under '' **TO SCREEN**.

8. SET '' **RF LEVEL OFFSET dB"= ON**

9. SET ''**RF IN/OUT" = -40**

10. Press '' **CELL CONTROL"**

11. SET '' **AMPLITUDE" = -70dBm**

12. SET **MOBILE PHONE '' TX LEVEL" = 5 @ GSM 900; 1@ GSM 1800**

13. Insert the **TEST SIM CARD** in the Mobile phone.

14. Power ON the mobile phone

15. After a few moments it should register with the test-set and 'camp' on the 8922s Network. (Most mobile phones display **001-01** when the mobile phone has camped.

Once these parameters given above are changed, we can make call from BSS as follows:

1. Press **ORIGINATE CALL**

2. Accept the call from the test set.

3. The connection status field changes from **ATTACHED** to **SET-UP REQEST** and then to **CONNECTED** when the call is established.

Procedure for Sensitivity Measurements:

1. Set the test-rig for the measurement as per as the figure shown above. Connection to the BSS using appropriate connection protocols-GSM

2. Start the phone call with the BSS and place it in *loop back mode**.

3. Rotate the phone to an angle of 30˚, set the output power level of BSS and record the BER.

4. Raise or lower the BSS Output power until the BER= Reference BER (2.44%GSM).

5. Repeat all angles (30˚) in both theta (θ) and phi (Ø) polarisations.

6. The test involves of making 60 Measurements at different positions on the sphere, which are integrated to yield a single figure of merit known as TOTAL ISOTROPIC SENSITIVITY (TIS).

7. Both polarisations are measured turning the dual-polarized antenna automatically.

8. Both field components are calculated as a completed field during post processing.

* In loop back mode, the BSS transmits a bit pattern to the phone and the phone transmits it back. The returned bit pattern is then compared and the BER is determined.

Appendix D

Snapshots of the software developed for calculating the Total Isotropic Sensitivity (TIS) and Total Radiated Power (TRP) of the mobile phone:
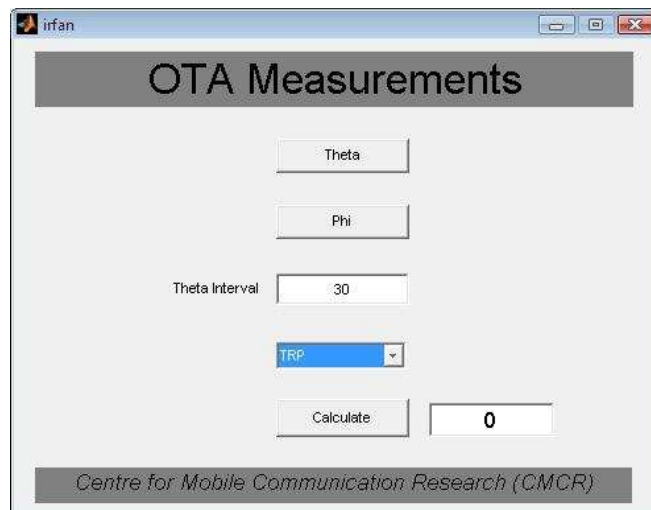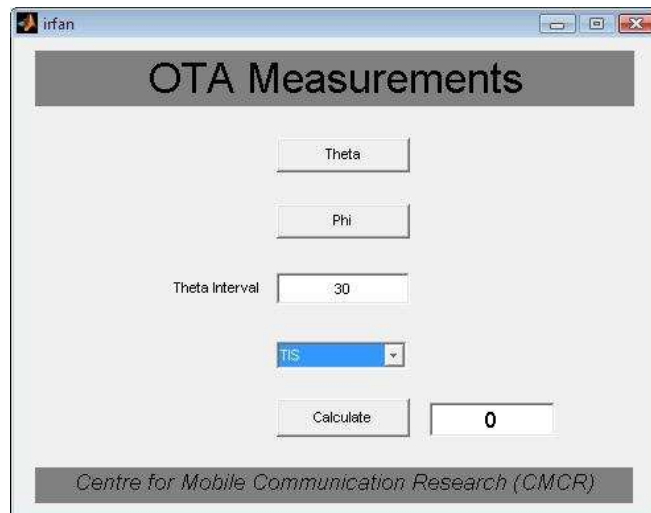
Code of the software used to calculated Total Isotropic Sensitivity (TIS) and Total Radiated Power (TRP) of the mobile phone:

```
function varargout = irfan(varargin)

% IRFAN M-file for irfan.fig
%      IRFAN, by itself, creates a new IRFAN or raises the existing
%      singleton*.
%
%      H = IRFAN returns the handle to a new IRFAN or the handle to
%      the existing singleton*.
%
%      IRFAN('CALLBACK',hObject,eventData,handles,...) calls the local
%      function named CALLBACK in IRFAN.M with the given input arguments.
%
%      IRFAN('Property','Value',...) creates a new IRFAN or raises the
%      existing singleton*.  Starting from the left, property value pairs
are
%      applied to the GUI before irfan_OpeningFunction gets called.  An
%       unrecognized property name or invalid value makes property
application
%      stop.  All inputs are passed to irfan_OpeningFcn via varargin.
%
%      *See GUI Options on GUIDE's Tools menu.  Choose "GUI allows only
one
%      instance to run (singleton)".
%
% See also: GUIDE, GUIDATA, GUIHANDLES

% Edit the above text to modify the response to help irfan

% Last Modified by GUIDE v2.5 06-Dec-2009 20:47:29

% Begin initialization code - DO NOT EDIT
gui_Singleton = 1;
gui_State = struct('gui_Name',       mfilename, ...
                   'gui_Singleton',  gui_Singleton, ...
                   'gui_OpeningFcn', @irfan_OpeningFcn, ...
                   'gui_OutputFcn',  @irfan_OutputFcn, ...
                   'gui_LayoutFcn',  [] , ...
                   'gui_Callback',   []);
if nargin && ischar(varargin{1})
   gui_State.gui_Callback = str2func(varargin{1});
end
```

```matlab
if nargout
    [varargout{1:nargout}] = gui_mainfcn(gui_State, varargin{:});
else
    gui_mainfcn(gui_State, varargin{:});
end
global piData;
global thetaData;
%piData=[];
%thetaData=[];
% End initialization code - DO NOT EDIT


% --- Executes just before irfan is made visible.
function irfan_OpeningFcn(hObject, eventdata, handles, varargin)
% This function has no output args, see OutputFcn.
% hObject    handle to figure
% eventdata  reserved - to be defined in a future version of MATLAB
% handles    structure with handles and user data (see GUIDATA)
% varargin   command line arguments to irfan (see VARARGIN)

% Choose default command line output for irfan
handles.output = hObject;

% Update handles structure
guidata(hObject, handles);

% UIWAIT makes irfan wait for user response (see UIRESUME)
% uiwait(handles.figure1);


% --- Outputs from this function are returned to the command line.
function varargout = irfan_OutputFcn(hObject, eventdata, handles)
% varargout  cell array for returning output args (see VARARGOUT);
% hObject    handle to figure
% eventdata  reserved - to be defined in a future version of MATLAB
% handles    structure with handles and user data (see GUIDATA)

% Get default command line output from handles structure
varargout{1} = handles.output;


% --- Executes on button press in pushbutton1.
function pushbutton1_Callback(hObject, eventdata, handles)
```

```matlab
[FileName,PathName] = uigetfile('*.xlsx','Select the M-file');
global thetaData;
thetaData=xlsread([PathName,FileName]);


% hObject    handle to pushbutton1 (see GCBO)
% eventdata  reserved - to be defined in a future version of MATLAB
% handles    structure with handles and user data (see GUIDATA)




% --- Executes on button press in pushbutton2.
function pushbutton2_Callback(hObject, eventdata, handles)
[FileName,PathName] = uigetfile('*.xlsx','Select the M-file');
global piData;
piData=xlsread([PathName,FileName]);


% hObject    handle to pushbutton2 (see GCBO)
% eventdata  reserved - to be defined in a future version of MATLAB
% handles    structure with handles and user data (see GUIDATA)


% --- Executes during object creation, after setting all properties.
function figure1_CreateFcn(hObject, eventdata, handles)
% hObject    handle to figure1 (see GCBO)
% eventdata  reserved - to be defined in a future version of MATLAB
% handles    empty - handles not created until after all CreateFcns called

function TISVal=TIS(piData,thetaData,thetaInterval)
[M,N]=size(piData);
[M2,N2]=size(thetaData);

if ((M==0)|(M2==0)|(N==0)|(N2==0))
    h = msgbox('Phi or Theta File not selected properly','Error','error');
    close(handles.gui);
end

if ((M~=M2) | (N~=N2))
    h = msgbox('Phi and Theta Dimensions do not agree','Error','error');
    close(handles.gui);
end

theta=thetaInterval;
phi=30;
%data1=xlsFilePi;
```

```matlab
%data2=xlsFileTheta;
data1=piData;
data2=thetaData;
TISVal=0;
temp=double(0);
temp2=0;
for i=2:N
    for j=1:M

temp2=((1/double(data1(j,i)))+(1/double(data2(j,i))))*sin(deg2rad(the
ta));
        temp=temp+ temp2;
         phi=phi+30;
    end
theta=theta+thetaInterval;
end


TISVal=(2*N*M)/(pi*temp);




% --- Executes on button press in pushbutton3.
function pushbutton3_Callback(hObject, eventdata, handles)

global piData;
global thetaData;
thetaInterval=get(handles.edit1,'String');
%piData
%thetaData
 if (get(handles.popupmenu1,'Value')==1)
   myResult=TIS(piData,thetaData,str2num(thetaInterval));
 else
    myResult=1/TIS(piData,thetaData,str2num(thetaInterval));
 end
set(handles.edit3,'String',num2str(myResult));

% hObject    handle to pushbutton3 (see GCBO)
% eventdata  reserved - to be defined in a future version of MATLAB
% handles    structure with handles and user data (see GUIDATA)
```

```
function edit1_Callback(hObject, eventdata, handles)
% hObject    handle to edit1 (see GCBO)
% eventdata  reserved - to be defined in a future version of MATLAB
% handles    structure with handles and user data (see GUIDATA)

% Hints: get(hObject,'String') returns contents of edit1 as text
%        str2double(get(hObject,'String')) returns contents of edit1 as
a double


% --- Executes during object creation, after setting all properties.
function edit1_CreateFcn(hObject, eventdata, handles)
% hObject    handle to edit1 (see GCBO)
% eventdata  reserved - to be defined in a future version of MATLAB
% handles    empty - handles not created until after all CreateFcns called

% Hint: edit controls usually have a white background on Windows.
%       See ISPC and COMPUTER.
if      ispc      &&      isequal(get(hObject,'BackgroundColor'),
get(0,'defaultUicontrolBackgroundColor'))
    set(hObject,'BackgroundColor','white');
end


function edit3_Callback(hObject, eventdata, handles)
% hObject    handle to edit3 (see GCBO)
% eventdata  reserved - to be defined in a future version of MATLAB
% handles    structure with handles and user data (see GUIDATA)

% Hints: get(hObject,'String') returns contents of edit3 as text
%        str2double(get(hObject,'String')) returns contents of edit3 as
a double


% --- Executes during object creation, after setting all properties.
function edit3_CreateFcn(hObject, eventdata, handles)
% hObject    handle to edit3 (see GCBO)
% eventdata  reserved - to be defined in a future version of MATLAB
% handles    empty - handles not created until after all CreateFcns called

% Hint: edit controls usually have a white background on Windows.
%       See ISPC and COMPUTER.
```

```matlab
if        ispc        &&        isequal(get(hObject,'BackgroundColor'),
get(0,'defaultUicontrolBackgroundColor'))
    set(hObject,'BackgroundColor','white');
end




% --- Executes on selection change in popupmenu1.
function popupmenu1_Callback(hObject, eventdata, handles)
% hObject    handle to popupmenu1 (see GCBO)
% eventdata  reserved - to be defined in a future version of MATLAB
% handles    structure with handles and user data (see GUIDATA)

% Hints: contents = get(hObject,'String') returns popupmenu1 contents as
cell array
%          contents{get(hObject,'Value')} returns selected item from
popupmenu1


% --- Executes during object creation, after setting all properties.
function popupmenu1_CreateFcn(hObject, eventdata, handles)
% hObject    handle to popupmenu1 (see GCBO)
% eventdata  reserved - to be defined in a future version of MATLAB
% handles    empty - handles not created until after all CreateFcns called

% Hint: popupmenu controls usually have a white background on Windows.
%      See ISPC and COMPUTER.
if        ispc        &&        isequal(get(hObject,'BackgroundColor'),
get(0,'defaultUicontrolBackgroundColor'))
    set(hObject,'BackgroundColor','white');
end
```

Appendix E

MICROWAVE BICONICAL BROADBAND ANTENNA SBA 9119

SPECIFICATIONS

LINEAR POLARISED MICROWAVE BICONICAL BROADBAND ANTENNA

NOMINAL FREQUENCY RANGE:	1 - 6 GHZ
USEABLE FREQUENCY RANGE:	0.5 - 6.5 GHZ
CONNECTOR:	FEMALE 50 Ω N
MOUNTING TUBE:	LH=560MM, D=22 MM
INDEX RING:	LR=190MM
ELEMENT LENGTH TOTAL:	LE = 50 MM
ELEMENT DIAMETER:	D = 28 MM
ISOTROPIC GAIN:	TYP. -10....+2 DBI
	(1 - 6 GHZ)
ANTENNA FACTOR:	32 ... 48 DB/M
	(1.5-5GHZ)

Description

The SBA 9119 has two main applications:

A passive field probe for frequency selective measurements of the generated field according to EN 61000-4-3, including the measurement of the uniform area. A further application is the validation of fully anechoic rooms for measurements above 1 GHz according the Site-VSWR-method, described in CISPR 16-1-4. In conjunction with the SBA 9112 a frequency range from 1 to 18 GHz can be covered with excellent antenna performance. Accepting some limitations (i.e. Antenna Factor and VSWR increase, symmetry reduction) the SBA 9119 can be used from 0.5 GHz on. The validation of test sites with commonly used Microwave antennas (e.g. Log.-Per. or Horn Antennas) leads to insufficient results, since these directive gain antennas with concentrated directional pattern do not take the test site characteristics into account.

Application

The typical applications of the microwave biconical Antenna are the evaluation of test sites, the (frequency selective) field strength measurement and the generation of defined field strength (e.g. ERP or EIRP). Thanks to the wide bandwidth there is no need for a time consuming change of the antenna elements as required when operating with tuned half-wave dipoles. The biconical elements allow a continuos sweep over the complete frequency range. Because of the dipole-like directional pattern, the fixed phase center and the high power handling capability the SBA 9119 may replace tuned half-wave dipoles in many applications. The SBA 9119 is not intended for emission testing with very low limits, horn and Log.-Per. Antennas are better matched for this purpose because of their better antenna factor. A typical application of the SBA 9119 is the use as a (highly linear) broadband nearfield probe thanks to its small dimensions.

Frequency MHz	Antenna Factor (dB/m)
501.5	55.4
519	55.82
540	56.16
561	55.53
578.5	54.32
599.5	52.81
620.5	51.84
641.5	51.15
659	50.96
680	50.21
701	49.77
718.5	49.08
739.5	48.67
760.5	48.08
781.5	47.55
799	46.79
820	46.25
841	45.48
858.5	44.83
879.5	44.05
900.5	43.42
921.5	42.86
939	42.36
960	41.94
981	41.53
998.5	41.06
1019.5	40.37
1040.5	39.83
1061.5	39.19
1079	38.73
1100	38.02
1121	37.53
1138.5	37
1159.5	36.47
1180.5	35.83
1201.5	35.19
1219	34.69
1240	34.12
1261	33.62
1278.5	33.15
1299.5	32.85

1320.5	32.62
1341.5	32.32
1359	32.24
1380	32.08
1401	32.1
1418.5	31.97
1439.5	31.95
1460.5	31.98
1481.5	32.08
1499	32.28
1520	32.49
1541	32.81
1558.5	33.01
1579.5	33.19
1600.5	33.27
1621.5	33.46
1639	33.64
1660	33.77
1681	33.9
1698.5	34.03
1719.5	34.29
1740.5	34.44
1761.5	34.61
1779	34.81
1800	35.06
1821	35.24
1838.5	35.31
1859.5	35.49
1880.5	35.71
1901.5	35.97
1919	36.2
1940	36.4
1961	36.64
1978.5	36.75
1999.5	36.88
2020.5	37.05
2041.5	37.31
2059	37.6
2080	37.7
2101	37.65
2118.5	37.61

2139.5	37.53
2160.5	37.5
2181.5	37.51
2199	37.64
2220	37.77
2241	37.76
2258.5	37.75
2279.5	37.94
2300.5	38.27
2321.5	38.59
2339	38.86
2360	39.14
2381	39.4
2398.5	39.55
2419.5	39.55
2440.5	39.53
2461.5	39.46
2479	39.4
2500	39.35
2521	39.36
2538.5	39.34
2559.5	39.34
2580.5	39.41
2601.5	39.54
2619	39.69
2640	39.73
2661	39.75
2678.5	39.75
2699.5	39.86
2720.5	39.86
2741.5	39.93
2759	40.07
2780	40.19
2801	40.33
2818.5	40.3
2839.5	40.4
2860.5	40.55
2881.5	40.61
2899	40.72
2920	40.75
2941	40.77

2962	40.63
2979.5	40.42
3000.5	40.31
3021.5	40.32
3039	40.38
3060	40.4
3081	40.54
3098.5	40.7
3119.5	40.9
3140.5	40.99
3161.5	41.1
3179	41.21
3200	41.28
3221	41.21
3238.5	41.26
3259.5	41.25
3280.5	41.32
3301.5	41.21
3319	41.16
3340	41.21
3361	41.23
3378.5	41.21
3399.5	41.14
3420.5	41.16
3441.5	41.28
3459	41.25
3480	41.38
3501	41.42
3518.5	41.56
3539.5	41.53
3560.5	41.52
3581.5	41.57
3599	41.53
3620	41.47
3641	41.38
3658.5	41.42
3679.5	41.45
3700.5	41.44
3721.5	41.47
3739	41.54
3760	41.66

3781	41.64
3798.5	41.62
3819.5	41.65
3840.5	41.65
3861.5	41.71
3879	41.74
3900	41.89
3921	42.04
3938.5	42.04
3959.5	41.97
3980.5	41.85
4001.5	41.83
4019	41.72
4040	41.72
4061	41.78
4078.5	41.97
4099.5	42.07
4120.5	42.07
4141.5	42.09
4159	42.06
4180	42.03
4201	42.04
4218.5	42.12
4239.5	42.29
4260.5	42.33
4281.5	42.31
4299	42.27
4320	42.25
4341	42.19
4358.5	42.08
4379.5	42.12
4400.5	42.25
4421.5	42.4
4439	42.42
4460	42.4
4481	42.43
4498.5	42.41
4519.5	42.35
4540.5	42.3
4561.5	42.37
4579	42.53

4600	42.62
4621	42.73
4638.5	42.78
4659.5	42.77
4680.5	42.74
4701.5	42.66
4719	42.72
4740	42.78
4761	42.93
4778.5	43.06
4799.5	43.17
4820.5	43.16
4841.5	43.11
4859	43.06
4880	43.08
4901	43.1
4922	43.15
4939.5	43.18
4960.5	43.22
4981.5	43.21
4999	43.17
5020	43.24
5041	43.42
5058.5	43.64
5079.5	43.76
5100.5	43.76
5121.5	43.86
5139	43.87
5160	43.84
5181	43.81
5202	43.88
5219.5	44.1
5240.5	44.39
5261.5	44.44
5279	44.37
5300	44.11
5321	44.04
5338.5	43.98
5359.5	44.08
5380.5	44.24
5401.5	44.46

5419	44.67
5440	44.84
5461	45.06
5478.5	45.13
5499.5	45.18
5520.5	45.35
5541.5	45.49
5559	45.6
5580	45.58
5601	45.66
5618.5	45.74
5639.5	45.69
5660.5	45.65
5681.5	45.58
5699	45.58
5720	45.51
5741	45.58
5758.5	45.85
5779.5	46.19
5800.5	46.62
5821.5	46.87
5839	46.77
5860	46.45
5881	46.11
5898.5	46.3
5919.5	46.69
5940.5	47.27
5961.5	47.67
5979	47.99
6000	48.14

References

[1] J. D. Krauss, "Antennas," *2nd Edition, New York ; London, McGraw- Hill,* 1992.

[2] C. A. Balanis, "Antenna theory analysis and design," *John Wily & Sons Inc,* 1997.

[3] S. FUJIWARA, "Antenna Effect of Human Body towards Electromagnetic Waves in Space," *Analytical Sciences,* vol. 6, pp. 143-144, 1990.

[4] M. Klemm and G. Troester, "EM energy absorption in the human body tissues due to UWB antennas," *Progress in Electromagnetics Research,* vol. 62, pp. 261–280, 2006.

[5] Wen-Tzu Chen and Huey-Ru Chuang, "Human body coupling effects on radiation characteristics of superquadric loop antennas for pagers' applications," *IEEE Antennas and Propagation Society, International Symposium, Montreal, Canada, July 1997, Pp. 1190-1193,* July 1997.

[6] K. Yoshida, A. Hirata, Z. Kawasaki and T. Shiozawa, "Human Head Modeling for Handset Antenna Design at 5 GHz Band," *Journal of Electromagnetic Waves and Applications,* vol. 19, pp. 401-411, 2005.

[7] S. M. Abdelsayed and N. K. N. M. J. Deen, "Radiation characteristics of loop antennas for biomedical implants," *XXVIIIth," General Assembly of the International Union of Radio Science CDROM,* 2005.

[8] Y. Okano and K. Ito, "Radiation characteristics of small slot antenna for wristwatch-type pager worn on human body," *Electronics & Communications in Japan, Part I: Communications(English Translation of Denshi Tsushin Gakkai Ronbunshi),* vol. 83, pp. 93-101, 2000.

[9] Z. N. Chen, A. Cai, T. S. P. See, X. Qing and M. Y. W. Chia, "Small planar UWB antennas in proximity of the human head," *IEEE Trans. Microwave Theory Tech.,* vol. 54, pp. 1846, 2006.

[10] N. Cho, J. Yoo, S. J. Song, J. Lee, S. Jeon and H. J. Yoo, "The human body characteristics as a signal transmission medium for intrabody communication," *IEEE Trans. Microwave Theory Tech.,* vol. 55, pp. 1080-1086, 2007.

[11] D. Marculescu, R. Marculescu, S. Park and S. Jayaraman, "Ready to ware," *IEEE Spectrum,* vol. 40, pp. 28-32, 2003.

[12] J. Lebaric and A. T. Tan, "Ultra-wideband RF helmet antenna," in *MILCOM 2000. 21st Century Military Communications Conference Proceedings,* Vol. 1, pp.591-594, 2000.

[13] R. Abramo, R. Adams, F. Canez, H. Price and P. Haglind, "Fabrication and testing of the COMVIN vest antenna," in *IEEE MILCOM,* Vol 1, pp. 595–598, 2000.

[14] E. Fear, S. Hagness, P. Meaney, M. Okoniewski and M. Stuchly, "Enhancing breast tumor detection with near-field imaging," *IEEE Microwave Magazine,* vol. 3, pp. 48-56, 2002.

[15] S. C. Hagness, A. Taflove and J. E. Bridges, "Two-dimensional FDTD analysis of a pulsed microwave confocal system for breast cancer detection: Fixed-focus and antenna-array sensors," *IEEE Transactions on Biomedical Engineering,* vol. 45, pp. 1470-1479, 1998.

[16] A. Smailagic, D. P. Siewiorek, R. Martin and J. Stivoric, "Very Rapid Prototyping of Wearable Computers: A Case Study of VuMan 3 Custom versus Off-the-Shelf Design Methodologies," *Des. Autom. Embedded Sys.,* vol. 3, pp. 219-232, 1998.

[17] J. Rantanen, T. Karinsalo, M. Mäkinen, P. Talvenmaa, M. Tasanen, J. Vanhala, N. Alfthan, J. Impiö, M. Malmivaara and R. Matala, "Smart clothing for the arctic environment," *Fourth International Symposium on Wearable Computers,* Atlanta, GA, Oct. 16-17, pp.15-23, 2000.

[18] J. Rantanen, T. Vuorela, K. Kukkonen, O. Ryynanen, A. Siili and J. Vanhala, "Improving human thermal comfort with smart clothing," in *2001 IEEE International Conference on Systems, Man, and Cybernetics,* 2001.

[19] J. W. Hines, "Medical and surgical applications of space biosensor technology," *Acta Astronaut.,* vol. 38, pp. 261-267, 1996.

[20] S. Park and S. Jayaraman, "Enhancing the quality of life through wearable technology," *IEEE Engineering in Medicine and Biology Magazine,* vol. 22, pp. 41-48, 2003.

[21] C. Pattichis, E. Kyriacou, S. Voskarides, M. Pattichis, R. Istepanian and C. N. Schizas, "Wireless telemedicine systems: an overview," *IEEE Antennas and Propagation Magazine,* vol. 44, pp. 143-153, 2002.

[22] i. Medtronic, "http://www.medtronic.com,"

[23] J. Cavuoto, "Neural engineering's image problem," *IEEE Spectrum,* vol. 41, pp. 32-37, 2004.

[24] R. Weir, P. Troyk, G. DeMichele and T. Kuiken, "Implantable myoelectric sensors (IMES) for upper-extremity prosthesis control-preliminary work," *Proceedins of EMBS Conference,* Cancun, Mexico, September 16-21, 2003, pp.1562-1565.

[25] W. Wiatr, "A broadband technique for one-port calibration of VNA," in *Microwaves and Radar, 1998. MIKON '98., 12th International Conference on,* 1998, pp. 363-367 vol.2.

[26] W. Wiatr, "A broadband technique for one-port VNA calibration and characterization of low-loss two-ports," in *Precision Electromagnetic Measurements Digest, 1998 Conference on,* 1998, pp. 432-433.

[27] V. Adamian, "Simplified automatic calibration of a vector network analyzer (VNA)," in *ARFTG Conference Digest-Fall, 44th,* 1994, pp. 1-9.

[28] U. Stumper, "Uncertainties of VNA S-parameter measurements applying the short-open-load-reciprocal (SOLR) calibration method," in *Precision Electromagnetic Measurements Digest, 2008. CPEM 2008. Conference on,* 2008, pp. 438-439.

[29] U. Stumper, "Influence of calibration uncertainties on VNA S-parameter measurements," in *Precision Electromagnetic Measurements, 2002. Conference Digest 2002 Conference on,* 2002, pp. 132-133.

[30] J. M. Golio, *The RF and Microwave Handbook.* CRC Pr I Llc, 2001, pp. 4.17-4.20.

[31] J. Demarinis, "The antenna cable as a source of error in EMI measurements," in *IEEE 1988 International Symposium on Electromagnetic Compatibility, 1988. Symposium Record.* 1988, pp. 9-14.

[32] M. I. Khattak, R. M. Edwards, S. Bashir, L. Ma, "A study of the on-body channel for a human male with wet and dry clothing," in WWRF 21st Meeting, 13th – 15th October 2008, Stockholm, Sweden.

[33] P. Clements, "Electrical Length Stability of Coaxial Cable in a Field Environment," *Techinal Report 32-1526,* Vol. VII, pp.97-100, Jet Propulsion Laboratory, Pasadena, Calif, February 15, 1972.

[34] D. Schnelle and R. Wetmore, "Evaluation of antenna and receiver mismatch effects on DTV reception," *IEEE Trans. Broadcast.,* vol. 48, pp. 365-369, 2002.

[35] S. Saario, D. V. Thiel, J. Lu and S. G. O'Keefe, "An assessment of cable radiation effects on mobile communications antenna measurements," in *IEEE Antennas and Propagation Society International Symposium,* 1997, pp. 24-24.

[36] C. Icheln, J. Ollikainen and P. Vainikainen, "Reducing the influence of feed cables on small antenna measurements," *Electron. Lett.,* vol. 35, pp. 1212, 1999.

[37]   http://en.wikipedia.org/wiki/Permittivity

[38] Italian National research Council, Institute for Applied Physics (Italy) Http://niremf.ifac.cnr.it/tissprop/htmlclie/htmlclie.htm#atsftag.

[39] W. Scanlon and N. Evans, "Numerical analysis of bodyworn UHF antenna systems," *Electronics & Communication Engineering Journal,* vol. 13, pp. 53-64, 2001.

[40] C. Johnson and A. Guy, "Nonionizing electromagnetic wave effects in biological materials and systems," *Proc IEEE,* vol. 60, pp. 692-718, 1972.

[41] F. T. Ulaby, R. K. Moore and A. K. Fung, "Microwave remote sensing: active and passive," *Artech House, Norwood, MA,* vol. 3, 1986.

[42] G. Roqueta, A. Fort, C. Craeye and C. Oestges, "Analytical propagation models for body area networks," in *Antennas and Propagation for Body-Centric Wireless Communications, 2007 IET Seminar on,* 2007, pp. 90-96.

[43] D. K. Cheng, *Field and Wave Electromagnetics.* Addison-Wesley Reading, MA, 1989.

[44] D. A. McNamara, C. W. I. Pistorius and J. Malherbe, *Introduction to the Uniform Geometrical Theory of Diffraction.* Artech House Norwood, MA, 1990.

[45] A. Fort, J. Ryckaert, C. Desset, P. De Doncker, P. Wambacq and L. Van Biesen, "Ultra-wideband channel model for communication around the human body," *IEEE J. Select. Areas Commun.,* vol. 24, pp. 927, 2006.

[46] H. Hashemi, "The indoor radio propagation channel," *Proc IEEE,* vol. 81, pp. 943-968, 1993.

[47] R. W. Y. Habash, *Electromagnetic Fields and Radiation: Human Bioeffects and Safety.* CRC, 2001.

[48] D. Poljak, *Electromagntec Modelling of Wire Antenna Structures.* WIT Press i Computational Mechanics Inc., 2002.

[49] D. Poljak, C. Y. Tham and N. Kovac, "The assessment of human exposure to low frequency and high frequency electromagnetic fields using the boundary element analysis," *Eng. Anal. Boundary Elements,* vol. 27, pp. 999-1007, 2003.

[50] S. Ullah, H. Higgin, M. A. Siddiqui and K. S. Kwak, "A study of implanted and wearable body sensor networks," *Lecture Notes in Computer Science,* vol. 4953, pp. 464, 2008.

[51] M. Schallner, J. Waldmann, S. Hübner and F. Landstorfer, "The Influence of the Human Body on Electric and Magnetic Field Components in the Immediate Vicinity of the Body," .

[52] M. Sanad, "Effect of the human body on microstrip antennas," in *Antennas and Propagation Society International Symposium, 1994. AP-S. Digest,* 1994, .

[53] O. P. Gandhi, *Biological Effects and Medical Applications of Electromagnetic Energy.* Prentice-Hall Englewood Cliffs, NJ, 1990.

[54] R. Adey, E. Albert, S. Allen, J. Allis, P. Barber, H. Bassen, E. Berman, C. Blackman, R. Carpenter and K. Chen, "Biological effects and medical applications of electromagnetic energy," *Proc IEEE,* vol. 68, pp. 5, 1980.

[55] A. Fort, C. Desset, J. Ryckaert, P. De Doncker, L. Van Biesen and P. Wambacq, "Characterization of the ultra wideband body area propagation channel," *Proc. IEEE Int. Conf. Ultra Wideband (ICU),* Zurich, Switzerland, Sep. 2005, pp. 22-27.

[56] A. Fort, C. Desset, P. De Doncker, P. Wambacq and L. Van Biesen, "An ultra-wideband body area propagation channel model-from statistics to implementation," *IEEE Trans. Microwave Theory Tech.,* vol. 54, pp. 1820, 2006.

[57] Skycross., "http://www.skycross.com,"

[58] A. Guraliuc, A. Serra, P. Nepa, G. Manara, F. Potortì and P. Barsocchi, "Body Posture/Activity Detection: Path Loss Characterization for 2.4 GHz On-Body Wireless Sensors,"

 http://fly.isti.cnr.it/curriculum/papers/pdf/PosturePathLoss-APS09.pdf, 2005.

[59] http://www.xbow.com

[60] A. Alomainy, Y. Hao, A. Owadally, C. G. Parini, Y. Nechayev, C. C. Constantinou and P. S. Hall, "Statistical analysis and performance evaluation for on-body radio propagation with microstrip patch antennas," *IEEE Transactions on Antennas and Propagation,* vol. 55, pp. 245, 2007.

[61] P. Hall and Y. Hao, "Antennas and Propagation for Body Centric Communications Systems," *Artech House, Norwood, MA, USA,* pp. 1-58053, 2006.

[62] P Hall, Y Nechayev, A. Alomainy, Y Hao, A Owadally, C Constantinou and C Parini, "On-body communications channel characterisation for wearable computer systems," in *IEEE/ACES Int. Conf. Wireless Communications and Applied Computational Electromagnetics, Honolulu, HI,2005.*

[63] Y. I. Nechayev, P. S. Hall, C. C. Constantinou, Y. Hao, A. Alomainy, R. Dubrovka and C. G. Parini, "On-body path gain variations with changing body posture and antenna position," in *IEEE AP-S International Symposium and USNC/URSI National Radio Science Meeting, Washington, DC,* 2005.

[64] P. S. Hall, Y. Hao, Y. I. Nechayev, A. Alomainy, C. C. Constantinou, C. Parini, M. R. Kamarudin, T. Z. Salim, D. T. M. Hee and R. Dubrovka, "Antennas and propagation for on-body communication systems," *IEEE Antennas and Propagation Magazine,* vol. 49, pp. 41-58, 2007.

[65] P. S. Hall, Y. I. Nechayev, Y. Hao, A. Alomainy, M R Kamarudin, C. C. Constantinou, R Dubrovka and C. G. Parini, "Narrowband and Wideband Radio Channel Characterisation and Antennas for On-Body Communication Systems," *2nd International Workshop on Wearable & Implantable Body Sensor Networks, 12-13 April, 2005, Imperial College, London UK.,*

[66] M. Kamarudin, Y. Nechayev and P. Hall, "Performance of antennas in the on-body environment," in *IEEE Antennas and Propagation Society International Symposium,* pp. 475, 2005.

[67] Hu, Z.H.; Gallo, M.; Bai, Q.; Nechayev, Y.I.; Hall, P.S.; Bozzettit, M.; , "Measurements and Simulations for On-Body Antenna Design and Propagation Studies," *Antennas and Propagation, 2007. EuCAP 2007. The Second European Conference on* , vol., no., pp.1-7, 11-16 Nov. 2007.

[68] T. Aoyagi, J. Takada, K. Takizawa, N. Katayama, T. Kobayashi, K. Y. Yazdandoost, H. Li and R. Kohno, "Channel model for wearable and implantable WBANs," *IEEE 802.15, Working Group Document, IEEE 802.15-08-0416-03-0006, Sep. 2008.*

[69] T. Zasowski, F. Althaus, M. Stager, A. Wittneben and G. Troster, "UWB for noninvasive wireless body area networks: Channel measurements and results," in *Proc. IEEE UWBST,* 2003, pp. 285–289.

[70] P. Hall, M. Ricci and T. Hee, "Measurements of on-body propagation characteristics," in *IEEE Antennas And Propagation Society International Symposium,* pp. 310-313, 2002.

[71] T. Zasowski, G. Meyer, F. Althaus and A. Wittneben, "Propagation effects in UWB body area networks," in *Proc. ICU,* 2005, pp. 16–21.

[72] A. Fort, C. Desset, P. De Doncker, P. Wambacq and L. Van Biesen, "An ultra-wideband body area propagation channel model-from statistics to implementation," *IEEE Trans. Microwave Theory Tech.,* vol. 54, pp. 1820, 2006.

[73] A. Fort, C. Desset, J. Ryckaert, P. De Doncker, L. Van Biesen and P. Wambacq, "Characterization of the ultra wideband body area propagation channel," in *2005 IEEE International Conference on Ultra-Wideband, 2005. ICU 2005,* pp. 6, 2005.

[74] J. Ryckaert, P. De Doncker, R. Meys, A. de Le Hoye and S. Donnay, "Channel model for wireless communication around human body," *Electron. Lett.,* vol. 40, pp. 543-544, 2004.

[75] S. Van Roy, C. Oestges, F. Horlin and P. De Doncker, "On-body propagation velocity estimation using ultra-wideband frequency-domain spatial correlation analyses," *Electron. Lett.,* vol. 43, pp. 1405-1406, 2007.

[76] P. Hall, M. Ricci and T. Hee, "Measurements of on-body propagation characteristics," in *IEEE Antennas and Propagation Society International Symposium,* 2002, pp. 310-313.

[77] S. L. Cotton and W. G. Scanlon, "A statistical analysis of indoor multipath fading for a narrowband wireless body area network," in *2006 IEEE 17th International Symposium on Personal, Indoor and Mobile Radio Communications,* 2006, pp. 1-5.

[78] S. Cotton and W. Scanlon, "Higher Order Statistics for Lognormal Small-Scale Fading in Mobile Radio Channels," *IEEE Antennas and Wireless Propagation Letters,* vol. 6, 2007.

[79] E. Reusens, W. Joseph, G. Vermeeren and L. Martens, "On-body measurements and characterization of wireless communication channel for arm and torso of human," in *IFMBE Proceedings*, pp. 264, 2007.

[80] H. Ghannoum, C. Roblin and X. Begaud, "Investigation of the UWB on-Body Propagation Channel," 2005.

http://www.ensta.fr/~roblin/papers/WPMC2006_HG_BAN_model.pdf.

[81] A. Alomainy, Y. Hao, X. Hu, C. Parini and P. Hall, "UWB on-body radio propagation and system modelling for wireless body-centric networks," *IEE Proceedings-Communications,* vol. 153, pp. 107-114, 2006.

[82] G. Dolmans and A. Fort, *Channel Models WBAN-Holst centre/IMEC-NL, IEEE 802.15-08-0418-01-0006,* July 2008.

[83] D. Miniutti, L. Hanlen, D. Smith, A. Zhang, D. Lewis, D. Rodda, B. Gilbert, "Narrowband channel characterization for body area networks," IEEE P802.15-08-0421-00-0006, July 2008.

[84] W. C. Y. Lee, *Mobile Communications Design Fundamentals.* John Wiley & Sons, Inc. New York, NY, USA, 1992,

[85] ANSI C63.4-1992, *"American National Standard for Methods of Measurement of Radio Noise Emissions from Low- Voltage Electrical and Electronic Equipment in the Range of 9 KHz to 40 GHz",*"

[86] *Method of measurement of radio-noise emissions from low-voltage electrical and electronic equipment in the range of 10 kHz to 1 GHz*, ANSI Standard C63.4, 1988.

[87] M. D. Foegelle, "An analysis of the complex fit normalized site attenuation method," *Electromagnetic Compatibility, 2002. EMC 2002. IEEE International Symposium on,* vol. 1; 1, pp. 23-28 vol.1, 2002.

[88] A. Sugiura, "Formulation of normalized site attenuation in terms of antenna impedances [EMI measurement applications]," *Electromagnetic Compatibility, IEEE Transactions on,* vol. 32; 32, pp. 257-263, 1990.

[89] P. T. Trakadas and C. N. Capsalis, "A mixed model for the determination of normalized site attenuation," *Electromagnetic Compatibility, IEEE Transactions on,* vol. 43; 43, pp. 29-36, 2001.

[90] A. Askri, C. Vollaire, L. Nicolas and D. Prebet, "Normalized site attenuation standard correction from numerical computing," *Magnetics, IEEE Transactions on,* vol. 38; 38, pp. 693-696, 2002.

[91] R. A. McConnell, "Antenna pattern effects in normalized site attenuation," *Electromagnetic Compatibility, 1999 IEEE International Symposium on,* vol. 2; 2, pp. 949-951 vol.2, 1999.

[92] E. R. Heise and R. E. W. Heise, "A method to compute open area test site uncertainty using ANSI C63.4 normalized site attenuation measurement data," *Electromagnetic Compatibility, 1996. Symposium Record. IEEE 1996 International Symposium on,* pp. 505-507, 1996.

[93] A. Smith, R. German and J. Pate, "Calculation of site attenuation from antenna factors," *IEEE Trans. Electromagn. Compat.,* pp. 301-316, 1982.

[94] Schwarzbeck Mess - Elektronik,

"http://www.schwarzbeck.de/Datenblatt/k9117.pdf,"

[95] Rohde and Schwarz,

"http://www2.rohde-schwarz.com/file_11384/HF906_brief_e.pdf,"

[96] Z. N. Chen, *Antennas for Portable Devices.* John Wiley & Sons, Inc. New York, NY, USA, 2007.

[97] Schmid & partner engineering AG, DASY4 manual V4.1, march 2003. Page No. 17-2.

[98] S. D. R. Braun and Y. Shavit, "Active Measurements for CTIA Compliant Mobile Phones," 2005.

http://www.orbitfr.info/Papers/ORFRAMTAPapers/2005/a05-pid355_dreizin.pdf

[99] Brock Butler,Hakan Alparslan,Michael D. Foegelle,Ronald Borsato, "
A-GPS antenna performance: Over-the-air test method," September 1, 2009. http://www.tmssales.com/Application_Notes/RF_and_Microwwave/AGPS%20Test%20Method.pdf

[100] C. Certification, "Test Plan for mobile station over the air performance," *CTIA Wireless Association,* 2005.

http://files.ctia.org/pdf/CTIA_TestPlaforMobileStationOTAPerformanceRevision_2_2_2_Final_121808.pdf

[101] S. I. Al-Mously and M. M. Abousetta, "Anticipated impact of hand-hold position on the electromagnetic interaction of different antenna types/positions and a human in cellular communications," *International Journal of Antennas and Propagation (IJAP),* Vol. 2008, Article ID: 102759, 22, 2008.

[102] Y. Nechayev, P. Hall, A. Alomainy, Y. Hao, C. Constantinou, and C. Parini, "Measurements and modelling of on-body transmission channels," presented at National URSI Symposium, University of Bath, 2004.

[103] D. Neirynck, C. Williams, A. Nix and M. Beach, "Channel characterisation for personal area networks," *European Cooperation in the Field of Scientific and Technical research (EURO- COST)*, COST 273 TD(05)115, Lisbon, Portugal, Nov. 10-11, 2005.

[104] Z. Hu, M. Gallo, Q. Bai, Y. Nechayev, P. Hall and M. Bozzettit, "Measurements and simulations for on-body antenna design and propagation studies"*, EuCAP 2007. the Second European Conference on Antennas and Propagation,* 2007, pp. 1-7, 2007.

[105] Y. Hao, A. Alomainy, Y. Zhao, C. G. Parini, Y. Nechayev, P. Hall and C. C. Constantinou, "Statistical and deterministic modelling of radio propagation channels in WBAN at 2.45 GHz," in *IEEE Antennas and Propagation Society International Symposium 2006,* 2006, pp. 2169-2172.

[106] A. Christ, T. Samaras, A. Klingenböck and N. Kuster, "Characterization of the electromagnetic near-field absorption in layered biological tissue in the frequency range from 30 MHz to 6000 MHz," *Phys. Med. Biol.,* vol. 51, pp. 4951-4966, 2006.

[107] R. Vaughan, A. Lea, P. Hui and J. Ollikainen, "Theory of propagation for direct on-body wireless sensor communications," *Antennas and Propagation for Body-Centric Wireless Communications, 2nd IET Seminar on Vol. no.,* pp.1-5, 20-20 April 2009.

[108] C. A. Balanis, *Antenna Theory.* Wiley New York, 1997, Page 722.

[109] Y. Koyanagi, H. Kawai, K. Ogawa and K. Ito, "Consideration of the local SAR and radiation characteristics of a helical antenna using a cylindroid whole body phantom at 150 MHz," *Electronics and Communications in Japan(Part I Communications),* vol. 87, pp. 48-60, 2004.

[110] W. S. Chen, "Inset-microstripline-fed circularly polarized microstrip antennas," in *IEEE Trans. on Antennas and Propagation*, Vol: 48, Issue: 8, Aug. 2000, pp. 1253-1254, 2000.

[111] C. L. Holloway, P. McKenna, and R. F. German, "On the application of computational electromagnetic techniques to the design of chambers for EMC compliance testing," Compliance Engineering, pp. 19-33, March/April 1994.

[112] B. K. Chung, H. T. Chuah, Design and construction of a multipurpose wideband anechoic chamber, IEEE Antennas and Propagation Magazine 45 (2003) 41–47.